



Federal University of São Carlos  
Chemical Engineering Department  
Graduate Program in Chemical Engineering



**Doctoral Exam**

# **Design and Automation of a New Reactor For Enzymatic Hydrolysis of Lignocellulosic Biomass at High Solids Loading**

Vitor Badiale Furlong M.Sc.

Supervisors:

Professor Marcelo Perencin de Arruda Ribeiro Ph.D.

Professor Roberto de Campos Giordano Ph.D.

São Carlos - SP

May 10<sup>th</sup>, 2019



Vitor Badiale Furlong M.Sc.

# **Design and Automation of a New Reactor For Enzymatic Hydrolysis of Lignocellulosic Biomass at High Solids Loading**

Doctorate exam text in the  
Graduate Program in Chemical  
Engineering, Center of Exact  
Science and Technology, Federal  
University of São Carlos.

Research Area: Simulation and Control of Chemical Processes

Adviser: Professor Marcelo Perencin de Arruda Ribeiro Ph.D.

Co-adviser: Professor Roberto de Campos Giordano Ph.D.

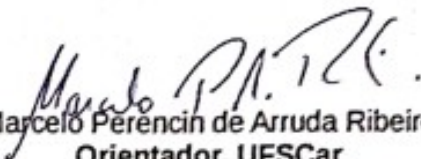
São Carlos - SP

May 10<sup>TH</sup>, 2019

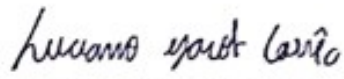


MEMBROS DA BANCA EXAMINADORA DA DEFESA DE TESE DE VITOR BADIALE FURLONG APRESENTADA AO PROGRAMA DE PÓS-GRADUAÇÃO EM ENGENHARIA QUÍMICA DA UNIVERSIDADE FEDERAL DE SÃO CARLOS, EM 10 DE MAIO DE 2019.

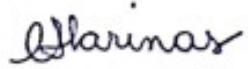
BANCA EXAMINADORA:

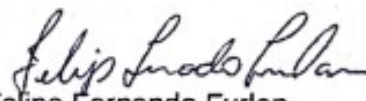
  
Marcelo Perencin de Arruda Ribeiro  
Orientador, UFSCar

  
Roberto de Campos Giordano  
Coorientador, UFSCar

  
Luciano Jacob Corrêa  
UFLA

  
Edson Romano Nucci  
UFSJ

  
Cristiane Sanchez Farinas  
EMBRAPA/UFSCar

  
Felipe Fernando Furlan  
UFSCar

*To my parents.*

*In retribution to all the love and care.*

*The feeling is mutual.*

## **ACKNOWLEDGMENTS**

I would like to thank;

- My supervisors, Marcelo and Roberto, for the dedication.
- The exam committee, for the suggestions.
- My family, for the love and patience.
- Thaís, for the love and support, despite my lack of patience.
- All my colleagues, old and current, friends, professors and any other person that withstands my daily mood.
- The Brazilian people, for the patronage.

*“So I strolled across old Main Street  
Walked down a flight of stairs  
Stepped into the hall  
And saw all my friends were there  
A neon sign was flashin', ‘Welcome, come on in  
It feels so good feelin' good again’.”*

*Robert Earl Keen*



## ABSTRACT

Several bottlenecks need to be overcome in order to establish the biorefinery concept as a feasible and lucrative second generation ethanol production technology. Lignocellulosic biomass enzymatic saccharification presents itself as one of the major challenges. This process needs high productivity while retaining low cost in order to become a regular practice. However, high enzymatic cocktail cost and complex phenomena makes its optimization a difficult task. Different strategies are necessary to deal with this task. In this work, different research fronts have been explored to improve the sugarcane bagasse enzymatic hydrolysis process performance. To improve modeling, a Fuzzy reaction rate model was proposed. Aiming to improve hydrolysis state prediction, specially under fed-batch conditions. This methodology proved to be useful in this situation, improving prediction both in training and validation assays. This model was coupled to a state estimator to enable monitoring of the hydrolysis process in real time. To do such, a Moving Horizon Estimator was implemented, and instrumentation data was obtained from a soft-sensor using an Artificial Neural Network to predict solids concentration from the reactor's mixing power requirement. This algorithm was able to predict the desired state variables, however, further studies are necessary before online implementation. Another research front explored in this work was the design of a new reactor architecture. A Semisolid Horizontal Saccharification Bioreactor was developed and coupled to a stirred reactor to compose a parallel reactor system. An automated solids feeder and liquid autosampler were also developed. These apparatus improved energy consumption of the process, while retaining performance indexes from other architectures. The development of the new reactor architecture opens new technologies possibilities inside the bioethanol biorefinery.

Key-words: Biomass Saccharification, Biorefinery, Fuzzy Modeling, Power Consumption, Reactor Development, State Estimation.

## RESUMO

Diversos desafios devem ser superados para assegurar o conceito de biorrefinaria como uma tecnologia de produção de etanol de segunda geração eficiente e lucrativa. Uma das etapas mais desafiadoras é a sacarificação enzimática da biomassa lignocelulósica. Esse processo necessita ter alta produtividade e baixo custo. No entanto, alto custo do complexo enzimático e fenômenos complexos fazem com que a otimização deste processo seja difícil. Diferentes estratégias devem ser usadas para lidar com essa tarefa. Neste trabalho, diferentes frentes de trabalho foram investigadas a fim de melhorar o desempenho do processo de hidrólise enzimática de bagaço de cana-de-açúcar. Para melhorar a modelagem do processo, um modelo de reação utilizando lógica *fuzzy* foi proposto. Seu objetivo foi prever a concentração de variáveis de estado com maior precisão do que modelos clássicos, especialmente de processos de batelada alimentada. Esta metodologia se provou eficiente, melhorando predição em ensaios de treinamento e validação, quando comparado a outros modelos usuais. Este modelo foi usado em um estimador de estado para viabilizar a predição em tempo real de variáveis de estado da hidrólise. Para tanto, um Estimador de Estado de Janela Móvel foi desenvolvido. Dados de instrumentação obtidos de uma Rede Neuronal Artificial que transcreve potência de agitação do reator para concentração de sólidos foram utilizados neste algoritmo. Este se provou capaz de prever concentração, no entanto, estudos ainda são necessários para aumentar sua robustez. Outra frente de trabalho foi o desenvolvimento de uma nova arquitetura de reator. Um Biorreator Horizontal Semi-sólido foi desenvolvido e acoplado a um reator agitado. Um aparelho de alimentação de sólidos e um amostrador automático de fase líquida foram desenvolvidos juntamente ao reator. Esta aparelhagem diminuiu a necessidade de energia do processo, enquanto manteve índices de produtividade semelhantes ao de outras arquiteturas de reatores. O desenvolvimento deste novo reator abre novas vias de produção no interior da biorrefinaria.

Palavras Chave: Biorrefinaria, Desenvolvimento de Reator, Consumo de Potência, Estimação de Estado, Modelagem com Lógica Difusa, Sacarificação de biomassa.

## SUMMARY

Acknowledgments.....	i
Robert Earl Keen.....	ii
Abstract.....	iii
Resumo.....	iv
Summary.....	v
Table Index.....	viii
Figures Index.....	ix
Abbreviations.....	x
Variables List.....	xi
Greek Letters.....	xiii
1. Introduction.....	1
2. Objective.....	4
2.1 Specific Objectives.....	4
3. Literature Review.....	5
3.1. Lignocellulosic Biomass.....	5
3.1.1. Sugarcane Bagasse.....	5
3.1.2. Cellulose Morphology.....	5
3.1.3. Hemicellulose And Lignin Morphology.....	7
3.2. Second Generation Biofuels Production in biorefineries.....	7
3.3. Biomass Pretreatment.....	10
3.4. Lignocellulosic Biomass Hydrolysis.....	12
3.4.1. Acid Hydrolysis.....	12
3.4.2. Enzymatic Hydrolysis.....	12
3.4.2.1. Carbohydrate Binding Module.....	13
3.4.2.2. Cellulose Hydrolysis.....	13
3.4.2.3. Hemicellulose Hydrolysis.....	16
3.4.2.4. Enzymatic Cocktail Inhibition and Inactivation.....	16
3.4.2.5. Biomass Enzymatic Hydrolysis Cost.....	18
3.5. High Solids Enzymatic Hydrolysis.....	18
3.5.1. Biomass Hydrolysis in Semi-continuous Operations.....	20
3.6. Modeling Enzymatic Lignocellulosic Biomass Hydrolysis.....	25
3.6.1. Michaelis-Menten Kinetics.....	27
3.6.2. Langmuir Type Kinetics.....	29
3.7. High Solids Hydrolysis in Nonconventional Architectures.....	30
3.8. Bioprocess Monitoring.....	33
3.8.1 Data Driven Soft Sensors.....	34
3.8.1.1. Principal Components and Partial Least Squares Regressions.....	34
3.8.1.2 Neural Networks.....	36
3.8.1.3. Torque Measurement.....	37
3.8.1.4. Visible and Ultra Violet Spectroscopy.....	38
3.8.1.5. Near Infrared Spectroscopy.....	38
3.8.1.6. Conductance/Capacitance Spectroscopy.....	38
3.8.2. State Estimation.....	39
4. Materials and Methods.....	40
4.1. Lignocellulosic Biomass.....	40
4.2. Enzymatic Hydrolysis.....	40
4.3. Carbohydrates Determination.....	41

4.3.1. Free Carbohydrates Analysis.....	41
4.3.2. Potential Carbohydrates Analysis.....	42
4.4. Enzyme Activity Analysis.....	42
4.4.1. Modified FPU Assay for Cocktail.....	44
4.4.2. Free Cellulase Activity.....	44
5. Hydrolysis Fuzzy-enhanced Modeling In Stirred Tank Reactor.....	45
5.1 Motivation and Objective.....	45
5.2 Materials and Methods.....	46
5.2.1 Hydrolysis Assays.....	46
5.2.2 Mathematical Modeling.....	47
5.2.2.1 Process Modeling.....	47
5.2.2.2 Standalone Reaction Rate Models.....	49
5.2.2.3. Fuzzy Kinetic Model.....	51
5.2.2.4. Fitting Algorithm and Statistics.....	52
5.3. Results and Discussion.....	53
5.3.1. Standalone Models Fitting.....	54
5.3.2. Fuzzy Kinetic Model Fitting.....	55
5.4. Conclusions.....	60
6. Hydrolysis State Estimation In Stirred Tank Reactor.....	61
6.1. Motivation and Objective.....	61
6.2. Materials and Methods.....	61
6.2.1 Hydrolysis Assays.....	61
6.2.2. Experimental Apparatus.....	62
6.2.3. Solids Monitoring.....	63
6.2.4. Instrumentation Data.....	63
6.2.5. Neural Network Architecture Optimization.....	64
6.2.6. Mathematical Modeling.....	65
6.2.7. Moving Horizon State Estimator.....	66
6.3. Results and Discussion.....	66
6.3.1. Neural Network Optimization.....	66
6.3.2. Moving Horizon Tuning.....	68
6.4. Conclusion.....	70
7. Semisolid Horizontal Saccharification Bioreactor Development.....	71
7.1. Motivation And Objective.....	71
7.2. Materials and Methods.....	74
7.2.1. Reactors Construction.....	74
7.2.1.1. Three Dimensional Modeling Software and Fast Prototype Hardware.....	75
7.2.2. System Control.....	75
7.2.3. Horizontal Reactor Power Consumption.....	75
7.3. Results and discussion.....	76
7.3.1. Solids Feeding Hardware.....	77
7.3.2 Autosampler.....	78
7.3.3 Semisolid Horizontal Saccharification Bioreactor.....	81
7.3.4 Stirred Tank Reactor and Liquid Recirculation.....	83
7.3.5 Power Consumption Estimate.....	85
7.4. Conclusion.....	86
8. Semisolid Horizontal Mesh Bioreactor Application.....	88
8.1. Motivation and Objective.....	88
8.2. Material and Methods.....	88

8.2.1. Batch and Fed-batch Assays.....	88
8.2.2. Analytical Procedures.....	89
8.2.2.1. Automated Sampling.....	89
8.2.2.2. Manual Sampling.....	89
8.2.3. Process Monitoring.....	89
8.2.3.1. Near Infrared Spectrum Scanning.....	90
8.2.3.2. Ultraviolet and Visible Spectrum Scanning.....	90
8.2.3.3. Capacitance and Conductance Scanning.....	90
8.2.3.4. Software Sensor Modeling.....	90
8.3. Results and Discussion.....	90
8.3.1. Analytical Results.....	90
8.3.2. Online Instrumentation Data.....	94
8.3.3. Software Sensor Monitoring.....	96
8.4. Conclusions.....	97
9. Conclusions.....	99
10. Further Studies.....	100
References.....	101

## TABLE INDEX

Table 3.1 Main Pretreatments Characteristics and Effects Summary.....	11
Table 3.2 Fed-Batch Lignocellulosic Biomass Enzymatic Hydrolysis Literature Review....	22
Table 3.3 Lignocellulosic Hydrolysis Modeling Classification.....	26
Table 3.4 Publications with Horizontal Reactors for Biofuels Production.....	33
Table 4.1 Pretreated Bagasses Compositions.....	40
Table 5.1 Assay Feeding Profiles.....	47
Table 5.2 Addressed Reaction Rates.....	50
Table 5.3 High and Low Heterogeneous Michaelis-Menten Model Parameters.....	56
Table 5.4 Fitting Error Summary for Proposed Models.....	57
Table 6.1 Assay Feeding Profiles.....	62
Table 6.2 Moving Horizon Estimator Tuning Pseudo-code.....	67

## FIGURES INDEX

Figure 3.1 Cellulose Transformation During Pretreatment.....	6
Figure 3.2 Lignocellulosic Biomass Processing for Bioethanol Production.....	9
Figure 3.3 Cellulases Synergistic Cellulose Hydrolysis.....	14
Figure 3.4 Conversions at Varying Solids Concentrations.....	19
Figure 3.5 Impellers for High Solids Operation.....	31
Figure 3.6 Perceptron Representation.....	36
Figure 3.7 Multilayer Perceptron Network.....	37
Figure 5.1 Fuzzy Model Reaction Rate Calculation.....	52
Figure 5.2 Standalone Models Fitting.....	55
Figure 5.3 High and Low Solids Models Fitting.....	56
Figure 5.4 Fuzzy, High and Low Solids Models Fitting.....	57
Figure 5.5 Fuzzy, High and Low Solids Validation Data Prediction.....	58
Figure 5.6 FM, HSM and LSM Reaction Rates.....	59
Figure 6.1 Experimental Apparatus.....	63
Figure 6.2 Cross Validation Procedure.....	64
Figure 6.3 Evaluated Transfer Functions.....	65
Figure 6.4 Training and Validation Errors Departure.....	65
Figure 6.5 Training and Validation Errors for Optimal Network.....	68
Figure 6.6 Training and Validation Errors Dispersion.....	68
Figure 6.7 Assay 1 and 2 State Estimation Prediction.....	69
Figure 6.8 Assay 3 State Estimation Prediction – Low Solids Fed-batch.....	69
Figure 7.1 Volumetric Power Consumption in Horizontal Reactor.....	71
Figure 7.2 Initial Proposal for Parallel Phase-Separated Hydrolysis Reactors.....	73
Figure 7.3 Parallel Phase-Separated Hydrolysis Reactors Design And Prototype.....	76
Figure 7.4 Solids Feeding System.....	77
Figure 7.5 Autosampler System.....	79
Figure 7.6 Manual and Autosampler Concentrations.....	81
Figure 7.7 Horizontal Filtering Media Drum.....	81
Figure 7.8 Horizontal Reactor with Screw Baffle – Mid Section Cut.....	82
Figure 7.9 Septa Positioning.....	83
Figure 7.10 Parallel Reactors Coupling.....	84
Figure 7.11 Horizontal Reactor Dripper.....	84
Figure 8.1 Parallel Reactors Batch Assay Analytical Data.....	92
Figure 8.2 Parallel Reactors Fed-batch Assay Analytical Data.....	93
Figure 8.3 Parallel Reactors Batch Assay Instrumentation Data.....	95
Figure 8.4 Parallel Reactors Fed-batch Assay Instrumentation Data.....	95
Figure 8.5 Cross Validation for PLS Fitting With UV/VIS Data.....	96
Figure 8.6 Prediction for PLS Regression With UV/VIS Data.....	97

## **ABBREVIATIONS**

bG -  $\beta$ -glucosidases  
CBH - Cellobiohydrolase  
CBM - Carbohydrate Binding Module  
EG – Endoglucanase  
FCA - Free Cellulase Activity  
FM - Fuzzy Model  
FPU - Filter Paper Unit  
GH - Glycoside Hydrolase  
HPLC - High Performance Liquid Chromatography  
HR - Horizontal Reactors  
HSB - High Solids Batch  
HSB - High Solids Fed-batch  
HSM - High Solids Model  
IF - Independent Fermentation  
IH - Independent Hydrolysis  
IU - International Unit of Enzyme Activity ( $\mu\text{Mol}\cdot\text{min}^{-1}$ )  
LK – Langmuir-type Kinetics  
LSF - Low Solids Fed-batch  
LSM - Low Solids Model  
MD - Membership Degree  
MLP - Multilayer Perceptron  
MMK - Michaelis-Menten Kinetics  
MMM - Modified Michaelis-Menten  
MSE - Mean Squared Error  
NIR - Near Infrared Spectroscopy  
NIRA - Near Infrared Reflectance Analysis  
PCR - Principal Components Regression  
PLS - Partial Least Squares  
PMM - Pseudo-Homogenous Michaelis-Menten  
PMO - Polysaccharide Monooxygenases  
PROALCOOL - National Ethanol Program  
PSR - Phase-Separated Reactor



SSF - Simultaneous Saccharification and Fermentation

STR - Stirred Tank Reactor

UV/VIS – Ultraviolet and Visible

## VARIABLES LIST

$A_{m,n}$  - Input Data Matrix

$B_{m,h}$  - Principal Components Projection Matrix

$C_{l_0}$  - Initial cellulose concentration ( $\text{g.kg}^{-1}$ )

$\text{Cov}(\theta)$  - Parameters Covariance Matrix

$D$  - Reactor Diameter (m)

$Em_i$  - Maximum adsorbed enzyme constant ( $\text{g}_{\text{Protein}}/\text{g}_{\text{Substrate}}$ )

$F$  - Objective Function Optimum Value

$F_r$  - Froude Number

$g$  - Gravity's Acceleration ( $\text{m.s}^{-2}$ )

$kc_i$  – Turnover Kinetic constant ( $\text{min}^{-1}$ )

$Kad_i$  - Dissociation constants for enzyme ( $\text{g}_{\text{Protein}}/\text{g}_{\text{Substrate}}$ )

$ke_i$  - First order inactivation constant ( $\text{min}^{-1}$ )

$Ki_{Cb}$  - Cellobiose Inhibition constant ( $\text{g.kg}^{-1}$ )

$Ki_{Gl}$  - Glucose Inhibition constant ( $\text{g.kg}^{-1}$ )

$Ki_{Xl}$  - Xylose Inhibition constant ( $\text{g.kg}^{-1}$ )

$Km_i$  - Michaelis-Menten constant ( $\text{g.L}^{-1}$ )

$Kp_i$  - Products competitive inhibition constant ( $\text{g.L}^{-1}$ )

$L$  - Reactor Length (m)

$L_v$  - Filtering Weights for Measurement Prediction

$L_w$  - Filtering Weights for Model Prediction

$l$  – Number of Predicted Variables

$m$  - Number of Data Points

$\text{MD}^{\text{HSM}}$  - Membership Degree of the High Solids Model

$\text{MD}^{\text{LSM}}$  - Membership Degree of the Low Solids Model

$N_{PL}$  - Reactor's Power Number With Liquid

$N_R$  - Reactor Rotational Speed ( $\text{s}^{-1}$ )

$N_{ps}$  - Reactor's Power With Slurry

$n$  - Input Data Dimension

$N$  - Estimation Window Size

$Q_{n,h}$  - Principal Components Matrix  
 $R_s$  - Substrate reactivity parameter  
 $R_e$  - Reynolds Number for Horizontal Reactors  
 $\underline{u}$  - Input Variables Vector  
 $Ve_{Max}$  - the Maximun Initial Velocity ( $g.L^{-1}.s^{-1}$ )  
 $V_L$  - Volume of Liquid Inside the Reactor ( $m^3$ )  
 $V_R$  - Reactor Total Volume ( $m^3$ )  
 $V_{T-N}$  - Arrival Cost  
 $\hat{y}$  - Projected Output  
 $\underline{y}_i$  - Partial Least Squares Eigenvectors  
 $\hat{Y}$  - Predicted Measurement  
 $Y$  - Instrumentation Measurement  
 $Y_{Cel-Ceb}$  - Pseudo-stoichiometric relation for cellulose and cellobiose ( $g_{Cellobiose}.g_{Cellulose}^{-1}$ )  
 $Y_{Cel-Glu}$  - Pseudo-stoichiometric relation for cellulose and glucose ( $g_{Glucose}.g_{Cellulose}^{-1}$ )  
 $Y_{Ceb-Gli}$  - Pseudo-stoichiometric relation for cellobiose and glucose ( $g_{Glucose}.g_{Cellobiose}^{-1}$ )  
 $Y_{He-Xyl}$  - Pseudo-stoichiometric relation for hemicellulose and xylose ( $g_{Xylose}.g_{Hemicellulose}^{-1}$ )  
 $Y_{Sol-Glu}$  - Pseudo-stoichiometric relation for solids and glucose ( $g_{Glucose}.g_{Solids}^{-1}$ )  
 $Y_{Sol-Xyl}$  - Pseudo-stoichiometric relation for solids and xylose ( $g_{Xylose}.g_{Solids}^{-1}$ )  
 $Y_{m,l}$  - Output Data Matrix  
 $\underline{w}$  - Nonlinear Weights Vector  
 $X$  - State Variable  
 $X_r$  - Regressors Matrix  
 $\hat{X}$  - Predicted State Variable  
 $X^*$  - Modeled State Variable  
 $\underline{x}_i$  - Principal Components Eigenvectors  
 $[Cb]$  - Cellobiose Concentration ( $g.L^{-1}$ )  
 $[C]$  - Cellulose Concentration ( $g.L^{-1}$ )  
 $[Eb_i]$  - Bounded enzyme concentration ( $g.L^{-1}$  or  $g.kg^{-1}$ )  
 $[Ef_i]$  - Free enzyme concentration ( $g.L^{-1}$  or  $g.kg^{-1}$ )  
 $[En]$  - Enzyme Concentration ( $g.L^{-1}$ )  
 $[Et_i]$  - Total Enzyme concentration ( $g.kg^{-1}$ )  
 $[G]$  - Glucose Concentration ( $g.L^{-1}$ )  
 $[He]$  - Hemicellulose Concentration ( $g.L^{-1}$ )

[ $L_g$ ] - Lignin Concentration ( $\text{g.L}^{-1}$ )

[ $P_i$ ] - Product concentration ( $\text{g.L}^{-1}$ )

[ $S_i$ ] - Substrate Concentration ( $\text{g.L}^{-1}$ )

[ $S_{0i}$ ] – Initial Substrate Concentration ( $\text{g.L}^{-1}$ )

[ $X_y$ ] - Xylose Concentration ( $\text{g.L}^{-1}$ )

### **GREEK LETTERS**

$\alpha_0$  - Initial Reaction Rate ( $\text{g.L}^{-1}.\text{min}^{-1}$ )

$\alpha^{\text{FUZZY}}$  - Fuzzy Model reaction rate ( $\text{g.L}^{-1}.\text{min}^{-1}$ )

$\alpha^{\text{HSM}}$  - High Solids Model reaction rate ( $\text{g.L}^{-1}.\text{min}^{-1}$ )

$\alpha_i$  - Reaction rate for “i” reaction, where “i” are reactions 1 through 6 ( $\text{g.L}^{-1}.\text{min}^{-1}$ )

$\alpha^{\text{LSM}}$  - Low Solids Model reaction rate ( $\text{g.L}^{-1}.\text{min}^{-1}$ )

$\alpha_r$  - Reactivity Constant

$\mu_L$  - Liquid Phase Viscosity ( $\text{Pa.s}$ )

$\rho_L$  - Liquid Phase Density ( $\text{kg.m}^3$ )

$\rho_{SL}$  - Slurry Density ( $\text{kg.m}^3$ )

$\phi$  - Solid Phase Volume Fraction



## 1. INTRODUCTION

The growing demand for energy, alongside with population growth and a relative decrease in fossil sources for fuels productions has led to investigations for new renewable energy sources. A possible solution to substitute some liquid fossil fuels is the use of bioethanol (Naik et al., 2010). Bioethanol has been a reliable and extensive renewable energy source used for several decades, with several countries committing to further expand the utilization of this fuel in their energetic matrix, in order to comply to targets for reduction of the carbon footprint. The technology for production of bioethanol from sugar cane juice or from corn is well established (Rastogi and Shrivastava, 2017).

In Brazil, large-scale production and feasibility of first generation bioethanol as an automotive fuel occurred in the 1970s when the Brazilian government initiated the National Ethanol Program (PROALCOOL) to diminish the national dependency on importing foreign refined oil used on gasoline production. The PROALCOOL program had as main feedstock material sugarcane. This culture was intensified during this period, especially in Brazil's southeast (Furlan et al., 2013).

A coproduct of the first generation ethanol production is sugarcane bagasse. Sugarcane bagasse is a lignocellulosic biomass and it is a byproduct of milling the sugarcane to produced juice (Carvalho et al., 2013). These materials are the basis of second generation biofuels. These are fuels produced from non-edible lignocellulosic feedstocks and biowaste (Özdenkçi et al., 2017). Thus, second generation biofuels can simultaneously increase productivity per land area, while diminishing competition with food production and reducing waste production (Zabed et al., 2017).

Lignocellulosic biomass is composed, mainly, by cellulose, hemicellulose and lignin. These are polymers formed by different molecules, but mostly, carbohydrates. One can then assume that these should be used to produce more bioethanol. However, these carbohydrates are not fermentable when using first generation production technology (Souza et al., 2013). Other processes are necessary to make these sugar available to fermentation, specially if the fermentation will be done using first generation microorganisms.

One of the main processes added to the production plant to adequate the lignocellulosic material for fermentation is the hydrolysis stage. The hydrolysis stage is where previously treated biomass is broken down to, mostly, fermentable monomers.

described as the most cost intensive stage. During initial biorefinery studies, enzymes cost alone would account to 50% of the bioethanol production cost (Chen and Qiu, 2010), and the energy necessary to mixing during hydrolysis can be more than half of the total energy contained in the produced bioethanol (Zhang et al., 2010). These figures have improved with research advances, but, if the establishment of the biorefinery is the final goal, the hydrolysis stage should be further optimized. This stage, as the technology stands, has small chances to overcome the described process. A drastic change is necessary, both in the reactor operation policy and, specially, in the reactor architecture itself. If this changes are not conducted in the near future, the entire biorefinery implementation remains in jeopardy.

## 2. OBJECTIVE

The main goal of this doctoral thesis is to advance the task of adequating the enzymatic hydrolysis process to an industrial scale within a biorefinery. This was done in two main work lines within the enzymatic hydrolysis stage. First by elucidating the hydrolysis kinetic behavior under different operating policies, monitoring the processes reliably, to ensure full process understanding and enable future process control. And second, by designing a new reactor architecture that promotes the hydrolysis stage energetic efficiency.

### 2.1 SPECIFIC OBJECTIVES

- Modeling the enzymatic hydrolysis of sugarcane bagasse under different operational policies.
- Monitoring the process by state estimation using instrumentation and kinetic model data.
- Developing a scalable bioreactor architecture that enables hydrolysis at high solids concentration, separation of solid-liquid phases, while keeping operational cost low.
- Operating the reactor and assess its performance.
- Estimating compounds concentration online in the new reactor architecture via instrumentation data.

### **3. LITERATURE REVIEW**

#### **3.1. LIGNOCELLULOSIC BIOMASS**

Lignocellulose are the fibrous materials found in plants and vegetables. Their main function is to provide structural support, however, other functions include microbiological and chemical protection. These compounds are an aggregation of several polymers, mostly composed by cellulose (32 – 55%), hemicellulose (19 – 24%), lignin (23 – 32%) and ashes (3.2 – 5.5%) varying with biomass and culture conditions (Santos et al., 2012).

Cellulose and hemicellulose are both carbohydrate polymers chains, as lignin is a three dimensional phenyl-propane polymer. These structures are highly linked by covalent and non-covalent bonds. This configuration makes for a strong matrix, resistant to digestion or saccharification (Sun et al., 2016).

##### **3.1.1. Sugarcane Bagasse**

Lignocellulosic biomass is obtained from several crops processing industries, waste management and even dedicated plantations. One of the most important is sugarcane bagasse, specially in tropical countries (Brazil, India, Cuba, China, Mexico, Indonesia and Colombia, to name a few). Sugarcane bagasse is obtainment from ethanol and sugar industries, where it is generated as a biproduct from sugarcane milling, used to extract the sugar rich juice from the plant. Each ton of sugarcane, after processing, can produce, approximately, 280 kg of bagasse (Cardona et al., 2010).

As it is the case for most crop based products, the composition of the biomass itself can vary with culture's condition, however, it is feasible to assume that average values for bagasse composition are 40% cellulose, 27% hemicellulose and 15% lignin, for its main components (Dyk and Pletschke, 2012).

##### **3.1.2. Cellulose Morphology**

Cellulose (molecular formula,  $(C_6H_{10}O_5)_n$ ) is the most abundant polysaccharide in lignocellulosic materials. Its ordered structure consists of several hundred glucose molecules (Xu et al., 2013).

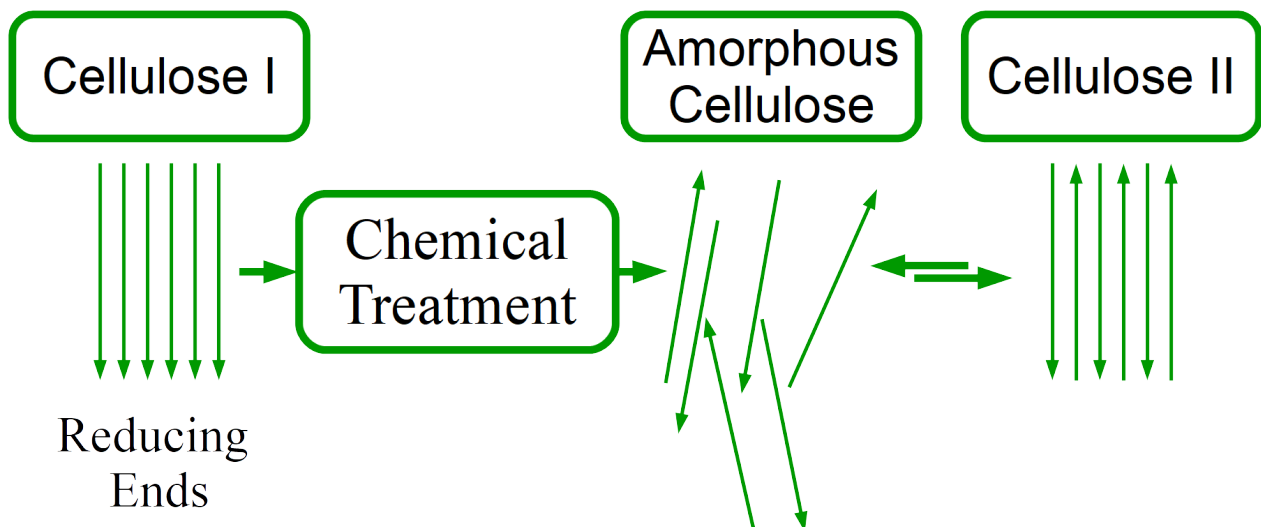
The cellulose spatial conformation is determined by three main interactions. The first interaction is the glycosidic linkage that unites a glucose to another glucose molecule through a covalent bound. This generates a unit of cellobiose, and this disaccharide is the repeating unit in the cellulose chain (Dias et al., 2011).



The second interaction is between hydrogen molecules from the same chain and the third is the between adjacent chains, both through hydrogen bridges (Corrêa et al., 2010). How the intermolecular interaction occurs between two separate chains dictates the degree of crystallinity. Due to these interactions, cellulose molecules can form high density areas, called crystalline regions, with high cohesiveness and resistant to hydrolysis, or amorphous regions, more susceptible to saccharification.

Amorphous cellulose can be obtained from crystalline cellulose through different processes, but, in the presence of water, the constructed amorphous cellulose is prone to retrograde into a crystalline structure (Karimi and Taherzadeh, 2016). This process is represented in Figure 3.1.

**Figure 3.1** Cellulose Transformation During Pretreatment



**Source:** Adapted from Karimi and Taherzadeh (2016)

The highly packed crystalline cellulose structure is called Cellulose I, and is the naturally occurring variety in most higher plants. Cellulose I is constructed from parallel chains of cellulose with the same orientations (as presented in the most left side of Figure 3.1), this type remains mostly unchanged during hydrolysis if no prior treatment is used in the biomass.

Cellulose II, III and IV don't occur naturally, and are obtained when cellulose I is subjected to chemical treatments (Phanthong et al., 2018). These structures are less crystalline and more susceptible to hydrolysis. Cellulose II is often called regenerated cellulose, and is generated when treated Cellulose I returns from amorphous organization to a more organized form during precipitation (Corrêa et al., 2010). However, this

reorganization is not enough to hinder saccharification to the same degree as Cellulose I (Sun et al., 2016).

### **3.1.3. Hemicellulose And Lignin Morphology**

Hemicellulose differs significantly from cellulose. It is a heteropolysaccharide composed by hexoses (glucose, galactose and mannose), pentoses (xylose and arabinose), acetic acid, glucuronic acid and 4-O-methy-glucuronic acid, this substances ratios differs among vegetables. Hemicellulose does not forms crystalline regions, thus it can be removed or hydrolyzed more easily than cellulose (Canilha et al., 2012).

Lignin is formed by the polymerization of, mainly, p-coumarilic alcohol, synapyl alcohol and coniferilic alcohol. It is the second most abundant polymer in the lignocellulosic biomass, and provides a barrier to the structure against foreign agents (Rahikainen et al., 2013). In order to prevent this effect, a delignification procedure may be applied, since the recuperated lignin mass may be used in other processes with in the refinery (Özdenkçi et al., 2017).

## **3.2. SECOND GENERATION BIOFUELS PRODUCTION IN BIOREFINERIES**

Second generation biofuels are produced from non-food feedstocks, usually lignocellulosic biomass and biowaste (Łukajtis et al., 2018). These are the only truly fuels that can be carbon neutral or even carbon negative. However, the production of these fuels may not yet be cost-effective, several hurdles have to be overcome to establish second generation production as a viable mean of production (Naik et al., 2010).

Therefore, to make biofuels production a feasible and lucrative venture the production plant needs to be highly optimized in terms of finances. Furthermore, the production of only one product from the biomass, the biofuel itself, may be insufficient to ascertain plant viability.

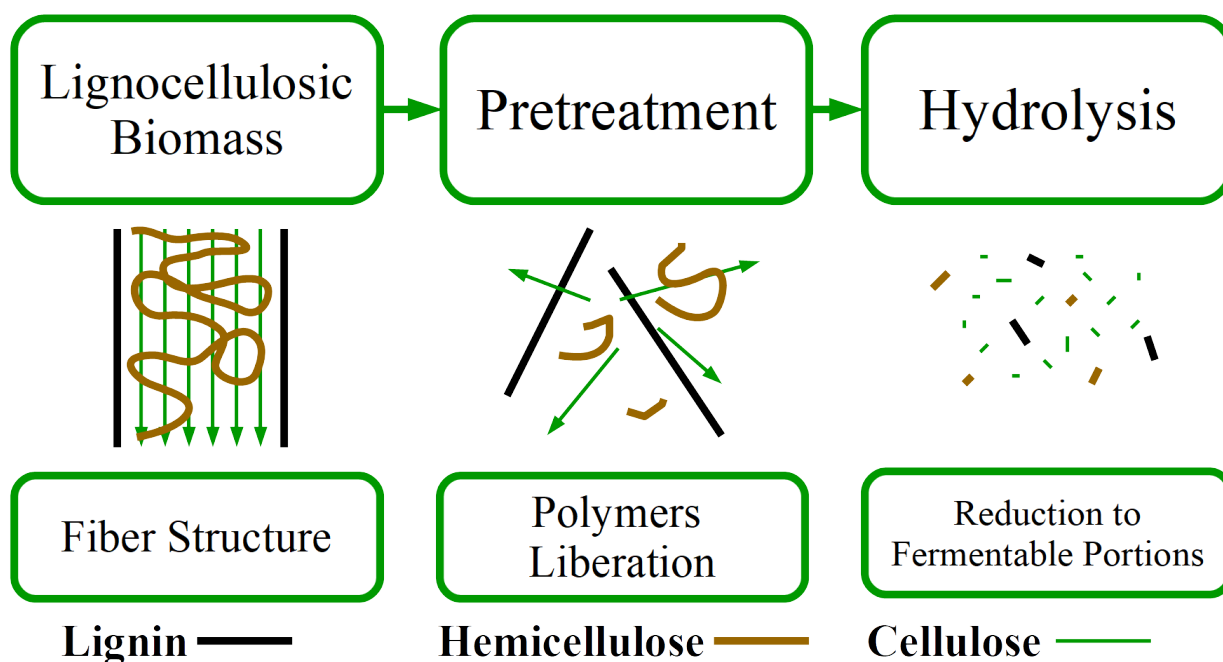
From this issue, the biorefinery concept arises. The International Energy Agency defines a biorefinery as a production plant that can synergistically and sustainably produce energy (fuels, power and heat), products (chemicals and materials) and food and feed ingredients from biomass (IEA Bioenergy, 2014). This sort of plant may be the solution to the hurdles in second generation biofuels production, since aggregating all that is necessary during the production process under a single company reduces overall cost (Longati et al., 2018).

The biorefinery design is greatly influenced by its surroundings, and are based on available feedstock. Plants can be based on commonly produced crops (corn, wheat, rice, barley and others) or using wood materials from natural or designed forests. Tropical countries, alongside the previously described biomasses, have more diversified feedstocks (coconut, sorgham, grass) (Bhowmick et al., 2018). One particular interesting biomass for biorefineries is sugarcane bagasse, specially in Brazil.

As previously described, sugarcane bagasse is a byproduct of first generation ethanol and refined sugar production. This technology is widely used in Brazil, and generates great amounts of bagasse. In the first generation technology, part of the total bagasse produced is burned in boilers to generate power for the plant, and the power surplus is sold to the grid to generate more profit (Dantas et al., 2013). The bagasse is then a readily available source of carbohydrates that is not currently used to produce ethanol in its entirety.

To produce ethanol from lignocellulosic materials the structural polysaccharides must be hydrolyzed, so that their monosaccharides units (mostly pentoses and hexoses) become available to fermentation by microorganisms (Souza et al., 2013). In addition, before the hydrolysis process, a pretreatment stage is required to separate and adequate the lignocellulosic compounds constituents (cellulose, hemicellulose and lignin) to a less recalcitrant form that is susceptible to hydrolysis. In particular, the crystalline structures in cellulose has to be destabilized, otherwise hydrolysis yield is very low. A representation of the entire process is presented in Figure 3.2.

**Figure 3.2** Lignocellulosic Biomass Processing for Bioethanol Production



**Source:** Adapted from Santos et al. (2012)

These processes are energy intensive, and increase the cost of the final product, to an extent that, under current economic market, may negate a stand-alone second generation bioethanol production plant (Dias et al., 2012).

However, adapting the current established Brazilian first generation ethanol production to also produce second generation ethanol can diminish installation costs and help control uncertainties in the production cost of the new technology. This alternative has been the most studied within Brazilian research groups (Longati et al., 2018).

Furthermore, extending the Brazilian production matrix update from first to second generation to a broader biorefinery concept, more products can be obtained from the biomass. The products range from; hydrocarbons, syngas, biogas and hydrogen production to generate bioenergy; to fine chemicals such as organic acids, phenolic compounds and materials based on nanocellulose fibers and crystals (Bhowmick et al., 2018; Farinas et al., 2018). The fabrication of these products depend on the plant's installation, especially in the choice of pretreatment and hydrolysis technologies.

Nevertheless, independent assessments of which pretreatment and hydrolysis technologies are to be used in a potential biorefinery is of little necessity or importance. All sub-processes must be taken into account at once when designing the production plant. A more expensive process may have its cost offset by smaller subsequent downstream

treatment. Yet, it is important that research projects retain a certain level of abstraction from these integration procedures. All basis can not be covered by a single assay or thesis, and a starting position needs to be established in order to generate reliable data, even if certain operational policies are changed in the production plant.

### 3.3. BIOMASS PRETREATMENT

The pretreatment procedure is conducted to destabilize the lignocellulosic structure, making it more susceptible to subsequent processes. This is achieved by increasing the material porosity and reducing cellulose crystallinity.

The entire procedure must be applied to an intensity that generates an optimum platform to subsequent operations, while considering the formation of inhibitors and cost effectiveness (Chiaramonti et al., 2012).

Several methodologies are available to this processes, each one with different necessities and, different end products. Thus, the choice of correct pretreatment varies with the feedstock, process plant design and financial situation. A summary of the main used pretreatments for biofuels production is presented in Table 3.1.

Analysis of Table 3.1 demonstrates that choosing the pretreatment to be used within a biorefinery is not a trivial task. Not only the change in biomass structures differs greatly from technology to technology, the liquid effluent from each also varies.

Since the biorefinery concept deals with the utilization of the whole biomass production potential, choosing only one technology can be difficult, if not impossible. It is possible to assume that an optimized biorefinery may need two or more pretreatment techniques depending on the targeted products (Bhowmick et al., 2018).

Among the several available pretreatments, special attention must be given to Liquid Hot Water and the Steam Explosion pretreatments, both are considered Hydrothermal pretreatments, but, in this work this name is used as a synonym to the Liquid Hot Water pretreatment. These technologies use small amounts of chemical compounds during the process, yielding a less toxic effluent than other operations. This can amount to a cheaper operation cost. However, this pretreatment generates little alteration and removal of lignin, and this can hinder downstream processes (Menon and Rao, 2012).

**Table 3.1** Main Pretreatments Characteristics and Effects Summary

Pretreatment	Action	Advantages	Disadvantages	Cellulose Decrystalization	Hemicellulose Removal	Lignin Removal
Mechanical	Milling	Surface area increase	High energy consumption	Minor Effect	No Effect	No Effect
Liquid Hot Water	Pressurized reactor with liquid water for a wide range of retention times	Low inhibitors production Low environment impact	High energy and water consumption	Minor Effect	Major Effect	Minor Effect
Steam Explosion	Exposure to steam for small retention time	Low water requirement Low environment impact	High inhibitors production High installation cost	Minor Effect	Major Effect	Minor Effect
Diluted Acid	Pressurized and unpressurized reactors with diluted acid solutions	High depolymerization Hemicellulose hydrolysis	High water consumption High effluent treatment cost	Minor Effect	Major Effect	Minor Effect
Alkali	Pressurized and unpressurized reactors with basic solutions	High depolymerization Facilitates lignin recuperation	High water consumption High effluent treatment cost	Major Effect	Minor Effect	Major Effect
Organosolv	Pressurized and unpressurized with organic and polar compounds	High lignin and hemicellulose depolymerization	High solvent recovery cost Fire and explosions risk	Minor Effect	Minor Effect	Major Effect
Ammonia Fiber Extension	Pressurized liquid ammonia at moderate temperature with sudden release	Low inhibitors production	High effluent treatment cost Lignin content sensible	Major Effect	Minor Effect	Major Effect

**Source:** Adapted from literature Gandla et al. (2018), Mosier et al. (2005) and Rastogi and Shrivastava (2017)

### 3.4. LIGNOCELLULOSIC BIOMASS HYDROLYSIS

The pretreated biomass must then be further processed to provide fermentable carbohydrates. This process is denominated hydrolysis, or saccharification. At this stage, the polymers released by the pretreatment stage are converted to free monomers, this is necessary since microorganisms responsible for the anaerobic fermentation, where the ethanol is produced, can not digest long polymers, or at least, not in a rate needed by industrial scale. Two main technologies are used in order to hydrolyze lignocellulosic materials, using acid solutions or using enzymatic complexes (Aditiya et al., 2016).

#### 3.4.1. Acid Hydrolysis

Acid hydrolysis is usually divided into two groups, diluted and concentrated acid hydrolysis. Diluted acid hydrolysis uses acid's concentrations below  $10 \text{ g} \cdot 100\text{g}_{\text{Media}}^{-1}$ , while concentrated acid operates above the  $10 \text{ g} \cdot 100\text{g}_{\text{Media}}^{-1}$  threshold and reaching concentrations of up to  $90 \text{ g} \cdot 100\text{g}_{\text{Media}}^{-1}$ . The most used acid is sulfuric, but others have been researched (Kumar et al., 2015).

Regardless of acid or concentration a high concentration of toxic and inhibitors compounds for downstream processes are expected from this technology. During acid hydrolysis, inhibitors are generated by degradation and condensation of hexoses and pentoses, mostly furfurals. This degradation does not only decreases the hydrolysis final yield, since part of the carbohydrates are being condensed, but also decreases downstream hydrolysis and fermentation yields (Limayem and Ricke, 2012). Furthermore, since acids are utilized, even at mild conditions, corrosive issues inside reactors are fairly common. In addition, disposal costs are also increased, since the acid needs to be recovered or treated (Bansal et al., 2009).

#### 3.4.2. Enzymatic Hydrolysis

The issues with acid hydrolysis leads to the necessity for a more environmental suitable process, one alternative is enzymatic hydrolysis. This procedure yields high conversions, with fewer risks of producing toxic secondary products (Limayem and Ricke, 2012).

Due to the high complexity of the lignocellulosic material, the enzymatic catalyst used in the biomass hydrolysis is not composed by only one active protein, but a cocktail of several molecules, each interacting with a portion of the lignocellulosic substrate (Sun

and Cheng, 2002).

This generates a large amount of proposed mechanisms, with varying degrees of complexity. In this item, the main groups and structures from fungal produced enzymatic cocktails are described.

It is important to remember that other cocktails are used, such as bacterial made cocktails. However, fungal cocktails are the most used both in academy and industry and, in this work, it will be used as the case studied (Teter et al., 2014).

#### 3.4.2.1. Carbohydrate Binding Module

Lignocellulose digesting enzymes are modular, meaning that more than one active site can be found within the protein molecule and they can differ in function. Within fungal secreted enzymes, it is common to find a catalytic center, where the hydrolysis occurs, and a Carbohydrate Binding Module (CBM). This region is responsible for directing the enzyme to its substrate, increasing activity (Zhang et al., 2017).

These structures are of extreme importance in a heterogeneous media. They can greatly increase the enzyme affinity when compared to the same molecule without a CBM site. These are also credited with being able to disrupt and make crystalline regions prone to hydrolysis (Hildén and Johansson, 2004).

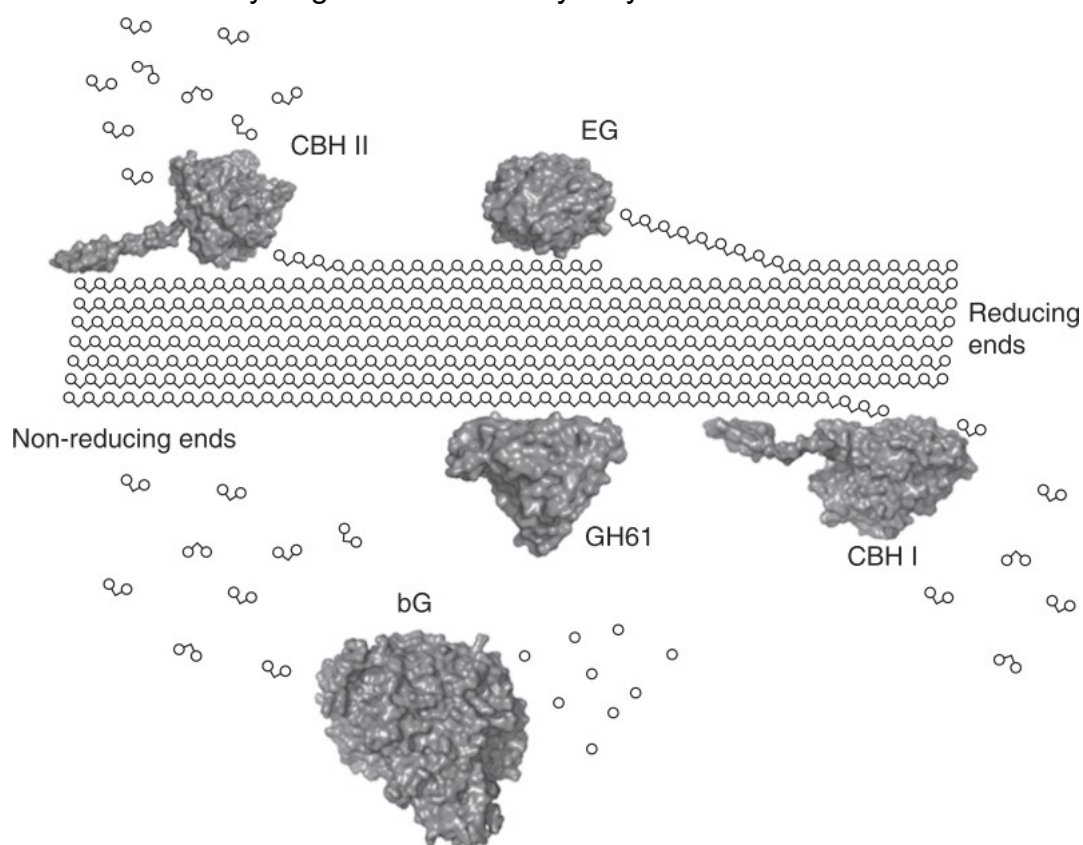
CBMs are found in both cellulose and hemicellulose digesting enzymes, and they can be divided into three different categories, CBM A binds to insoluble, crystalline substrates, CBM B binds to soluble polysaccharides and CBM C binds to small sugars (Dyk and Pletschke, 2012).

#### 3.4.2.2. Cellulose Hydrolysis

The portion of active proteins that interacts with cellulose, and hydrolysis intermediates from cellulose, are called cellulases. Cellulases are divided into four main groups. Endoglucanases (endo-1,4- $\beta$ -glucanase, abbreviation EG), Cellobiohydrolases, or Exoglucanases (exo-1,4- $\beta$ -glucanase, abbreviation CBH),  $\beta$ -glucosidases (bG) and Polysaccharide Monooxygenases (PMO) also know as GS61. The interaction of these enzymes are presented in Figure 3.3.



**Figure 3.3** Cellulases Synergistic Cellulose Hydrolysis



**Source:** Teter et al. (2014)

EG works in the uninterrupted region of available cellulose molecule and binds randomly, liberating reductive ends in the polymer chain. EGs are usually linked to CBMs A, they adhere to crystalline structures, cleave the internal glycosidic bonds in the cellulose where the chain is susceptible. This activity may not generate a free carbohydrate, but generates two ends in the cellulose chain, one reducing and one non-reducing. Since the attack is random, the length in each side of the chain is also random, from one glucose unit to almost a full chain (Balat, 2011; Teter et al., 2014).

The chain ends newly formed by EG activity and the naturally occurring ones in the cellulose molecule are the binding site for CBHs. These are the bulk of the enzymatic cocktail and can be divided into two groups. CBH I acts in the reductive ends of the chain, as CBH II binds to the non-reducing end of the chain. Both produce soluble cellobiose and are usually associated to a CBM A (Zhang et al., 2017). This is the main reaction responsible for the biomass liquefaction, since it is the primary mechanism by which the insoluble matter becomes soluble.

Some authors propose loosening the strict division between EGs and CBHs as the

mechanisms for each is more elucidated. Some EGs appear to present CBHs activity, as some CBHs can modify their structure to achieve EG activity (Hildén and Johansson, 2004).

This idea is strengthened when the mechanisms for EG and CBH are considered, and how similar they seem. The most accepted mechanism is that first the enzymes are adsorbed to cellulose with the help of the CBM. The adsorbed enzymes then slide through the cellulose fibril until a reactive site is found, a susceptible bond to EG and a chain end to CBH. Then the enzyme-substrate complex is formed. This is followed by the hydrolysis of the glycosidic bond and sliding of the enzymes along the polymer. The enzyme can then desorb from the cellulose molecule or continue sliding to find another reactive site and repeat the process (Bansal et al., 2009).

However, this is not a consensus in the literature. Authors have reported that EG does not slide on top of the cellulose molecule after hydrolysis and the mechanism through which the CBH deals with the cellulose is still a point of much debate (Bansal et al., 2009; Hildén and Johansson, 2004; Teter et al., 2014).

Regardless of the mechanism from each enzyme, their synergistic cooperation is undeniable. The utilization of a EG improves the substrate concentration for CBHs, improving hydrolysis productivity. Both enzymes use CBM to react with heterogeneous substrates, and the product of their cooperation are small soluble carbohydrates, mostly glucose or cellobiose (Dyk and Pletschke, 2012).

Cellobiose and other small soluble polymers need further hydrolysis to be readily fermentable. These hydrolysis reactions are catalyzed by bGs. Since this stage of hydrolysis occurs in liquid phase, bGs are not usually linked to CBM (Reilly, 2007).

The last group is a somewhat new addition to describe lignocellulosic biomass hydrolysis, PMOs. PMOs are metalloenzymes that can cleave glycosidic bonds without the need for a polymer end, generating either a new end or small molecules. These enzymes require molecular oxygen and reductant cofactors. The cofactors can be supplied by adjacent enzymes in the cocktail or chemically supplemented (Beeson et al., 2011).

With the reaction substrates allocated the reaction occurs. However, the reaction mechanism is still under debate. What is clear is that the PMO inserts molecular oxygen within the carbon-hydrogen bonds adjacent to glycosidic bonds, destabilizing them and

leading to cleave. Similar to CBHs and EGs, PMOs are usually bounded to CBMs (Li et al., 2007).

#### 3.4.2.3. Hemicellulose Hydrolysis

Hemicellulose hydrolysis is more complex than cellulose due to its composition, requiring a wider group of proteins. Core groups of enzymes are endo-xylanases, that cleave xylan polymer to shorter chains, and  $\beta$ -xylosidases to hydrolyze the xylan chains into xylose. The same manner occurs with mannans chains, where endo-mannanase breaks the backbone of the chain, and  $\beta$ -mannosidase reduces the chains to mannose. Since xylose and mannose are not the only constituents of hemicellulose, several other secondary enzymes also take part in this hydrolysis process (Dyk and Pletschke, 2012).

#### 3.4.2.4. Enzymatic Cocktail Inhibition and Inactivation

Inactivation and inhibition of enzymes are issues well covered in literature ever since the early studies in enzymology. Studies have tried to explain varying reaction rates since before the publication of, the now famous, Michaelis-Menten enzymatic kinetics paper (Cornish-Bowden, 2013). The hydrolysis of lignocellulosic material differs from those initial studies conditions, however, several effects described in the past can be extended to this process with minor alterations.

The enzymatic cocktail is susceptible to denaturation, as other more simple and isolated proteins are. Enzyme activity increases with temperature until it reaches a certain level that the molecule is unstable, and the molecule is unable to retain its conformity. Alterations in quaternary, tertiary and secondary structures of the enzyme renders it inactive, this process is called denaturation, and it is, often, irreversible (Campbell and Farrel, 2007).

Temperature denaturation is among, if not, the first efforts in enzymes kinetics inhibition studies, and advances in this field are still being made more than a century later (Daniel and Danson, 2013). This only demonstrates how complex the reaction mechanism is, even for simple solutions, containing few reactants. The complexity is multiplied by a large factor when the entire hydrolysis of lignocellulosic material is considered. Thus, even areas considered simple and well described should be investigated.

Similarly to temperature, enzymatic complexes have an optimum pH and salinity range. Below and above the thresholds of the range, sharp decreases in the enzyme

activity are to be expected. These are related to several effects in the protein, but the most important can be attributed to the solubility of the enzyme within its medium. The amount of charges surrounding the enzyme, if outside the optimum range, can impede catalyst activity, or, in more extreme concentrations, destabilize the entire molecule, precipitating it and ceasing activity. Opposite to temperature, loss of activity due to solubility issues are, usually, reversible (Trevor Palmer, 1985).

As is the case for most enzymes, enzymatic cocktails for lignocellulosic biomass hydrolysis operates in, relative, mild temperature and pH conditions. It is widely accepted that optimum values for these enzymes are around 40-50 °C and pH 4.50-5.00 (Battista and Bolzonella, 2018).

However, pH and temperature are important variables for process design and they can be changed if the loss of enzymatic hydrolysis does not hinder the whole plant economic optimization. Thus, it is of little meaning the search for optimum temperature and pH ranges for a given cocktail. Instead, the research effort should be focus in constructing robust models for the entire operational range.

Another important plant wide design task is the selection of pretreatment technology considering the inhibitors produced in this stage that can hinder the subsequent hydrolysis. Degradation products from lignocellulose, such as weak acids, furfurals, 5-hydroxymethyl furfural and soluble phenolic compounds, can all be produced during pretreatment and they are of great toxicity to subsequent fermentation (Sun et al., 2016).

During the hydrolysis itself, the generation of smaller saccharides causes a decrease in productivity, due to product inhibition, a well documented effect. Enzyme activity inhibition by products is well documented. Cellulases are inhibited by cellobiose, as bG is inhibited by glucose. The reaction decrease can even surpass the productivity loss by inhibitors from other processes upstream (Dyk and Pletschke, 2012).

With the description of recent mechanism proposals, new inhibition sources have been described. Lignin inactivation onto the several enzymes involved in the biomass hydrolysis is an effect that has been the focus of several research groups efforts (Guo et al., 2014).

Lignin can hinder the hydrolysis in three ways, physically shielding the cellulose and hemicellulose surface: soluble lignin can interact with catalytic sites, rendering the

molecule inactive; enzymes can adsorb non-productively onto insoluble lignin surface. The non-productivity, together with the shield effect, have been considered the major effects in enzyme activity depletion (Rahikainen et al., 2013). The shielding effect may be mitigated with the choice of pretreatment, since the lignin extraction is dependent on the technology used.

The non-productivity aspect has more of a connection with the enzyme structure itself. As previously described, the enzymes involved in heterogeneous reactions (EGs, CBHs, PMOs, xylanases and mannanases) are linked to CBMs to improve reaction site location capacity. However, the CBM can also bind to lignin, often in a non-reversible manner. This can account to as much as a 50% loss of the total hydrolysis activity to non-productivity lignin interactions (Jørgensen and Pinelo, 2017).

#### 3.4.2.5. Biomass Enzymatic Hydrolysis Cost

From the described mechanisms and issues within the reactive system, it is possible to see how sensible the enzymatic hydrolysis process is, and furthermore, how cost can increase rapidly when more cocktail is used to cope with activity depletion. Therefore, the amount of enzyme used is a very important parameter since, with current technology, enzymatic complex cost can amount to 50% of the total second generation bioethanol production cost (Chen and Qiu, 2010).

To adequate enzymatic hydrolysis to a financial feasible technology, several research fronts are being explored to diminish cost; Enzyme production within the biorefinery (Farinas et al., 2018); enzymatic complex recycling (Jørgensen and Pinelo, 2017); elucidation of inhibition mechanisms (Li and Zheng, 2017); additives to diminish inhibition (Rocha-martín et al., 2017); and process intensification, especially through the utilization of high solids concentration within the enzymatic hydrolysis bioreactor (Modenbach and Nokes, 2013).

### 3.5. HIGH SOLIDS ENZYMATIC HYDROLYSIS

In order to adequate enzymatic hydrolysis to a more profitable state, a higher ratio of substrate, i. e., solids loading, is necessary, generating a more concentrated carbohydrate solution at the end of the process. A more concentrated final product could possibly generate more ethanol in subsequent stages, and enable the integration of the second generation process with the first generation facility (Dias et al., 2013).

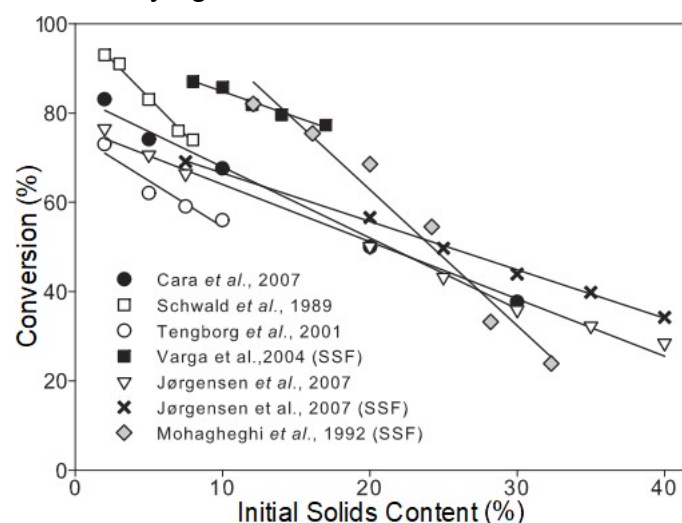
Solids are the dispersed phase of lignocellulosic biomass suspended inside the reactor liquid phase, the continuous phase. Several manners can be used to express the concentration of solids in the reactor, in this work, % will be used, and this is the mass of insoluble material per 100 units of reactor media ( $\text{g}_{\text{Solids}} \cdot \text{g}_{\text{Media}}^{-1}$ ).

High solids reactor also generates economical advantages, since the operational volume is lower than in a low-solids operation, resulting in less energy to heat or cool the reactor, as well as reduce effluent disposal and treatment costs due to lower water usage (Hodge et al., 2008).

High Solids processes are those where the ratio of solid material to aqueous phase is such that very little free liquid is present (Hodge et al., 2009). As water becomes sparse within the reactor, issues arise.

It is well documented that conversion decreases when enzymatic hydrolysis is carried out at increasing solids concentrations. This effect is related to the previously described enzymatic cocktails inhibition phenomena. Several authors have described this phenomenon, both for hydrolysis and for when hydrolysis and fermentation occurs simultaneously, known as Simultaneous Saccharification and Fermentation (SSF) processes. This trend is presented in Figure 3.4, where data from several authors are combined into one plot.

**Figure 3.4** Conversions at Varying Solids Concentrations



**Source:** Adapted from Kristensen et al. (2009). Data taken from; Cara et al. (2007) ● Hydrolysis; Schwald et al. (1989) □ Hydrolysis; Varga et al. (2004) ■ SSF; Jørgensen (et al., 2007) ▽ Hydrolysis and × SSF, Mohagheghi et al. (1992) ◇ Hydrolysis.

The data in Figure 3.4 is from different sources of lignocellulosic biomasses and

with different initial solids concentrations. A negative linear relation between the solids concentration and conversion can be observed.

It is easy to attribute this tendency to the inhibition effects described in Item 3.4.2.4., and these are only intensified when using a high solids operation policy. With the higher products concentration, product competitiveness is enhanced. More solids also mean more lignin, if this fraction was not removed in other upstream processes, within the reactor, increasing shielding and unproductive binding. More substrate also brings in more pretreatment generated inhibitors (Kristensen et al., 2009).

Furthermore, new activity hindering effects, previously negligible at low solids concentrations, are established. Water is also necessary in order to provide a medium in which the enzyme is suspended the lack of it can interfere in the enzyme solubility. Water and its ions are also frequently substrates or cofactors in the hydrolysis reaction. All of these can interfere with the cocktail activity (Modenbach and Nokes, 2013).

Another issue is the reactive media lubricity. Normally the continuous phase (liquid water) viscosity is low, but with the addition of high amounts of disperse phase (solids) interaction between both phases increases, this causes a behavior in the medium rheology, changing from a Newtonian fluid to a non-Newtonian one. The change in the fluid apparent density and viscosity requires alterations in the reactor's mixing apparatus and vessel design, otherwise, the mixture departs greatly from a uniform state (Battista and Bolzonella, 2018). Even with the change in the reactor hardware, an increase in the energy necessary to agitate the reactor is to be expected, specially if the standard reactor agitation hardware is used (Wang et al., 2013).

These characteristics of high solids systems may indicate that this is not a feasible manner to operate the hydrolysis reactor. However, the benefits of high product concentration can outweigh the described issues. Therefore, several authors have dedicated efforts to increase this technology feasibility, particularly by altering the reactor's operation policy and design.

### **3.5.1. Biomass Hydrolysis in Semi-continuous Operations**

Biomass hydrolysis in fed-batch processes appears as a promising strategy since adverse conditions of the standard high solids batch are diminished. A process policy where substrate is fed into the reactor continuously avoids the necessity of beginning the

process with high solids loading, facilitating system initial homogenization. Furthermore, adding solids after the previously added substrate are already liquefied can not only increase media homogenization, but also decrease the energy necessary to mix the reactor (Corrêa et al., 2016a; Hernández-beltrán and Hernández-escoto, 2018). Table 3.2 presents the main cited publications that investigate fed-batch strategies for enzymatic hydrolysis of lignocellulosic biomass.

The analysis of Table 3.2 brings important discussing points.

First point is the wide range of conversions obtained by the several works presented. Calculating cellulose conversion seems straightforward, most papers calculate it by subtracting the fraction of hydrolyzed substrate, calculated stoichiometrically from the products, from the initial substrate concentration.

This methodology assumes; a constant slurry density; that the volume of liquid is equal to the total slurry; that the volume of liquid remains unchanged in the reactor. All of these can be altered during hydrolysis. And with the increase of solids, the deviations from this characteristics are further increased (Zhu et al., 2011). Thus, even though important, the conversion data should be interpreted carefully.

Table 3.2 also demonstrates how modeling of fed-batch processes usually involves altering a previous batch generated model to fit the fed-batch assay. This seems trivial, since during batches the kinetic parameters are more easily predicted, and these models can be used in fed-batch processes by alternating the systems mass balances. However, this is not straightforward for high solids enzymatic hydrolysis. The kinetic model may not hold when the new substrate feeding policy is introduced.

Previously unforeseen phenomena can arise with the addition of fresh solids. The work of Chandra et al. (2011), for instance, demonstrated that at low enzyme loadings (5 FPU.g<sub>Cellulose</sub><sup>-1</sup>) the cocktail appeared to irreversibly bound in a non-productive way to inactive solids, this behavior was accessed via free protein analysis during hydrolysis. This can demonstrate that even though two processes amount to the same substrate concentrations, their performances can differ, furthermore, it is reasonable to assume that addition of fresh enzymatic complex is as important as solids feeding.



**Table 3.2** Fed-Batch Lignocellulosic Biomass Enzymatic Hydrolysis Literature Review

Publication	Feeding Variable	Addition Control Policy	Kinetic Model	Principal Results and Conclusions	Cellulose Conversion
Rosgaard et al. (2007)	Solids Enzyme	Empirical discrete addition	No model fitting	Conversions with batch policies superior than with fed-batch; Viscosity in fed-batch lower	83.3 %
Hodge et al. (2009)	Solids Enzyme	Optimum control profile to maintain 15% solids; Discrete addition	Previously fitted Langmuir-type kinetic model (Kadam et al., 2004)	Controlled fed-batch reached batch conversion with 25% solids; High retention time (300 h)	82.0 %
Morales-Rodríguez et al. (2010)	Solids Enzyme	Simulation of Proportional-Integral control used with different controlled variables	Re-calibration of Langmuir-type kinetic model (Kadam et al., 2004)	No validation essay performed; Reduction of 107% in Enzyme Addition	88.9 %
Chandra et al. (2011)	Solids	Empirical discrete addition	No model fitting	Irreversible cellulase binding; Batch conversion superior to fed-batch	66.0 %
Yang et al. (2011)	Solids Enzyme	Empirical discrete addition	No model fitting	Fed-batch policy improved conversion and retention time over batch process	85.1%
Gupta et al. (2012)	Solids Enzyme	Open loop simulation of different feeding; Validation with discrete feeding	First order kinetic model fitted with batch assay data	Experimental fed-Batch conversion superior to batch	63.5%
Wang et al. (2012)	Solids Enzyme	Empirical discrete addition	No model fitting	Conversion superior with lower solids concentrations; Fed-batch policy superior over batch	68.6 %
Zhang et al. (2012)	Solids	Empirical discrete addition	No model fitting	High product concentrations; Conversion decreased with final solids addition.	50.8 %

**Table 3.2** Fed-Batch Lignocellulosic Biomass Enzymatic Hydrolysis Literature Review - Continued

Publication	Feeding Variable	Addition Control Policy	Kinetic Model	Principal Results and Conclusions	Cellulose Conversion
Cavalcanti-montaño et al. (2013)	Solids Enzyme	Optimal control to maximize product and conversion; Empirical control to maintain rates; Discrete feeding	Michaelis-Menten kinetic model fitted with batch assay data	200 g.L <sup>-1</sup> experimental glucose concentration; Simulation of successive batches show process economy improvement	66,4 %
Tai et al. (2015)	Solids Enzyme	Optimal control to maximize product and conversion with automated feeding	Previously established Epidemic Based kinetic model (Tai et al., 2014)	Experimental fed-Batch conversion superior to batch;	72.1%
Corrêa et al. (2016a)	Solids Enzyme	Empirical discrete addition	No model fitting	Fed-batch conversion superior to batch; Fed-batch strategies improved power requirement	52.0%
Eko et al. (2016)	Solids Enzyme	Empirical discrete addition	No model fitting	Sequential cocktail feeding improved hydrolysis performance	55,2 %
Sotaniemi et al. (2016)	Solids	Empirical discrete addition; Open loop to maintain power	No model fitting	Fed-batch strategies improved power requirement	49.0%
Tervasmäki et al. (2017)	Solids	Empirical discrete addition; Addition schedule to maintain stirring power constant	Langmuir-type model discretized between an initial adsorption and an adsorption model with inhibitions	Model separation improved prediction; Adsorption parameters and activity are influenced by conversion	40,0%
Battista et al. (2018)	Solids	Empirical discrete addition	No model fitting	Fed-batch strategies improved power requirement	20.2%
Ren and Zhang (2018)	Solids	Empirical discrete addition	No model fitting	Experimental fed-batch conversion superior to batch	83.0%

**Source:** Literature review, sources within the table.

The improvement of performance when enzyme is added throughout the process statement is supported by the works of Corrêa et al. (2016) and Eko et al. (2016), where feeding policies with addition of fresh solids and enzyme cocktail obtained conversions better than the same solids addition with the total amount of cocktail added in the beginning of the process.

From the 6 presented papers that either did model fitting, or used a model in some manner, only one had a dedicated structure to deal with fed-batch operation, the rest were either modified, re-calibrated parameters or used without any alteration batch reaction rates to simulate fitting profiles.

Tervasmäki et al. (2017) used a Langmuir-type adsorption kinetic model to describe both batch and fed-batch operations in the same model. However, to do so, the model was discretized between initial kinetics, where only the adsorption phenomena are occurring in a significant rate, and a complete model, where the initial kinetics are coupled to terms describing decrease in enzyme adsorption and activity and product competitive inhibition.

This structure performed well not only for Tervasmäki's and collaborators data, but also to other literature data analyzed by these authors. This demonstrates that a single model may be insufficient to represent hydrolysis data, and some manner of discretization and interpolation between models may be needed to describe different operation policies.

However, from all the studies containing modeling, only Morales-Rodríguez et al. (2010), considered cellobiose as a state variable, and none used hemicellulose or its products in the process description. It is clear then that several advances are still needed in fed-batch modeling until a definitive strategy is created. Specially if the model is to be used in monitoring and control, where high extrapolation capacities are necessary.

Concurrently, with advances in fed-batch technology, and the establishment of better performance over batch operations, authors began to focus in the energy required to agitate the reactor. In this subject the advantages of fed-batch were overwhelming over batch operation.

Sotaniemi et al. (2016) based the feeding scheduling to minimize power requirements. The methodology was successful, diminishing the agitation power necessity to less than 10 W over the more than 20 W for the equivalent batch, while improving conversion, 49% for fed-batch and 38% for batch. The same trend was found in all papers

that evaluated energy efficiency.

However, in the same papers the best conditions obtained for total mixing energy were  $1500 \text{ W.m}^{-3}$  in Corrêa et al. (2016),  $6000 \text{ W.m}^{-3}$  in Sotaniemi et al. (2016) and  $15.000 \text{ W.m}^{-3}$  in Battista et al. (2018). All are above the lower bound of  $100 \text{ W.m}^{-3}$  and upper bound of  $500 \text{ W.m}^{-3}$  for typical volumetric power range for industrial stirred tank reactor (Bouquet and Morin, 2006).

This may indicate that the Stirred Tank Reactor (STR), used in all the described publications, is not the adequate architecture to conduct lignocellulosic material at high solids concentration. A change in the reactor structure is necessary to enable the enzymatic hydrolysis technology inside the biorefinery with low energy requirements.

### 3.6. MODELING ENZYMATIC LIGNOCELLULOSIC BIOMASS HYDROLYSIS

As described, modeling enzymatic lignocellulosic biomass hydrolysis is a grueling task. Specially if the model is composed to describe batches and fed-batches in different conditions simultaneously.

To cope with such complexity, a large number of publications are dedicated to the research of models that can elucidate the saccharification process. Several categories of models have been used to describe the process, a summary of these are presented in Table 3.3.

The analysis of Table 3.3 demonstrates that the model choice must be based in the situation's goal. As the model's phenomenon explanation degree rises, so does its complexity, generating the necessity of more specific data.

The least complex structures are non-mechanistic models. These are not based in any information regarding the reactions and kinetics of the hydrolysis process, and thus, can not elucidate reaction mechanisms (Sousa Jr et al., 2011). Nevertheless, they are useful in initial studies, since they are of easy implementation and use (Bansal et al., 2009).

On the other hand, models designed from the ground up to generate a high level of details can elucidate several underlying phenomena otherwise overlooked. However, some saccharification assays or substrates characterization methods may not provide the detailed level necessary to more complex models. To produce such data, several particular reaction conditions are necessary to decouple masquerading phenomena. These

conditions can be difficult to maintain among replication trials and scale-up (Sousa Jr et al., 2011).

**Table 3.3** Lignocellulosic Hydrolysis Modeling Classification

Model Category	Basis	Properties	Limitations
Non-mechanistic Models	Based on data correlation; No mechanism basis	Good data adherence and easy of use	Little extrapolation capacity; No phenomenon understanding
Semi-mechanistic Models	Based on Enzyme/ Substrate interactions	Enables reactor design; Identification of main mechanism effects	No understanding of reactants features besides concentration
Functionally Based	Based on Enzyme/ Substrate interactions and features	Enables mechanism and substrates changes and types description	Data availability; Model complexity increases rapidly; Hinder reactor and molecular design
Structurally Based	Based on cellulases features	Enables molecular design	Very specific model; Hard development
Fractal Based	Based on jamming effects of spatially confined kinetics	Realistic assumptions generates better adherence	Difficult interpretation; Utility and extrapolation capacity to be determined

**Source:** Adapted from Zhang and Lynd (2004) and (Bansal et al., 2009)

Such is the case for most Functionally and Structurally based models. These contribute greatly to enhance understanding of enzymes and substrate interaction, in particular those that require adsorption, and the substrate itself, since as previously described cellulose is a heterogeneous substrate when considering its reactive sites distribution. However, the very capacity to elucidate secondary kinetics altering phenomena is its hindering point when reactor design and control is considered. Their complexity makes deriving kinetics behavior from then a difficult task, if not, unfeasible (Zhang and Lynd, 2004). The amount of details in these models may not even be significant to the process itself in larger scales. Thus adequate trade-off between available data and model complexity must be observed.

A new approach to deal with this trade-off is the utilization of Fractal Kinetics. These occur in spatially confined reactions, generating apparent rate orders and time-dependent parameters from non-uniform mixing (Kopelman, 1988). Furthermore, these models can be modified to cope with heterogeneous substrate surfaces (Haerifar and Azizian, 2014).

and fractal parameters can be coupled to preexisting classical kinetic models (Bansal et al., 2009). It is easy to acknowledge how similar conditions are found in lignocellulosic material hydrolysis, thus, several studies using this model type have been published (Aguilar et al., 2013; Berry, 2002; Våljamäe et al., 2003; Wang and Feng, 2010; Xu and Ding, 2007; Yao et al., 2011). However, one of the most important point when generating this type of model is describing which reaction rate is limiting, as it is the case with most models. But in fractal kinetics, the time dependency of parameters can make this task more difficult. Thus, significant research is still needed to validate this approach as a robust modeling methodology (Bansal et al., 2009).

A good trade-off between model simplicity and mechanism elucidation, while using a proven modeling methodology, are semi-mechanistic models. These can be based in several assumptions generating different reaction rates equations. Two of the most used in lignocellulosic saccharification, with high solids operations in particular are Michaelis-Menten Kinetics (MMK) and Langmuir-Type Kinetics (LK)

### **3.6.1. Michaelis-Menten Kinetics**

The most popular semi-mechanistic model for lignocellulosic biomass enzymatic hydrolysis are Michaelis-Menten models. These are derived from the early works of, arguably, the pioneers of modern enzymology professors Leonor Michaelis Ph.D. and Maud Leonora Menten Ph.D., more precisely their work on the description of the inversion of sucrose catalyzed by a invertase enzyme (Cornish-Bowden, 2013). Since then, their model has been altered and applied to several enzymatic reactions.

MMK are based in mass action laws that are only valid to homogeneous reaction systems, this is not true for lignocellulosic hydrolysis since the substrate is suspended in the reactive media. The excess substrate concentration ( $[S]$ ) to enzyme concentration ( $[E]$ ) condition ( $[S] \gg [E]$ ), necessary to the quasi-steady-state condition, if achieved, is quickly dismissed, since the fraction of glucosidic bounds available to hydrolysis is not high enough to establish the excess. Furthermore, the hydrolysis of cellulose itself is usually described as a one dimensional procedure, since CBHs bind to cellulose and slides through the molecule to search for new reactive sites. (Lynd et al., 2002; Zhang and Lynd, 2004). All of these depart from the assumptions of the MMKs.

Nevertheless, literature has shown that a pseudo-homogenous assumption for the biomass as soluble substrate and using MMK usual formulation is sufficient to model

lignocellulosic material hydrolysis (Bezerra and Dias, 2004). This is a Pseudo-homogenous Michaelis-Menten (PMM) and does not differ from the classical MMK rate equation, presented in Equation 3.1.

$$\alpha_i = \frac{kc_i \cdot [E_i] \cdot [S_i]}{Km_i + [S_i]} \quad \text{Equation 3.1}$$

Where  $\alpha_i$  is the reaction rates ( $\text{g.L}^{-1} \cdot \text{min}^{-1}$ ), where the subscripted "i" denotes the reaction where it is used, the same nomenclature is used in the subsequent variables,  $kc_i$  is turnover kinetic constant ( $\text{min}^{-1}$ ),  $[E_i]$  is enzyme concentrations ( $\text{g.L}^{-1}$ ),  $[S_i]$  is substrate concentrations ( $\text{g.L}^{-1}$ ) and  $Km_i$  is the Michaelis-Menten constant ( $\text{g.L}^{-1}$ ).

Another proposed alteration based on the MMK is using a modification within the model to consider the substrate solid and that the soluble enzyme has to adsorb to the substrate and adsorption sites are rapidly occupied.

This modification is derived from the work of Bailey (1989), where it is first stated that cellulose hydrolysis is slow enough that researchers can not assume an infinitely small enzyme concentrations ( $[S] \gg [E]$ ), and thus, MMK assumptions can not be upheld.

Bailey (1989) proceeds to describe that it is more feasible to use as reaction velocity calculation base the total amount of soluble enzyme in the medium, and not the substrate concentration, as it is the case for the classical MMK convention. This is feasible since for a given amount of solid substrate, the initial velocity increases with total enzyme concentration growth until a saturation point. Thus, the new underlying assumption is that in the steady-state it is the free enzyme concentration that is in excess over substrate ( $[E] \gg [S]$ ), Equation 3.1 is then modified to its new modified form presented in Equation 3.2.

$$\alpha_0 = \frac{Ve_{Max} \cdot [E_i] \cdot [S_i]}{Km_i + [E_i]} \quad \text{Equation 3.2}$$

Where  $\alpha_0$  is the initial reaction rate ( $\text{g.L}^{-1} \cdot \text{min}^{-1}$ ),  $Km_i$  is the Michaelis-Menten constant ( $\text{g.L}^{-1}$ ) but has a different physical meaning, is the half enzyme saturation constant and  $Ve_{Max}$  is the maximum initial velocity ( $\text{g.L}^{-1} \cdot \text{s}^{-1}$ ) for the Modified Michaelis-Menten (MMM) model. The modified structure has been proven to enhance initial rate prediction in lignocellulosic biomass hydrolysis (Carrillo et al., 2005).

To enable the utilization of the MMM with data from the entire assay, and not only with initial reaction rates, two other assumptions are added, first is that the adsorption sites

change with the saccharification progress, according to Equation 3.3 and that the amount of bounded enzyme ( $[Eb_i]$ ) is far lower than the free enzyme ( $[Ef_i]$ ) in the solution ( $[Ef_i] \gg [Eb_i]$ ) (Carvalho et al., 2013).

$$[S_i] = [S_{i0}] - [P_i] \quad \text{Equation 3.3}$$

Where  $[S_i]$  is the available substrate concentration ( $\text{g.L}^{-1}$ ),  $[S_{i0}]$  is the initial substrate concentration ( $\text{g.L}^{-1}$ ), and  $[P_i]$  is the reaction product concentration ( $\text{g.L}^{-1}$ ). With these alterations Equation 3.2 is modified into Equation 3.4.

$$\alpha_i = \frac{kc_i \cdot [E_i] \cdot [S_i]}{Km_i + [E_i]} \quad \text{Equation 3.4}$$

Both models are showed to be able of fitting hydrolysis data. However, they do not account for inhibitions present in the process. Literature has shown that utilizing a PMM or MMM with product competitive inhibition improved both models performance (Bezerra and Dias, 2004; Carvalho et al., 2013). Thus Equation 3.1 is modified to Equation 3.5.

$$\alpha_i = \frac{kc_i \cdot [E_i] \cdot [S_i]}{Km_i \cdot \left(1 + \frac{[P_i]}{Kp_i}\right) + [S_i]} \quad \text{Equation 3.5}$$

Where  $Kp_i$  is the product competitive inhibition constant ( $\text{g.L}^{-1}$ ). The same addition can be applied to Equation 3.4 to generate a modified MMM with product inhibition, presented in Equation 3.6.

$$\alpha_i = \frac{kc_i \cdot [E_i] \cdot [S_i]}{Km_i \cdot \left(1 + \frac{[P_i]}{Kp_i}\right) + [E_i]} \quad \text{Equation 3.6}$$

### 3.6.2. Langmuir Type Kinetics

Kinetics based on Langmuir adsorption isotherm are another way to incorporate adsorption kinetics into lignocellulosic biomass hydrolysis.

This type of model has been adapted to cellulose hydrolysis since the late nineteen seventies (Huang, 1975). Many derivations of this model class have been proposed to contemplate different lignocellulosic materials and assay conditions. Perhaps one of the most popular and cited versions of the LK is the one presented by Kadam et al. (Kadam et al., 2004), the Langmuir-type isotherm used in this paper is presented in Equation 3.7.

$$[Eb_i] = \frac{Em_i \cdot Kad_i \cdot [Ef_i] \cdot [S_i]}{1 + Kad_i \cdot [Ef_i]} \quad \text{Equation 3.7}$$

Where  $Kad_i$  is the dissociation constants for the enzyme adsorption/desorption



reaction ( $\text{g}_{\text{Protein}} \cdot \text{g}_{\text{Substrate}}^{-1}$ ). This was coupled to an enzyme mass balance to account for the different states in which the enzyme presents itself during hydrolysis. This balance is presented by Equation 3.8.

$$[Et_i] = [Ef_i] - [Eb_i] \quad \text{Equation 3.8}$$

Where  $[Et_i]$  is the total enzyme concentration ( $\text{g} \cdot \text{kg}^{-1}$ ).

Kadam et al. (2004) model considers three reactions. The breakdown of cellulose into cellobiose and glucose, as two heterogeneous separate reactions, thus an adsorption isotherm was considered for EG and another for CBH. After that, for both reactions, a first order reaction, with competitive inhibition by glucose, cellobiose and xylose, was assumed in the surface of substrate. The breakdown of cellobiose by bG was modeled by a MM kinetic model with competitive inhibition by glucose and xylose.

The authors also introduced a “substrate reactivity” parameter, related to the amount of substrate that can be hydrolyzed within the system. This is an empirical parameter that correlates to the degree of polymerization of the lignocellulosic material, and to other transport phenomena hindering interactions. Indeed, the degree of polymerization may be considered an important parameter for modeling reaction rates, since different biomasses or pretreatment methods may generate different crystallinity indexes. These directly correlates to the amount of cellulose that is available to the enzymatic complex (Karimi and Taherzadeh, 2016). Thus, using a “reactivity” parameter, or alternatively, evaluating the amount of available substrate, can improve model prediction.

In fact, all these lumping structures and simplifications generated a widely usable and adaptable model. However, some of their underlying assumptions may not hold throughout the entire assays, since significant changes in the reaction media occur during the liquefaction of biomass. For instance, the rheology of the reaction medium may change drastically throughout the process (Samaniuk et al., 2011).

### 3.7. HIGH SOLIDS HYDROLYSIS IN NONCONVENTIONAL ARCHITECTURES

As described previously, a highly optimized fed-batch operation still generates a power consumption beyond of what is generally considered to be suitable for industrial operation.

To deal with this situation, several author's have dedicated efforts to alter STRs in

order to extend the solids concentrations that these can operate while diminishing agitation energy. The most common manner to do such is to alter the reactor mixing system, particularly by altering impellers geometry. The main impeller types used in biomass saccharification are presented in Figure 3.5.

**Figure 3.5** Impellers for High Solids Operation

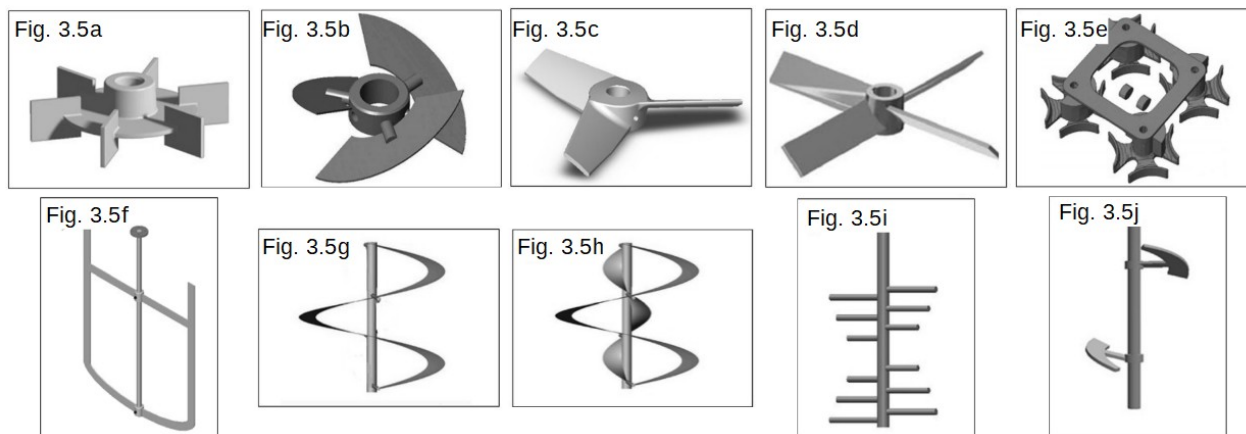


**Figure 3.5a** Rushton impeller; **Figure 3.5b** Elephant Ear impeller; **Figure 3.5c** Triple paddles impeller; **Figure 3.5d** Quadruple paddles impeller; **Figure 3.5e** S shaped impeller; **Figure 3.5f** Anchor impeller; **Figure 3.5g** Helical Ribbon impeller; **Figure 3.5h** Double Helical Ribbon impeller; **Figure 3.5i** Peg impeller; **Figure 3.5j** Segmented Helical impeller.

**Source:** Adapted from Liguori et al. (2015)

The most common impeller in bioreactor is the Rushton type (Figure 3.5a). With this type of impeller, in high apparent viscosity media, stagnated zones are generated, hindering homogenization (Pino et al., 2018). These stagnated zones generation are called Cavern Effect, since only the media adjacent to the impeller is moved, while the media close to the reactor's walls remains still (McCabe et al., 2005). Thus, this impellers are usually changed for other configurations.

Elephant ear impellers (Figure 3.5b) were used with success to increase media homogenization and energetic efficiency during high solids hydrolysis of pretreated sugarcane bagasse (Corrêa et al., 2016b). This configuration also generates an agitation in the axial direction of the reactor in addition to a radial direction, increasing media circulation.

Impellers similar to the previously described are the Triple paddles (Figure 3.5c), Quadruple paddles (Figure 3.5d) and S shaped paddles (Figure 3.5e). These are used in high solids concentrations, but can suffer from the same issues presented by Rushton

impellers (Liguori et al., 2015). The same is true for Elephant ears impellers.

To diminish stagnated zones, specifically designed impellers can be constructed to deal with high solids loadings. These impellers are less susceptible to inefficient mixing since they usually operate in the entire reactor volume (Modenbach and Nokes, 2013). Examples of these impellers are the Anchor (Figure 3.1f), Helical Ribbon (Figure 3.1g), Double Helical Ribbon (Figure 3.1h), Peg (Figure 3.1i) and Segmented Helical (Figure 3.1j) impellers.

However, even when using optimized special impellers, operating in STRs with high solids can still not obtain suitable power consumption. The necessary energy to agitate the hydrolysis reactor can be so large, that can account to more than half the energy contained in the final product (Zhang et al., 2010). This value, as it stands, can prevent the implementation not only of the enzymatic hydrolysis process, but the entire biorefinery.

Therefore, a change in architecture is necessary in this process. A non-conventional design that not only can cope with high solids operation, but also reduce energy consumption is necessary.

Horizontal Reactor (HR) is a type of reactor used in production plants to mix solids and liquids in high viscosity systems using low shear forces. This incentives their use as bioreactors (Wang et al., 2013). In addition, these reactors also demand low energy consumption by usable volume (Dasari et al., 2009).

These reactors can be agitated either by rotating themselves along their longitudinal axis, containing baffles or not, in this cases they are called Rotating Drum reactor, or by using an impeller in the longitudinal axis of the reactor (Liguori et al., 2016).

Studies of biomass saccharification with HR are scarce, specially when compared to the amount of studies in STR and in orbital agitated flasks. The main publications using HR for Independent Hydrolysis (IH), Independent Fermentation (IF) and Simultaneous Saccharification and Fermentation (SSF) of lignocellulosic biomass are presented in Table 3.4.

Table 3.4 demonstrates how researches with this type of reactor are recent, with different structures and operation policies. However, throughout the cited works, HRs improve or matches STRs performances in equivalent operation. This characteristic, together with the expected energy demand improvement, makes this a promising

architecture for the biorefinery hydrolysis stage. This is supported by already operating pilot plants (Jørgensen et al., 2007; Larsen et al., 2012).

**Table 3.4** Publications with Horizontal Reactors for Biofuels Production

Publication	Biomass	Process	Operation	Agitation	Solids	Main Conclusion
Jørgensen et al. (2007)	Wheat straw	IH SSF	Batch	Vertical paddles	2–40%	IH and SSF in pilot scale
Dasari et al. (2009)	Corn stover	IH	Batch	Scraping blades	10–25%	60% glucose conversion
Roche et al. (2009)	Corn stover	IH	Batch	Rotating drum	15–30%	170 g.L <sup>-1</sup> glucose concentration
Larsen et al. (2012)	Wheat straw	IH IF	Batch	Vertical paddles	25–30%	6 h for biomass liquefaction
Salles (2013)	Sugarcane bagasse	IH	Batch Fed-batch	Rotating drum	10%	Conversion in HR better than flasks
Lin et al. (2013)	Sugarcane bagasse	SSF	Batch	Rotating drum	10%	92,2% of total ethanol theoretical yield
Du et al. (2014)	Corn stover	IH	Batch Fed-batch	Rotating drum with paddles	20–25%	Product concentration improved over STR
Pino et al. (2019)	Agave bagasse	IH	Batch Fed-batch	Peg mixer	20–30%	Conversions close to 98%

**Source:** Literature review, sources within the table.

### 3.8. BIOPROCESS MONITORING

With new reactor architectures, and after the reaction process within them is elucidated to a sufficient degree, the next step is applying process control to further improve saccharification performance economy. Modern control techniques, such as optimal control, have been used to improve reactor performance indexes (Cavalcanti-montaña et al., 2013; Fenila and Shastri, 2016; Furlong, 2015; Tai et al., 2015).

However, most efforts in controlling the hydrolysis reactor are not validated, and even more rarely are operated in closed loop. Close loop operations requires the utilization of data feedback to the controller in order to update the controlled variable setpoint. In bioprocesses, feedback is specially difficult since the reaction's products are usually not covered by commercial sensors. Thus, monitoring hardware has to be, frequently, tailor-made to the application where it is used (Vojinovi et al., 2006).

Another scenario is when instrumentation hardware to monitor a desired variable is

unfeasible. This may be the case of biomass saccharification at high solids, the media high viscosity and heterogeneous nature can impede single instrument utilization.

From this situation, new techniques that can compose predictions from several simultaneous measurements and filter the inherent noise in the prediction, have arisen.

Data from established instrumentation from secondary variables can be processed by a soft sensor, a software aided sensor, to predict more complex variables, mainly state variables (Luttmann et al., 2012).

However, the soft sensor may be unable to predict all the state variables involved in the reaction, or the noise from the data can be high, hindering the usage of this data in subsequent stage, mainly the reactor control. A possible alternative to circumvent these issues is to use a State Estimator. State estimation is a type of algorithm that uses a previously established kinetic model with instrumentation data to enhance the state variables prediction, or to estimate variables that are not monitored on-line (Dochain, 2003).

### **3.8.1 Data Driven Soft Sensors**

When the direct instrumentation of a process is unfeasible a soft sensor can be applied. Soft sensor are softwares capable of predicting non-measured process variables from readily available process data (Sagmeister et al., 2013).

Soft sensor performance is closely related to the data from the instrumentation used to generate the prediction, and the support model used to translate the data from the instrumentation to appreciable process variables, usually reactants concentrations. The models used in data driven soft sensor are usually empirical models and several algorithms alternatives are presented in literature (Kadlec et al., 2009).

#### **3.8.1.1. Principal Components and Partial Least Squares Regressions**

Data driven soft sensors are usually generated utilizing several instrumentation sensors running simultaneously inside the reactor, this can lead to an amount of data that needs to be pre-processed in order to reduce the dimensionality of the modeling stage. This is particularly expected with modern spectroscopy hardware, where scans of the entire available spectrum are performed continuously. Thus, a data reduction stage may be necessary.

Two widely used algorithms for this purpose are Principal Components Regression

(PCR) and Partial Least Squares (PLS).

PCR is a methodology to transcribe available data into new domains to reduce dimensionality. The underlying assumption in this methodology is that the data can be describe in terms of linear combinations, new axis can be generated to describe the data with fewer values (Wold et al., 2001).

The generic formulation for a PCR (as presented by Nelles (2001)) is to maximize data variance from a data matrix  $A_{m,n}$  where  $m$  is the number of data points and  $n$  the dimension of the input data, along new separate axis  $\underline{x}_i$ . The new axis is a vector, and has the dimension of the input data, and as many axis as the number of data points can be obtained ( $i=1, \dots, m$ ). A generic axes is presented in Equation 3.9.

$$\underline{x}_i = [x_{i1}, x_{i2}, \dots, x_{in}]_{1,n}^T \quad \text{Equation 3.9}$$

The variance in the new axes is obtained with the square of the projection of  $A$  over  $\underline{x}_i$  ( $A_{m,n} \cdot \underline{x}_i$ ). The axes vector also need to be normalized to prevent infinite solutions to the system ( $\underline{x}_i^T \cdot \underline{x}_i = 1$ ). Thus the constrained optimization problem becomes:

$$(A_{m,n} \cdot \underline{x}_{in,1})_{1,m}^T \cdot (A_{m,n} \cdot \underline{x}_{in,1})_{m,1} + \lambda \cdot (1 - \underline{x}_{in,1}^T \cdot \underline{x}_{in,1}) \rightarrow \max_{\underline{x}_i} \quad \text{Equation 3.10}$$

Where  $\lambda$  is the Lagrangian multiplier for the constraint. The solution of this problem is:

$$(A_{m,n}^T \cdot A_{m,n}) \cdot \underline{x}_{in,1} = \lambda \cdot \underline{x}_{in,1} \quad \text{Equation 3.11}$$

The eigenvectors are the optimal axis, and they are organized by their conjugated eigenvalue, the one with the highest value is the first component and the other are organized in a decreasing manner. The eigenvectors and eigenvalues can be calculated with singular value decomposition.

The components are concatenated column-wise in a matrix  $Q_{n,h}$  where  $h$  are the chosen components to be used in the modeling. The number of regressors ( $h$ ) should be enough to describe the data reasonably, and should be restricted to prevent overtraining. The utilization of a model optimization procedure is advised.

With the appropriate  $Q_{n,h}$ , the projection matrix  $B_{m,h}$  is obtained by projecting  $A_{m,n}$  onto  $Q_{n,h}$ .

$$B_{m,h} = A_{m,n} \cdot Q_{n,h} \quad \text{Equation 3.12}$$

The projection matrix  $B_{m,h}$  is a dimensionally reduced matrix from matrix  $A_{m,n}$ , and can be used in the regression rather than the initial input data matrix.

However, this methodology uses only data from the input independent variables, and the relation between  $A_{m,n}$  and the output data  $Y_{m,l}$ , where  $l$  is the number of predicted variables, is neglected.

A PLS algorithm is similar to the PCA algorithm, however, it uses the data from matrix  $Y_{m,l}$  with  $A_{m,n}$  data to produce the new axis. To do so, if the system is linear, in Equations 3.10 and 3.11 the matrix  $A_{m,n}$  needs to be substituted by the cross-relation matrix  $A_{m,n} \cdot Y_{m,l}$  and the output variable  $x_i$  is substituted by  $y_i$  before the eigenvectors calculation.

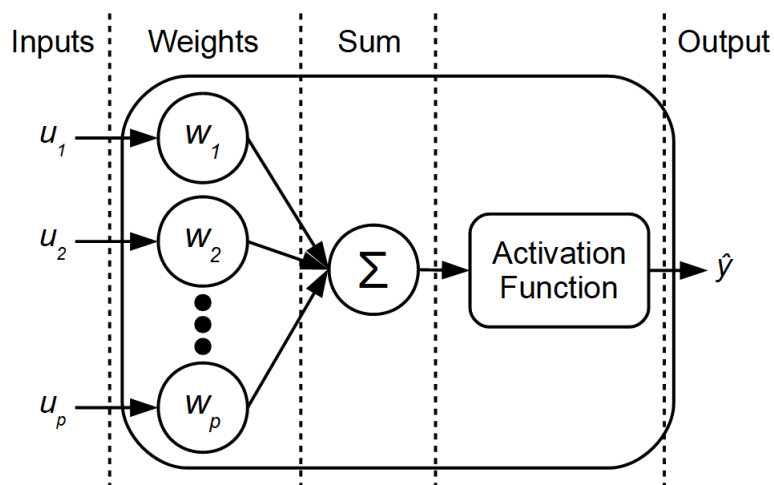
This increases synergy between the input and output data before dimensions decrease and can improve model prediction over PCR (Haaland and Thomas, 1988).

### 3.8.1.2 Neural Networks

Artificial Neural Networks (ANN) are empirical mathematical models based in how the human brain handles information, and are used for pattern recognition. The definition of an ANN varies with the used literature, in this thesis the description used is the one developed by Nelles (2001).

ANNs models are organized as a network of artificial neurons called perceptrons. Figure 3.6 presents a perceptron example.

**Figure 3.6** Perceptron Representation



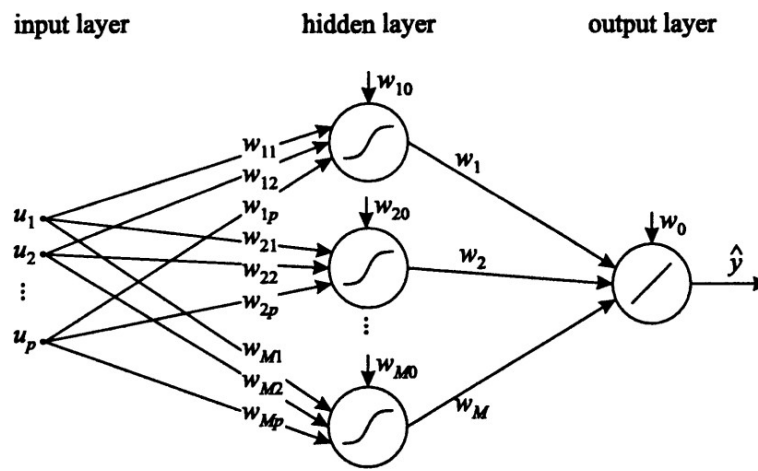
**Source:** Adapted from Nelles (2001)

A perceptron works by first taking input variables vector ( $\underline{u}$ ), projecting it onto nonlinear weights parameters vector ( $\underline{w}$ ) and adding all transformed variables to a scalar vector, this process is called ridge construction. The scalar variable is then transformed by

an activation function to generate a projected output ( $\hat{y}$ ). The weights vector, as well as the parameters inside the activation function can be subjected to optimization to achieve a predicted output that correlates to analytical data (Nelles, 2001).

ANN are networks of independent perceptrons. Several methodologies can be used to connect the perceptrons and generate the network. One that it is important to highlight is the Multilayer Perceptron (MLP) architecture. Figure 3.7 presents an example of this network.

**Figure 3.7** Multilayer Perceptron Network



**Source:** Nelles (2001)

In this architecture several neurons are used in parallel in a same layer, this is the hidden layer. Each neuron receives input data and is connected to a single neuron output neuron. As the input data is provided by analytical data, using only one hidden layer with neurons facilitates the control of the model complexity, i. e., its number of parameters, by adding neurons to the internal layer as needed to improve prediction (Nelles, 2001).

ANNs are used as models for several tasks in second generation biofuels production, from hydrolysis kinetic data modeling (Nikzad et al., 2012), substrate enzymatic digestibility prediction from composition (O'Dwyer et al., 2008), and to monitor and control of ethanol production (Amornchai and Shomchoam, 2009; Xiong and Zhang, 2005).

### 3.8.1.3. Torque Measurement

Torque measurement is an important variable when analyzing the rheometry of a solution or suspension. Usually, torque measurement is done in an off-line, where a sample of the reactive media is conducted to a bench rheometer (Corrêa et al., 2016b;



Scott et al., 2011). In studies that monitor rheometry throughout the process a clear decrease in the torque necessary to agitate the media is observed when the solids in the reactor are hydrolyzed (Palmqvist and Lidén, 2012; Samaniuk et al., 2011), demonstrating that this measurement can be used to monitor the reactor in some capacity

More recently, this was realized with biomass hydrolysis to some success. However, data from the instrumentation retains high inherent noise, and no filtering or state estimation methodology was used (Jawad et al., 2019), thus several improvements can be achieved with data processing improvement.

#### 3.8.1.4. Visible and Ultra Violet Spectroscopy

An analytical inline system, capable of analyzing the supernatant optical properties, alongside the hydrolysis reactor can uncover new behaviors in the hydrolysis kinetics. Specially the kinetics of inhibitors within the reactor.

This is supported by the fact that lignin absorbs electromagnetic radiation strongly in the ultraviolet region, and some methodologies use this characteristic in order to ascertain lignin content in the biomass (Gouveia et al., 2009; Kline et al., 2010; Sluiter et al., 2012).

#### 3.8.1.5. Near Infrared Spectroscopy

In the same field of spectroscopy data is Near Infrared Spectroscopy (NIR). This technology is used in a much broader range of reactants determinations. Both in offline methodologies (Rambla et al., 1997; Ribeiro et al., 2008; Xie et al., 2009), and online operation (Dodds and Heath, 2005). These studies also point out the diversity of compounds that can be analyzed by NIR, carbohydrates, proteins and antibiotics.

Furthermore, this technology has been proved to suit bioprocesses containing biomass (Rodríguez-zúñiga et al., 2014). However, few measurements are realized online. Nevertheless, the high adaptability of this equipment to several molecules motivates its use in biomass hydrolysis (Skvaril et al., 2017).

#### 3.8.1.6. Conductance/Capacitance Spectroscopy

Conductance and Capacitance Spectroscopy is the generation of alternating electrical fields in the reactive media inside the reactor with varying frequencies, some groups of molecules are polarized by this field. The polarization changes the dielectric constant of the media. This can be measured as variations in the conductance, the

capacity of the media to allow an electrical current to travel inside itself, and permittivity, the capacity of a media to maintain an electromagnetic field (Vojinovi et al., 2006).

This sort of measurement has been used in order to monitor lignocellulosic material hydrolysis (Bryant et al., 2013), in which a linear correspondence between the capacitance and the reduction of solids inside the reactor was found.

Therefore, an instrument of this sort can be used to aide in the reactor monitoring as a standalone instrument or as an input to the soft sensor layer.

### 3.8.2. State Estimation

Coupling untreated measurements or soft sensor predictions to a state estimator can increase state estimation precision. State observers are algorithm used to estimate state variables that are not direct measured, either by lack of instrumentation or sensor high price, or to diminish estimation error in the measured variables (Mohd et al., 2015).

Several observers can be used and have been described, one of the most used is a Moving Horizon Estimator (MHE). This sort of algorithm uses a dynamic window and optimization steps to predict the desired state variables, based on both measurements and model data.

MHE are very well established as state estimators for chemical processes because they can deal with the nonlinear dynamics and state constraints, inherent to most bioprocesses systems, in a fairly straightforward manner (Haseltine and Rawlings, 2005).

The moving horizon estimator is a modification of the full information estimator in order to diminish the total number of parameters to be optimized with a moving estimation window. The cost function of the optimization problem is presented to Equation 3.13.

$$\min_{X(T-N:T)} = V_{T-N}(X(T-N)) + \sum_{j=T-N}^{T-1} L_w(\hat{X} - X^-) + \sum_{j=T-N}^T L_v(\hat{Y} - Y) \quad \text{Equation 3.13}$$

Where  $N$  is the size of the estimation windows,  $V_{T-N}$  is the arrival cost, representing the information in the previous prediction window,  $X$  is the state variable,  $\hat{X}$  is the predicted state variable,  $X^-$  and is the modeled state variable,  $\hat{Y}$  is the predicted measurement,  $Y$  is the instrumentation measurement,  $L_w$  and  $L_v$  are the filtering weights for the model prediction and the measurement prediction, respectively. By correctly tuning the filter weights, the moving horizon can estimate the current value of a given state variable.

## 4. MATERIALS AND METHODS

The materials and methodologies described in this chapter are used in the following chapters. Which methodologies are used in a particular chapter, and previously not described special methodologies, are described within it.

### 4.1. LIGNOCELLULOSIC BIOMASS

Sugarcane bagasse was used as lignocellulosic material, it was pretreated in two different manners, steam-explosion and hydrothermal pretreatments.

The hydrothermally pretreated bagasse was obtained from bagasse donated by Usina Ipiranga S/A (Descalvado, SP). The pretreatment was carried out in pressurized reactor, with a maximum pressure of 200 psi, at 200 RPM. The reactor was loaded with 0.010 grams of dry bagasse per milliliter of reactor media. The reactor heating element was then programmed to reach 195°C and hold this temperature for 10 min. After the pretreatment, the bagasse was placed in a sleeve cloth filter and washed with distilled water for 2 h. The pretreated bagasse was, then, dried in kiln for 24h at 60°C, reaching a humidity of approximately 5 %.

The steam-exploded bagasse (1667 kPa and 205 °C for 20 min) was provided by the Centro de Tecnologia Canavieira (CTC, Piracicaba, São Paulo, Brazil).

The pretreated bagasse composition was determined in previous researches via literature established methodology (Gouveia et al., 2009). Their main components are presented in Table 4.1.

**Table 4.1** Pretreated Bagasses Compositions

Bagasse	Cellulose	Hemicellulose	Lignin	Ash
Hydrothermal	60.1±0.2 %	4.76±0.5 %	27.3±0.3 %	1.1±0.1%
Steam-explosion	43.1±0.1%	12.4±0.1 %	28.8±1.9%	4.7±0.1%

Values in the table are average of triplicates and followed by the distribution standard deviation (Average±Standard Deviation).

**Source:** Previously established experimental data.

These data were used to in calculations when needed.

### 4.2. ENZYMATIC HYDROLYSIS

The biomass was hydrolyzed under different operating policies and reactors. Each condition are presented in its pertinent chapter, as well as the reactor architecture. All

enzymatic hydrolysis were carried with enzymatic complex CELIC CTEC 2, donated by Novozymes Latin America (Araucária, Paraná, Brazil), and the hydrolysis media was citrate buffer with pH 4.80 and ionic force of 50 mM.

### 4.3. CARBOHYDRATES DETERMINATION

Glucose, cellobiose and xylose were the soluble products quantified in the hydrolysis liquid phase samples. The analysis was performed through High-Performance Liquid Chromatography (HPLC) methodology as described by Sluiter et al. (2008). These were analyzed in a Shimadzu SCL-10A chromatograph, with refraction index detector RID10-A, column Animex HPX-87H Bio-rad, mobile phase sulfuric acid 5 mM at 0.6 mL.min<sup>-1</sup>.

Calibration curves of each compounds were constructed to calibrate linear models between the standard concentration and a peak area in a given retention time, determined in the pure standard injection. Glucose standard ranged from 0.5 to 15.0 g.L<sup>-1</sup>, cellobiose from 0.2 to 2.0 g.L<sup>-1</sup> and xylose from 0.5 to 8 g.L<sup>-1</sup>. All samples were suspended in the buffer used in the reaction.

A curve validation standard was also generated by mixing all carbohydrates standards with concentrations in the midpoint of their ranges. This solution is used to evaluate both the analysis in itself, as well as the linear model prediction.

These curves were used to estimate concentration of two groups of carbohydrates in the hydrolysis, free and potential carbohydrates.

“Free” carbohydrates are those hydrolyzed by enzymes in the process, i. e., those in the reactive media when the sample was withdrawn, the potential carbohydrates are the sum of free and those still binded to other molecules, i. e., still polymerized.

The term free in this analysis denotes that no further hydrolysis procedure was applied to the sample. Thus, even though cellobiose is a polymer, it is considered to be free in the solution, due to its small size. Any carbohydrates larger than 2 glucose units is considered polymerized, and are part of the potential concentration. The same liquid sample is quantified for its free and potential carbohydrates.

#### 4.3.1. Free Carbohydrates Analysis

Free carbohydrates were quantified by injecting the raw liquid fraction from the sample. Before each injection, samples and standards were filtered through 0.22 µm

hydrophilic polyvinylidene fluoride filter and injections were performed in triplicate. This generated three separated curves, one for each analyzed carbohydrate, and these were used to quantify their concentration in the process samples.

#### **4.3.2. Potential Carbohydrates Analysis**

To obtain the potential carbohydrates concentrations, 200  $\mu\text{L}$  of the free sample was combined with 50  $\mu\text{L}$  of fresh enzymatic cocktail and 1.5 mL of distilled water. This mixture was then incubated at 50  $^{\circ}\text{C}$  for 6h. After this period, the samples were placed in boiling water for 10 min to denature enzymes and stop the reaction. These were then filtered through 0.22  $\mu\text{m}$  hydrophilic polyvinylidene fluoride filter and injected in the chromatograph.

This procedure was applied to both the samples and standards, apart from cellobiose calibration standards. Cellobiose was not quantified after the analytic depolymerization stage since it is considered that it would be broken into glucose, and thus, is already quantified by the potential glucose concentration.

Thus, two calibration curves were generated, one for potential glucose and one for potential xylose. These were used only to quantify depolymerized samples.

It is important to highlight that other methodologies can be used to determine soluble polymers, specially when using other HPLC columns and detectors. However, this methodology can be a useful indication of these polymers when the mentioned hardware is not available.

#### **4.4. ENZYME ACTIVITY ANALYSIS**

Enzymatic cocktail activity is determined with a modification of the procedure delineated in the guidelines of the International Union of Pure and Applied Chemistry, as described by Adney and Baker (2008) which is itself a modification of the methodology proposed by Ghose (1987). The method is used to ascertain the Filter Paper Units (FPU) per mL of enzymatic complex.

One FPU unit is the amount of enzyme necessary to generate 2 mg of glucose from 50 mg of Whatman<sup>®</sup> Number 1 filter paper (4% conversion) in 60 min at 50  $^{\circ}\text{C}$ .

The reasoning behind this methodology is that several enzymes are involved in the reaction and the reactions are complex, resulting in a non-linear production rate. Using an activity unit in the International Unit (IU,  $\mu\text{Mol}\cdot\text{min}^{-1}$ ) based in product formation for initial

rates over small time periods would hinder comparison between different cocktails. The activity of cellulase cocktails should be instead based on a, relatively, large conversion of a standard substrate over long periods of time (Ghose, 1987). To do so, several dilutions of the initial cocktail are prepared. The dilutions are combined with a strip of Whatman® Number 1 filter paper cut in a rectangular shape that amounts to 50 mg (roughly a rectangle of 6 cm by 1 cm), and citrate buffer. Samples containing; each dilution of the cocktail and citrate buffer (enzyme control assays), filter paper and buffer (paper control assay); citrate buffer (blank assay) are also prepared. A glucose standard calibration curve is also prepared.

All samples, controls and blank assays are incubated for 60 min at 50 °C. At the end of the incubation period, dinitrosalicylic acid color development reagent is added. The reagent is part of the methodology proposed by Miller (1959) and is used to quantify reducing sugar (carbohydrate molecules with at least one reducing end) in solutions. The tubes with the acid solution are boiled for 5 minutes for color development. The solutions are then diluted with water, and the absorbance at 540 nm of all tubes are measured.

With the glucose standard curve, a linear model between absorbance at 540 nm and reducing sugar concentration is constructed. With the model, reducing sugar concentrations are determined in all the assays, controls and blanks. The effect of the controls and blanks are subtracted from the enzyme dilutions. An interpolation is carried with the logarithmic transformed enzyme concentrations (inverse of the dilution) to predict the concentration that relizes 2 mg of sugars in these conditions, the Critical Enzyme Concentration ( $\text{mL}_{\text{Enzyme}} \cdot \text{mL}_{\text{Solution}}^{-1}$ ). The FPU is then determined by the Equation 4.1.

$$FPU = \frac{0.37}{\text{Critical Enzyme Concentration}} \quad \text{Equation 4.1}$$

The value 0.37 in the numerator of the right hand side of Equation 4.1 is the derivation of FPU unit. It is generated by altering the international unit for enzyme activities. 2 mg of reducing sugar converted to mols is 0.18  $\mu\text{Mol}$ , when using glucose as calculation basis, this is produced by 0.5 mL, the enzyme volume in the assay, over 60 min, generating 0.37  $\mu\text{Mol} \cdot \text{mL}^{-1} \cdot \text{min}^{-1}$ . Even though the dimensional analysis shows that the FPU should have a time component in its denominator, as previously described, Ghose (1987) argues that it should be suppressed, and thus, the cellulase activity is  $\text{FPU} \cdot \text{mL}^{-1}$ .

#### **4.4.1. Modified FPU Assay for Cocktail**

This work uses a minimization of the original FPU assay, validated by the author (unpublished data). In the original methodology, 0.5 mL of enzymatic cocktail dilutions is used to hydrolyze the filter paper, and 1.5 mL of buffer are added, these quantities were also used in the modified method. The incubation time and temperature were also the same as the original proposal. The modifications were performed in the carbohydrate analysis. Standards of glucose were used in the same range as the one in item 4.3, five concentrations equally distributed from 0.5 to 15 g.L<sup>-1</sup>.

The original method used 3.0 mL of color generating reagent added to the tubes containing the samples, and after incubation, 0.2 mL of sample were diluted in 2.5 mL of water. The modification was in another vessel, combine 0.1 mL of the hydrolysis assay with 0.3 mL of color generating reagent, incubating for the same period as the original description, 10 min at 100 °C, and diluting the mixture with 1.5 mL of water. This modification proved to generate the same results as the original methodology, and was applied to the cocktail used in the hydrolysis assays.

#### **4.4.2. Free Cellulase Activity**

A separate methodology was generated following the principle of the FPU determination methodology and was used to determine cellulase activity in the liquid phase. When the liquid phase cellulase activity was desired, 3 mL of solution were sampled. Half was placed in a vessel containing the same filter paper used in the FPU assay (activity assay). The other half was placed in an empty vessel (control assay). These were incubated following the FPU methodology, for 60 min at 50 °C. After the incubation, the modified reducing sugars method was applied to the samples, and the reducing sugars concentration after incubation was determined with previously established calibration curves.

The control assay reducing sugar concentration was subtracted from the activity assay. This procedure ensures that the hydrolysis of polymers already in the sample, that were going to be hydrolyzed in the reactor, would not interfere in the activity determination. The treated value is divided by the vessel volume (1.5 mL) to generate the Free Cellulase Activity (FCA, mg<sub>Reducing Sugar</sub>·mL<sup>-1</sup>·min<sup>-1</sup>).

## 5. HYDROLYSIS FUZZY-ENHANCED MODELING IN STIRRED TANK REACTOR

### 5.1 MOTIVATION AND OBJECTIVE

As previously described, several models have been proposed to describe biomass saccharification in high solids operations. However, the models may not fully describe the system behavior change during the whole long-term process (in fed-batch operation, for instance). Yet, adding complexity to the model, by acknowledging other effects during its mathematical formulation, by using structurally or functionality, or adding these features to semi-mechanistic models, will demand more parameters, which, can be very correlated when estimated from the same empirical data. As a result, the parameters frequently loose physical meaning.

An alternative approach is using a simpler structure, with fewer parameters fitted in different regions. These regions can be obtained by using feeding policies where all the substrate is added prior to enzymes addition, generating a high solids content at the beginning, or a more liquefied medium with, generated by scattered solids feeding, and using as model an interpolation between the models fitted in other solids concentrations. Another alternative is using different models in the same process. Some authors proposed to separate the process into two separate dynamics, liquefaction, when the solids concentration is very high in the slurry and saccharification reactors/reactions, when most of the substrate has been liquefied (Liu et al., 2015). This methodology is fairly straightforward for a batch reactor. However, during a fed-batch process liquefaction and saccharification occur simultaneously, since new solid material is added throughout the process. This is probably the reason for the lack of fit when model predictions are extrapolated to operational conditions different to those used for parameter fitting.

This chapter proposes to include a model layer that can smoothly drive the model switches. This idea comes from the previously described fact that the hydrolysis process goes through different stages of liquefaction of the biomass. Besides, when fresh material is fed to the reactor, two mechanisms may co-exist: one driven by the enzymatic attack of the solid by the enzymes, and the other reflecting the fact that part of the substrate present in the reactor has already been, at least partially, hydrolyzed. Therefore, only one simple class of model may not be sufficient to describe the reaction kinetics. Using computational intelligence, different classes of models can be combined in certain regions where no clear mechanism prevails. Instead of just an on-off shifting between kinetic models, their action



will be combined.

To guarantee a smooth transition between models, a Takagi-Sugeno (TS) fuzzy system was implemented. The TS fuzzy model may be composed by several models, all connected via a set of fuzzy membership rules. In other words, each model represents part of the system behavior and the degree of membership varies with a set of established rules (Al-hadithi et al., 2012). Fuzzy logic has been shown to improve the estimation of lignocellulosic material in a hydrolysis process with different combinations of substrates in a robust and reliable manner (Suarez et al., 2014).

Moreover, using a fuzzy logic addendum to the kinetic model can improve the model extrapolation capability. A consortium of models, coordinated by the fuzzy logic layer, can increase the overall robustness of the predictions, spanning regions of the state variables regions that were not used to fit each model of the consortium. This approach may be useful for a system that undergoes drastic physical transformations along process time.

In short, we propose a methodology where simple models may describe the behavior of the enzymatic hydrolysis of sugarcane bagasse in reactors under batch and fed-batch operation. Initially, semi-mechanistic Michaelis-Menten and Langmuir-based models were evaluated as a basis to predict batch and fed-batch data. When the utilization of only one model is not enough accurate, a novel modeling methodology enters into action: a consortium of simplified kinetic models coupled to a fuzzy logic membership rule, which combine the responses of the simple standalone models.

## 5.2 MATERIALS AND METHODS

### 5.2.1 Hydrolysis Assays

Different feeding policies of solids were evaluated. Enzymatic complex was CELIC CTEC 2 and lignocellulosic substrate was steam-exploded sugarcane bagasse. The assays were conducted in duplicates in a 3 L working volume stirred reactor with two elephant ear impellers, the one in the top of the axle generating a flow downward, and the one in the bottom generating flow upward, at 50°C and 470 RPM. Manual sampling was performed at 0.5, 1, 2, 4, 6, 8, 12, 24, 36, 48, 60, 72 and 96 h and supernatant free carbohydrates were determined.

Three feeding profiles were assessed. A High Solids Batch (HSB) process, Assay 1, where 200 g.L<sup>-1</sup> of substrate and 3.7 mg<sub>protein</sub>.g<sub>substrate</sub><sup>-1</sup> (approximately 10 FPU.g<sub>substrate</sub><sup>-1</sup>) of

enzymatic complex were added in the beginning of the process. And two fed-batches, where the feeding profiles amounted to the same substrate mass as the batch process. However, the lignocellulosic material was distributed in four discrete feeding times, with different addition times. These feeding profiles generated two assay conditions a Low Solids Fed-Batch (LSF) and a Mixed Profile Fed-Batch (MPF). Table 5.1 presents the three assays feeding profiles.

**Table 5.1** Assay Feeding Profiles

Fitting Assays						Validation Assays		
Assay 1 – High Solids Batch			Assay 2 – Low Solids Fed-Batch			Assay 3 – Mixed Profile Fed-Batch		
Feeding Time (h)	Solids Feeding (g.L <sup>-1</sup> )	Enzyme Feeding (mg.g <sup>-1</sup> )	Feeding Time (h)	Solids Feeding (g.L <sup>-1</sup> )	Enzyme Feeding (mg.g <sup>-1</sup> )	Feeding Time (h)	Solids Feeding (g.L <sup>-1</sup> )	Enzyme Feeding (mg.g <sup>-1</sup> )
0	200	3.70	0	50	3.70	0	50	3.70
-	-	-	2	50	-	0,5	50	-
-	-	-	12	50	-	1	50	-
-	-	-	24	50	-	2	50	-

**Source:** Author's library

The first two assays (Fitting Assays) were used for model fitting, and the third one was the Validation Assay, used to check models' prediction capacity.

## 5.2.2 Mathematical Modeling

### 5.2.2.1 Process Modeling

Six reactions were considered.

Reaction 1: Cellulose  $\rightarrow \gamma_{Cel-Ceb}$  Cellobiose

Reaction 2: Cellulose  $\rightarrow \gamma_{Cel-Glu}$  Glucose

Reaction 3: Cellobiose  $\rightarrow \gamma_{Ceb-Gli}$  Glucose

Reaction 4: Hemicellulose  $\rightarrow \gamma_{He-Xyl}$  Xylose

Reaction 5: Lignin  $\rightarrow$  Lignin

Reaction 6: Enzyme  $\rightarrow$  Inactive Enzyme

In the reaction scheme,  $\gamma$  are the pseudo-stoichiometric mass relations between substrates and products for each reaction. The values used for these parameters were:

$\gamma_{Cel-Ceb} = 1.056 \text{ g}_{\text{Cellobiose}} \cdot \text{g}_{\text{Cellulose}}^{-1}$  (Kadam et al., 2004),  $\gamma_{Cel-Glu} = 1.111 \text{ g}_{\text{Glucose}} \cdot \text{g}_{\text{Cellulose}}^{-1}$  (Kadam et al., 2004),  $\gamma_{Ceb-Gli} = 1.056 \text{ g}_{\text{Glucose}} \cdot \text{g}_{\text{Cellobiose}}^{-1}$  (Kadam et al., 2004),  $\gamma_{He-Xyl} = 0.841 \text{ g}_{\text{Xylose}} \cdot \text{g}_{\text{Hemicellulose}}^{-1}$  (Yao et al., 2015).

Throughout the modeling stages reactions 1, 2 and 4 are considered to be heterogeneous, since they represent the breakdown of cellulose (reactions 1 and 2) and hemicellulose (Reaction 4). Both substrates are solids that are hydrolyzed into soluble sugars.

The hydrolysis of cellobiose into glucose (Reaction 3) is considered to be homogeneous, since cellobiose has a solubility far superior than the cellulose polymers.

Reaction 5 is included, despite lignin is an inert. Thus, this “reaction” just reflects the accumulation of lignin in the reactor when it operates in fed-batch mode.

As previously described, several effects are responsible for enzyme inactivation and inhibition. Here, Reaction 6 represents a generic inactivation of the enzymatic complex. Using such a simple mechanism may not fully elucidate how the several effects affect each enzyme during hydrolysis. However, the underlying idea is to use as few parameters as possible, while retaining a robust model.

Mass balances for the components in the reactor are in Equation 5.1, following the formalism proposed by Bastin and Dochain (1990). Since feeding was accomplished discretely, the addition of substrate was calculated outside the model integration. In other words, when substrate addition was performed, the integration was re-initialized with proper initial conditions. Thus, the total mass balance of the system became a sequence of batch processes.

$$\frac{d}{dt} \cdot \begin{bmatrix} Cl \\ Cb \\ Gl \\ He \\ Xy \\ Lg \\ E \end{bmatrix}_{7 \times 1} = \begin{bmatrix} -1 & -1 & 0 & 0 & 0 & 0 \\ Y_{Cel-Ceb} & 0 & -1 & 0 & 0 & 0 \\ 0 & Y_{Cel-Gli} & Y_{Ceb-Gli} & 0 & 0 & 0 \\ 0 & 0 & 0 & -1 & 0 & 0 \\ 0 & 0 & 0 & Y_{He-Xi} & 0 & 0 \\ 0 & 0 & 0 & 0 & 0 & 0 \\ 0 & 0 & 0 & 0 & 0 & -1 \end{bmatrix}_{7 \times 6} \cdot \begin{bmatrix} \alpha_1 \\ \alpha_2 \\ \alpha_3 \\ \alpha_4 \\ \alpha_5 \\ \alpha_6 \end{bmatrix}_{6 \times 1} \quad \text{Equation 5.1}$$

The column vector in the right-hand side of the equations are the concentrations of reactive cellulose ( $[Cl]$ ), cellobiose ( $[Cb]$ ), glucose ( $[Gl]$ ), hemicellulose ( $[He]$ ), xylose ( $[Xy]$ ), lignin ( $[Lg]$ ) and enzymatic complex activity ( $[E]$ ). The 7 by 6 matrix at the right-hand side of the equation is the pseudo-stoichiometric matrix and the vector ( $\alpha_i$ ) is the instant

reaction rate calculated with different models.

The first approach, called “standalone reaction rate models”, was based on the previously described models, Michaelis-Menten Kinetic and Langmuir-Type Kinetics, within the conventional implementation, i. e., using one set of parameters to fit the models to all data of training assays (1 and 2) simultaneously, and checking prediction capacity through validation data (Assay 3), not used for parameter estimation. Item 5.2.2.2. describes the models used in this stage. It is important to emphasize that this strategy applies each individual model throughout each complete assay’s experimental data.

The second strategy, called “fuzzy kinetic model”, consists in using the models from the first strategy with best adherence to experimental data, but instead of fitting the two training assays simultaneously, one specific model, with the best fit, was parametrized with data from Assay 1 and another one with data from Assay 2. Following, an optimized TS fuzzy system was implemented, to interpolate between these models, according to the state of the system with respect to the amount of solids inside the reactor. The quality of fit of this consortium of models was checked for both the training and the validation assays. This modeling technique is described in Item 5.2.2.3.

#### 5.2.2.2 Standalone Reaction Rate Models

The kinetic models tested in this chapter are depicted in Table 5.2. Equations 5.2 and 5.3 are Michaelis-Menten based models (equivalent to Equations 3.1 and 3.4 in Item 3.6.1). Equations 5.4 to 5.8 are kinetic models based on the Langmuir adsorption isotherm, as described by Kadam et al. (2004) and extended to hemicellulose hydrolysis (Angarita et al., 2015). The parameters in these equations follow the same units used by Kadam et al. (2004). Equation 5.8 are the equations that described the enzyme adsorption itself (equivalent to Equations 3.7 and 3.8 in Item 3.6.2.), in these equations, a subscribed number in the enzyme concentrations variables denotes the enzymes in that equation, 1 is for is for CBH and EG together, 2 is for bG and 4 is for hemicellulose hydrolyzing enzymes.

**Table 5.2** Addressed Reaction Rates

Model Type	Used in Reaction	Model	Equation Number
Pseudo-Homogeneous Michaelis-Menten with Competitive Product Inhibition	3	$\alpha_i = \frac{k_i \cdot [E_i] \cdot [S_i]}{K m_i \cdot \left(1 + \frac{[P_i]}{K_{P,i}}\right) + [S_i]}$	5.2
Modified Michaelis-Menten with competitive product inhibition	1, 2 and 4	$\alpha_i = \frac{k_i \cdot [E_i] \cdot [S_i]}{K m_i \cdot \left(1 + \frac{[P_i]}{K_{P,i}}\right) + [E_i]}$	5.3
Langmuir Based Model with competitive inhibition by several inhibitors	1	$\alpha_1 = \frac{k_1 \cdot [E b_1] \cdot R_s \cdot [Cl]}{1 + \frac{[Cl]}{K i_{1Cb}} + \frac{[Gl]}{K i_{1Gl}} + \frac{[Xy]}{K i_{1Xl}}}$	5.4
	2	$\alpha_2 = \frac{k_2 \cdot ([E b_1] + [E b_2]) \cdot R_s \cdot [Cl]}{1 + \frac{[Cb]}{K i_{2Cb}} + \frac{[Gl]}{K i_{2Gl}} + \frac{[Xy]}{K i_{2Xy}}}$	5.5
	4	$\alpha_4 = \frac{k_4 \cdot [E b_4] \cdot R_s \cdot [He]}{1 + \frac{[Cb]}{K i_{4Cb}} + \frac{[Gl]}{K i_{4Gl}} + \frac{[Xy]}{K i_{4Xy}}}$	5.6
	1	$R_s = \alpha_R \frac{[Cl]}{[Cl_0]}$	5.7
	6	$[E b_i] = \frac{E m_i \cdot K a d_i \cdot [E f_i] \cdot [S_i]}{1 + K a d_i \cdot [E f_i]},$ $E t_i = E f_i + E b_i$	5.8
	Enzyme inactivation	6	$v = k_e \cdot [E]$

**Source:** Carvalho et al. (2013); Kadam et al. (2004)

Equations 5.4 to 5.6 are the first rate with products inhibition reactions occurring in the solid substrate surface,  $Ki_{Cb}$ ,  $Ki_{Gl}$  and  $Ki_{Xl}$ , are the inhibition constants ( $\text{g.kg}^{-1}$ ) for cellobiose, glucose and xylose, respectively.

Equation 5.7 is the equation that models the change in substrate reactivity,  $R_s$  is the substrate reactivity,  $\alpha_r$  is reactivity dimensionless constant,  $Cl_0$  is the initial cellulose concentration ( $\text{g.kg}^{-1}$ ).

It is important to notice that the information regarding the amount of each enzyme within the enzymatic complex was unavailable. In order to use the described model, the

enzymatic complex mass was divided equally between the different types of enzymes. Since the real fraction of certain type of enzyme is always constant, the activity of a specific enzyme will be lumped into their kinetic constants, and the model can be used, but its parameters do not relay the correct value.

Two sets of kinetic models were used in the standalone fitting stage. One set was based on Michaelis-Menten Kinetics (MMK), where the reactions involving solid substrates (Reactions 1, 2, and 4) were represented by a Modified Michaelis-Menten models with product inhibition (Equation 5.3). Cellobiose hydrolysis (Reaction 3), where the substrate is soluble, was represented by a classical Michaelis-Menten with product inhibition. First order inactivation was assumed for the whole enzymatic complex (Equation 5.9, where  $k_e$  is a first order inactivation parameter ( $\text{min}^{-1}$ )).

The other set was based on the Langmuir Kinetics (LK), where Reactions 1, 2 and 4 were represented by Equations 5.4, 5.5 and 5.6 respectively. The cellobiose hydrolysis (Reaction 3) was also represented by a classical Michaelis-Menten equation with product inhibition (Equation 5.3).

#### 5.2.2.3. Fuzzy Kinetic Model

The Fuzzy Model (FM) used a TS Fuzzy system (Takagi and Sugeno, 1985). The fitting procedure for the FM was carried out in three steps. Firstly, a standalone High Solids Model (HSM) was fitted using the MMK reaction rates as described in Item 5.2.2.2., and data from Assay 1 (HSB). Second, a Low Solids Model (LSM) was fitted in the same manner, but only using data from Assay 2 (LSB). Both models generated independent reaction rates ( $\alpha^{HSM}$  and  $\alpha^{LSM}$ ) for every equation in a same reaction instant. Until this point, no fuzzy methodology was used. Figure 5.1 illustrates how the FM weighs the two models.

The third step was optimizing a Membership Function (MSF) to dictate how the total reaction rate of the FM should smoothly change between the HSM and LSM. An MSF is used to calculate the Membership Degree (MD) of each model,  $MD^{HSM}$  for the HSM and  $MD^{LSM}$  for LSM, the latter obtained by subtracting  $MD^{HSM}$  from 1.

The MSF calculates the MD using the total amount of Reactive Solids (RS). RS is the sum of solid cellulose and hemicellulose concentrations. A pure positive piece-wise linear MSF was used, as presented in Figure 5.1b.

**Figure 5.1** Fuzzy Model Reaction Rate Calculation

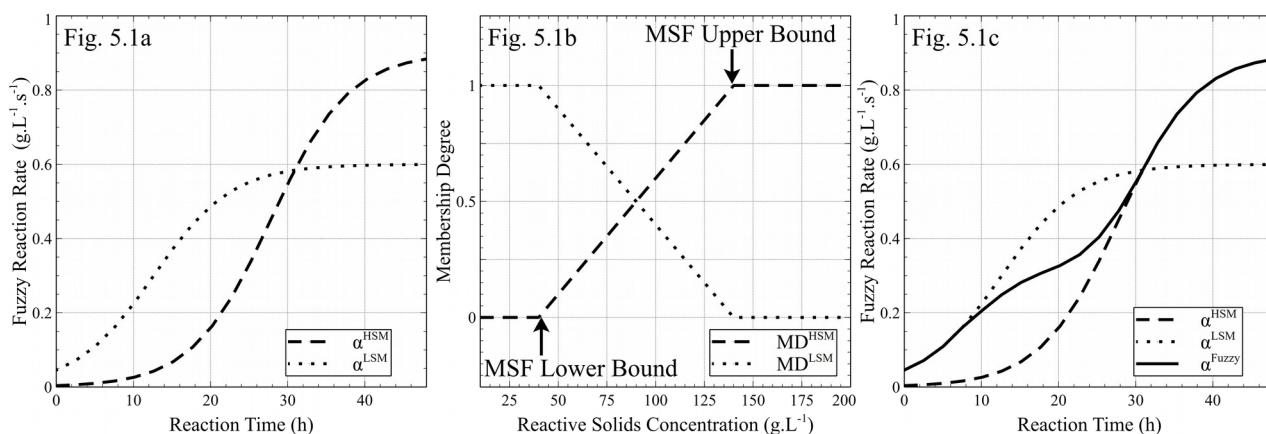


**Fig. 5.1a** Example Rates for Independent HSM and LSM; **Fig. 5.1b** Example MSF for HSM and LSM; **Fig. 5.1c** Resulting Hypothetical FM Rate from HSM and LSM Rates.

**Source:** Author's library

With the HSM and LSM membership degrees, the reaction rate for the FM is the output of the Takagi-Sugeno System (Nelles, 2001) was calculated with Equation 5.10, where  $\alpha^{FUZZY}$  are the reaction rates for each hydrolysis reaction.

$$\alpha^{Fuzzy} = MD^{HSM} \cdot \alpha^{HSM} + (1 - MD^{HSM}) \cdot \alpha^{LSM} \quad \text{Equation 5.10}$$

The MSF optimization stage was performed to determine where lower and upper bounds of the  $MD^{HSM}$  should be placed. These parameters were optimized via Levenberg-Marquardt algorithm using the data from Assays 1 and 2, the optimization procedure is described in Item 5.2.2.4.

To evaluate the model prediction capacity, the previously unused data of Assay 3 were used for validation of the procedure.

#### 5.2.2.4. Fitting Algorithm and Statistics

To estimate the different models' kinetic parameters and  $MD^{HSM}$  lower and upper bounds, a Levenberg-Marquardt algorithm was used.

The sum of weighted squares errors ( $F$ ) was used as cost function, it was calculated via Equation (5.11).

$$F = e^T \cdot Q \cdot e \quad \text{Equation 5.11}$$

Where  $Q$  is an  $n \times n$  diagonal weight matrix,  $e$  is the error column vector,  $n$  is the number of experimental data. The elements  $Q_{ii}$  are the inverse of the carbohydrate replicate variance ( $\sigma^2_i$ ). The variance estimated for glucose was  $0.392 \text{ g}^2/\text{L}^2$ , and for xylose was  $0.773 \text{ g}^2/\text{L}^2$ .

To obtain the standard errors of the optimized parameters, Equation 5.12 was used. The equation is based on the linearization of the model in relation to the parameters at their optimum values.

$$\text{Cov}(\theta) = (Xr^T \cdot Q \cdot Xr)^{-1} \cdot \frac{F}{m-n} \quad \text{Equation 5.12}$$

Where  $\text{Cov}(\theta)$  is the parameters covariance matrix,  $Xr$  is the linear sensitivity matrix, with derivatives approximated via finite differences,  $Q$  is the diagonal weight matrix.  $F$  is the objective function at the optimum value. The parameters standard error was estimated by the square root of the parameters' matrix main diagonal.

All fitting procedures were implemented in SCILAB 6.0.0. To integrate the state variables, with the generated model parameters, SCILAB's default ordinary differential equation solver was used, with the option for stiff systems enabled in a computer with an AMD FXTM-8350 and 15,7 Gb of random access memory running, as operating system, 64-bit Linux Mint 18.3

### 5.3. RESULTS AND DISCUSSION

It is important to emphasize once again that any model here presented is a strong simplification of the phenomenology behind the saccharification of lignocellulosic materials. Several other reactions are occurring within the reactor. Specially when using new enzymatic complexes, with improved bG activity and the addition of new cellulose oxidizing enzymes such as PMOs (Bansal et al., 2009). Furthermore, different molecules not considered here are generated during the hydrolysis, specially from hemicellulose (Yao et al., 2015).

However, modeling such complex interactions can be strenuous and the complexity of the generated model can compromise future studies, such as applications in reactor monitoring and control. The consortium of simple models here proposed intends to have enough complexity to predict the concentrations of the main compounds, while retaining enough simplicity and flexibility to be applied to engineering problems.

The distinct feeding profiles generated different situations within the reactor, as expected. In Assay 1 (HSB), the amount of substrate added in the beginning of the process generated a very high viscosity medium, where there was little visible free water within the reactor before the initial solids liquefaction. As the hydrolysis occurred, the viscosity of the media decreased rapidly. In Assay 2 (LSF), the feeding of substrate



occurred sparsely enough as not to build a load of solids within the reactor that could cause a significant visual change in the reactive medium, and the amount of visible free water remained constant. In Assay 3 (MPF), the initial substrate concentration was not enough to change the medium pseudo-viscosity greatly; however, the subsequent small intervals between feedings modified the medium towards a high-solids state. As the hydrolysis continued, the reactor once again returned to a low solids state. Thus, Assay 3 is a strong validation test, since the path of the reaction system was very different from the two first assays.

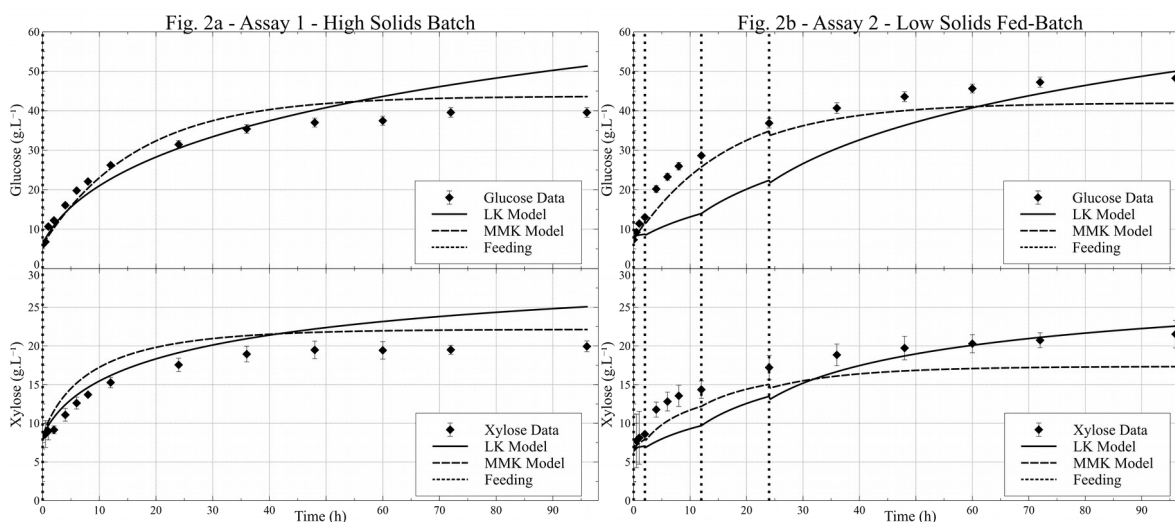
### **5.3.1. Standalone Models Fitting**

Assay 1 and 2 data were first used to test the prediction capacities of the LK and MMK models structures. The optimized models' fitting for these kinetics are presented in Figure 5.2.

Both models present the same fitting trend: overestimation of final glucose and xylose concentrations in HSB (Assay 1), and with similar predictions for products final concentrations in the LSF (Assay 2) However, a deviation from initial sugar concentration occurs. This behavior may indicate that both model sets are being compromised when their parameter are forced to cope with slower reaction rates in the LSF and higher rates in the HSB.

It is important to notice that the Mean Squared Error (MSE) for the LK kinetics was  $27.77 \text{ g}^2.\text{L}^{-2}$ , using 23 parameters, while the MMK model set, containing 13 parameters, obtained a MSE of  $8.90 \text{ g}^2.\text{L}^{-2}$  after optimization. In this case, the model that contained almost 60% more parameters showed no improvement over the simpler model.

**Figure 5.2 Standalone Models Fitting**



Error bar in data points are the assay standard error for the compound concentration; Vertical dotted lines are the solids feeding time; **Fig 2a** Fitting for Assay 1; **Fig. 2b** Fitting for Assay 2.

**Source:** Author's library

### 5.3.2. Fuzzy Kinetic Model Fitting

Using one model alone for a wide range of solids' concentrations was not enough to take into account the reactor medium change during liquefaction. Here, the FM was built using the MMK models, since they have fewer parameters (13) than then LK (23), when all equations are considered.

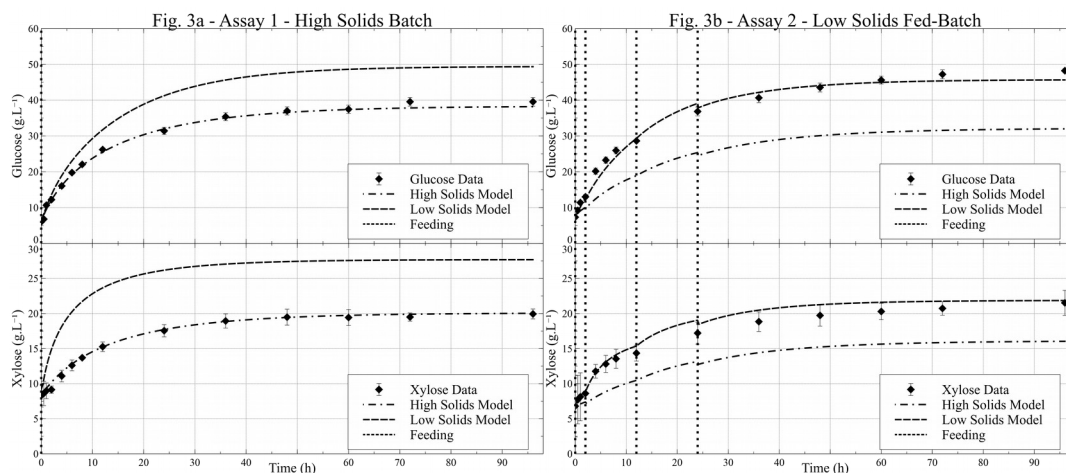
Firstly, two different sets of MMK parameters were obtained: the HSM set was obtained using data from Assay 1 only, and the LSM set from Assay 2, these models are presented in Figure 5.3 and the parameters resulting from the optimization of HSM and LSM are in Table 5.3. Figure 5.3a shows the LSM only to enable a comparison between this model and the HSM, as described, the data in this figure was not used to fit the LSM. The same occurs in Figure 3b but this time for HSM presence.

The models performed well within their fitting data, however, their prediction capacity with validation data is subpar. The LSM greatly overestimates the concentration of products in the end of Assay 1, and the HSM cannot describe the reaction rate of Assay 2.

The models were then used in the fuzzy optimization, as reaction rates generators. The lower and upper bounds of the FM (see Fig. 5.1) were then optimized. After optimization, the Low and High thresholds for the linear fuzzy rule were 70.56 g.L<sup>-1</sup> and

74.70 g.L<sup>-1</sup> respectively. This is an interesting result, since the threshold of the upper bond agrees with the empirical observations during the assays: visually, around this load of solids, the reactor seems to change its behavior from an almost semisolid process to one with high free water content. The resulting fitting of the FM, alongside the HSM and LSM for comparison, are presented in Figure 5.4.

**Figure 5.3** High and Low Solids Models Fitting



Error bar in data points are the assay standard error for the compound concentration; Vertical dotted lines are the solids feeding time; **Fig 3a** Fitting for Assay 1; **Fig. 3b** Fitting for Assay 2.

**Source:** Author's library

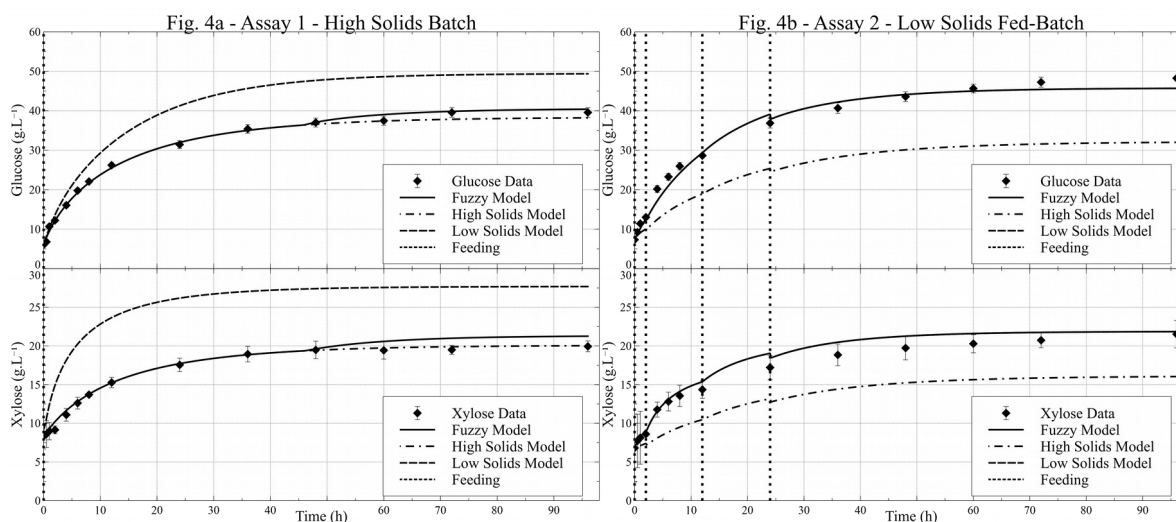
**Table 5.3** High and Low Heterogeneous Michaelis-Menten Model Parameters

Reaction	Solids Model	Parameters			
		k (min <sup>-1</sup> )	Km (g.L <sup>-1</sup> )	Kp (g.L <sup>-1</sup> )	ke (min <sup>-1</sup> )
1	High	$(1.01 \pm 9.57) \cdot 10^{-3}$	$(4.96 \pm 2.11) \cdot 10^{-2}$	$(6.06 \pm 4.22) \cdot 10^{-6}$	-
	Low	$(0.51 \pm 1.70) \cdot 10^{-2}$	$(0.50 \pm 2.31) \cdot 10^{-6}$	$(1.60 \pm 1.03) \cdot 10^{-4}$	-
2	High	$(1.24 \pm 2.91) \cdot 10^{-3}$	$(7.74 \pm 5.38) \cdot 10^{-3}$	$(0.49 \pm 2.14) \cdot 10^{-1}$	-
	Low	$(4.60 \pm 6.47) \cdot 10^{-4}$	$(0.31 \pm 1.48) \cdot 10^{-2}$	$(1.62 \pm 0.00) \cdot 10^{-2}$	-
3	High	$(3.93 \pm 6.53) \cdot 10^{-2}$	$(5.06 \pm 0.12) \cdot 10^{-4}$	$(0.93 \pm 3.32) \cdot 10^{-1}$	-
	Low	$(5.41 \pm 2.68) \cdot 10^{-2}$	$(0.10 \pm 3.58) \cdot 10^{-9}$	$(2.27 \pm 0.00) \cdot 10^{-1}$	-
5	High	$(2.11 \pm 1.29) \cdot 10^{-3}$	$(2.76 \pm 0.73) \cdot 10^{-2}$	$(1.80 \pm 1.25) \cdot 10^{-1}$	-
	Low	$(3.11 \pm 0.69) \cdot 10^{-3}$	$(7.13 \pm 0.16) \cdot 10^{-2}$	$(1.17 \pm 0.01) \cdot 10^{-1}$	-
6	High	-	-	-	$(8.43 \pm 2.09) \cdot 10^{-1}$
	Low	-	-	-	$(1.06 \pm 0.01) \cdot 10^{-1}$

Values are presented as (Parameter ± Standard Error)

**Source:** Author's library

**Figure 5.4** Fuzzy, High and Low Solids Models Fitting



Error bar in data points are the assay standard error for the compound concentration; Vertical dotted lines are the solids feeding time; **Fig 4a** Fitting for Assay 1; **Fig. 4b** Fitting for Assay 2.

**Source:** Author’s library

A summary of the fitting errors for all assays and models are presented in Table 4.

**Table 5.4** Fitting Error Summary for Proposed Models

Model		Assay 1 High Solids Batch	Assay 2 Low Solids Fed-batch	Assay 3 Mixed Profile Fed- batch	Total Training MSE	Total Validation MSE
Langmuir- Type Kinetics	Usage	Training	Training	No Prediction	27.77 g <sup>2</sup> .L <sup>-2</sup>	No Prediction
	MSE	12.72 g <sup>2</sup> .L <sup>-2</sup>	42.82 g <sup>2</sup> .L <sup>-2</sup>			
Michaelis- Menten Kinetics	Usage	Training	Training	No Prediction	8.90 g <sup>2</sup> .L <sup>-2</sup>	No Prediction
	MSE	7.12 g <sup>2</sup> .L <sup>-2</sup>	10.69 g <sup>2</sup> .L <sup>-2</sup>			
High Solids Model	Usage	Training	Validation	Validation	0.39 g <sup>2</sup> .L <sup>-2</sup>	42.77 g <sup>2</sup> .L <sup>-2</sup>
	MSE	0.39 g <sup>2</sup> .L <sup>-2</sup>	61.51 g <sup>2</sup> .L <sup>-2</sup>	24.03 g <sup>2</sup> .L <sup>-2</sup>		
Low Solids Model	Usage	Validation	Training	Validation	1.81 g <sup>2</sup> .L <sup>-2</sup>	30.44 g <sup>2</sup> .L <sup>-2</sup>
	MSE	49.48 g <sup>2</sup> .L <sup>-2</sup>	1.81 g <sup>2</sup> .L <sup>-2</sup>	11.40 g <sup>2</sup> .L <sup>-2</sup>		
Fuzzy Model	Usage	Training	Training	Validation	1.16 g <sup>2</sup> .L <sup>-2</sup>	6.18 g <sup>2</sup> .L <sup>-2</sup>
	MSE	0.51 g <sup>2</sup> .L <sup>-2</sup>	1.81 g <sup>2</sup> .L <sup>-2</sup>	6.18 g <sup>2</sup> .L <sup>-2</sup>		

**Source:** Author’s library

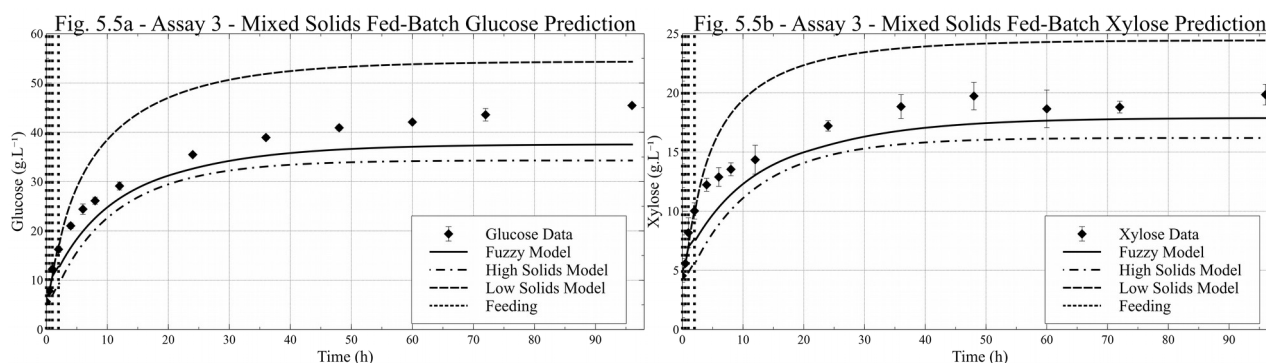
Analysis of Table 4 demonstrates several interesting aspects of the fuzzy modeling methodology. The FM has a higher MSE (0.51 g.L<sup>-1</sup>) than HSM (0.39 g.L<sup>-1</sup>) when predicting data used in the training of the latter model. This is to be expected, as the HSM is

generated with a smaller data sets, using only one batch assay condition.

However, using restrict data sets decreases model flexibility. This is presented in Figure 5.4, where a poor adherence from the HSM to the data in Assay 2 and from the LSM to the data in Assay 1 is clear. The fuzzy model, through its model's interpolation capacity, generates a much better fit in both assays simultaneously using only one model.

When the FM is compared to standalone models trained with the same data, it is clear that FM gives a much better fitting. The FM fitted with data from assays 1 and 2 obtained a MSE ( $1.16 \text{ g}^2.\text{L}^{-2}$ ) 23 times smaller than a LK model ( $27.07 \text{ g}^2.\text{L}^{-2}$ ) and 7 times smaller than the MMK model ( $8.90 \text{ g}^2.\text{L}^{-2}$ ) trained with the same data. However, the FM greatest feature is its prediction outside training data. As presented in Figure 5.5.

**Figure 5.5** Fuzzy, High and Low Solids Validation Data Prediction



Error bar in data points are the assay standard error for the compound concentration; Vertical dotted lines are the solids feeding time; **Fig 5a** Fitting for Glucose in Assay 3; **Fig. 5b** Fitting for Xylose in Assay 3.

**Source:** Author's library

The Fuzzy Model extrapolation ability clearly is superior. MSEs for the validation assay data (MPF), predicted by FM, HSM and LSM were respectively  $6.18 \text{ g}^2.\text{L}^{-2}$ ,  $24.03 \text{ g}^2.\text{L}^{-2}$  and  $11.40 \text{ g}^2.\text{L}^{-2}$ . These results indicate that the use of Fuzzy logic to coordinate a consortium of simple models is a powerful methodology when applied to enzymatic saccharification of sugarcane bagasse, an extremely complex reaction system. This is achieved by the fuzzy model's capacity to interpolate between its predecessor models when necessary. Figure 5.6 demonstrates the change in reaction rates for the training and validation assays for the FM and its parent models, HSM and LSM, as a function of the solids concentration.

**Figure 5.6** FM, HSM and LSM Reaction Rates

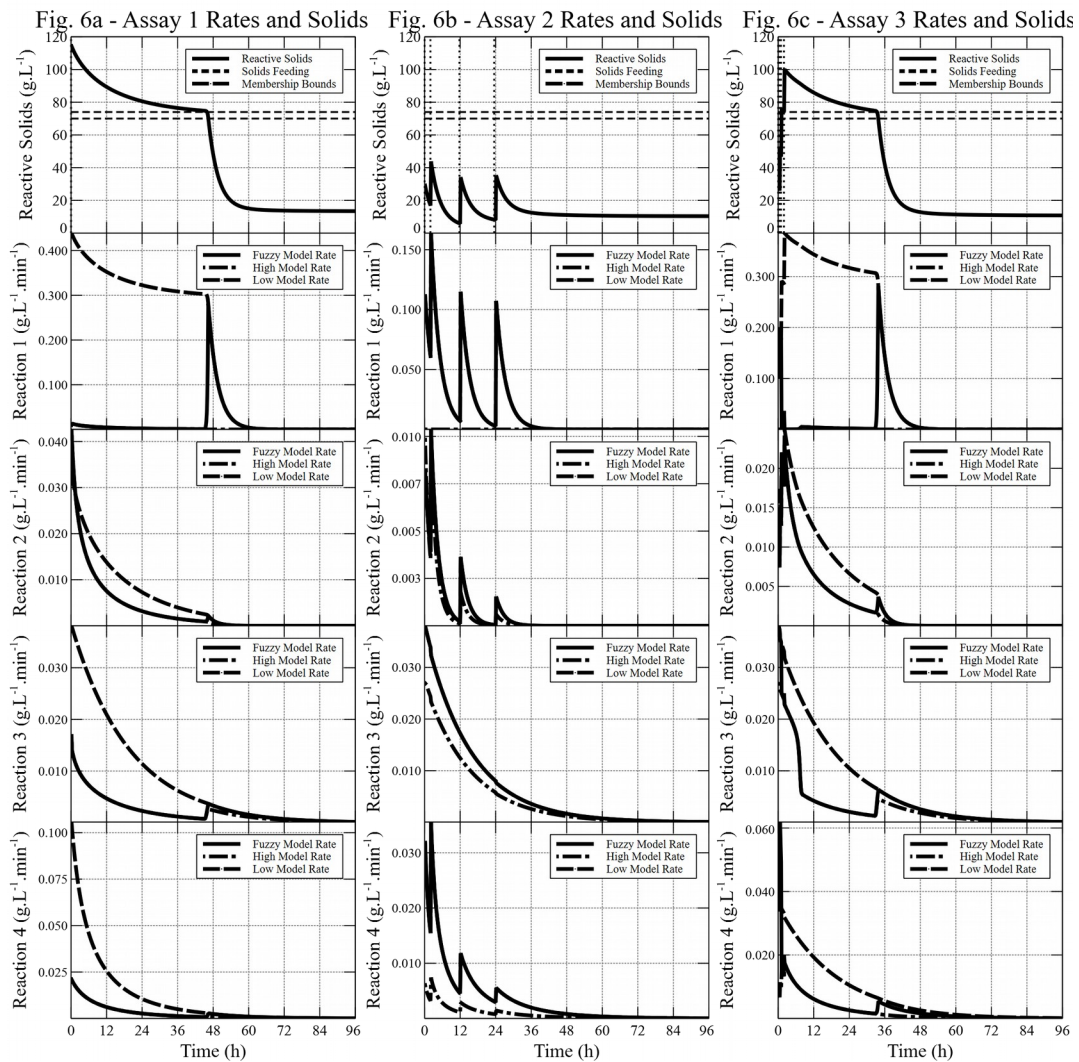


**Fig. 6a** Solids concentration and rates for reactions 1 through 4 for the models in Assay 1; **Fig. 6b** Solids concentration and rates for reactions 1 through 4 for the models in Assay 2; **Fig. 6c** Solids concentration and rates for reactions 1 through 4 for the models in Assay 3; Horizontal lines in the first row are the optimized thresholds for the Membership Degree of the High Solids Model during the Fuzzy optimization (Item 5.2.2.3) and vertical lines are biomass feedings.

**Source:** Author's library

The first row of figures in Figure 5.6 displays the reactive solids concentration for each assay, it is calculated by adding the concentration of cellulose and hemicellulose, these are calculated using the predicted value of its hydrolysis products. The solids value is the one used to calculate the membership degree for each parent model used in Equation 10 to generate the fuzzy reaction rate. This relationship explains the correlation between the solids concentration and the most pertinent reaction rate. For instance, during Assay 1 the reactive solids concentration remains above the upper bound of the high

model membership function until halfway through the process, thus, up until this point, the Fuzzy Reaction Rate (FRR) is equal to the HSM reaction rate, and switches to the LSM reaction rates in the second half of the assay. The LSM has a faster dynamic than the HSM, and thus, after the change in predominant reaction rate, the apparent reactive solids hydrolysis seems to accelerate.

For Assay 2, the opposite is true. The assay begins with a small solids concentration, and thus, the FRR is equivalent to the LSM rate. The subsequent solids addition does not amount to a solids concentration that can cause the FRR to deviate from the HSM reaction rate.

This is a very interesting capability, as the model can be adapted quickly to situations not present in the training data using only the knowledge of apparent reactive solids concentration. And such is what occurs in the reaction rates from Assay 3. The FM starts in the LSM rate and quickly changes to the HSM rate with the close feeding time periods. As the solids are liquefied, the model becomes a halfway interpolation of the two precursor models, and continues to approach the LSM rate at the process' end. This improves validation data prediction greatly, as presented in Figure 5.5.

Thus, the FM methodology can be used to predict the trajectory of the reactor for operational conditions different from those used for training the algorithm. Furthermore, this methodology requires little alterations in software development and can be applied to small datasets.

#### 5.4. CONCLUSIONS

In this chapter a Fuzzy Model (FM) for reaction rates was proposed to describe the enzymatic saccharification of sugarcane bagasse. Simple models, such as those based on Michaelis-Menten Kinetics (MMK) fit well to the data for a particular feeding policy. However, the same model could not be used to predict with accuracy the process behavior when the feeding policy was changed. The use of a fuzzy rule to weight between two simple models, each one fitted for different solids' concentrations, has greatly improved the bioreactor trajectory prediction for different operation modes. This approach seems to be a good trade-off between phenomenological and empirical-driver model, and was able to describe a very complex system. Of course, the methodology can be applied to different systems, for example, the enzymatic liquefaction of other lignocellulosic materials.

## **6. HYDROLYSIS STATE ESTIMATION IN STIRRED TANK REACTOR**

### **6.1. MOTIVATION AND OBJECTIVE**

Optimization of reactors to operate at high solids concentrations is an important step to enable enzymatic hydrolysis biomass as a feasible technology. However, due to several phenomena, operating under high solids conditions can cause several issues in the saccharification kinetics. Some issues can be traced to reactor homogenization, a difficult task at high apparent viscosity. The suspended solids also increase greatly the power for the stirring motor itself, creating the necessity to study the reactor and propellers architectures.

These sort of bottlenecks are overcome by studying the torque necessary to stir the reactor, and thus, indirectly, the reactor rheology. Stirring torque is a measurement widely used to design reactor and their coupled stirring apparatus, as well as the power consumption of a given reactor architecture during operation (Bondancia et al., 2018; Corrêa et al., 2016b). Furthermore, torque dynamometers can also be used to monitor reaction rates and fluid rheology during process (Jawad et al., 2019).

Nonetheless, torque measurement can be susceptible to a lot of noise. Coupling the torque measurement to a state estimator can increase state estimation precision. State observers are algorithm used to estimate state variables that are not directly measured (either by lack of instrumentation or sensor high cost) and to diminish estimation error in the measured variables (Mohd et al., 2015).

Several observers can be used, one possible approach is the Moving Horizon Estimator (MHE). This sort of algorithm uses a dynamic window and optimization steps to predict the observed state variables, based on both measurements and model data. MHE are very well established as state estimators for chemical processes because it can deal with the nonlinear dynamics and state constraints inherent to most reaction systems in a fairly straightforward manner (Lima and Rawlings, 2011).

Thus, the aim of this work was to design and test an MHE estimator based in torque measurements of suspended solids during fed-batch operation of sugarcane bagasse enzymatic hydrolysis.

### **6.2. MATERIALS AND METHODS**

#### **6.2.1 Hydrolysis Assays**



Different feeding policies of solids were evaluated. Enzymatic complex was CELIC CTEC 2 and lignocellulosic substrate was steam-exploded sugarcane bagasse. The assays were conducted in duplicates in a 3 L working volume stirred reactor with two elephant ear impellers, the one in the top of the axle generating a flow downward, and the one in the bottom generating flow upward, at 50°C and 470 RPM. Manual sampling was performed at 0.5, 1, 2, 4, 6, 8, 12, 24, 36, 48, 60, 72 and 96 h and supernatant free carbohydrates were determined.

Three feeding profiles were assessed. A High Solids Fed-Batch (HFB) process, Assay 1, where 300 g of substrate and  $3.7 \text{ mg}_{\text{protein}} \cdot \text{g}_{\text{substrate}}^{-1}$  (approximately  $10 \text{ FPU} \cdot \text{g}_{\text{substrate}}^{-1}$ ) of enzymatic complex were added in the beginning of the process, and after 1 and 2 h, 150 g were added. And two fed-batches, where the feeding profiles amounted to the same substrate mass as the first fed-batch process. However, the lignocellulosic material was distributed into four feeding times. These feeding profiles generated two assay conditions a Low Solids Fed-Batch (LSF) and a Mixed Profile Fed-Batch (MPF). Table 6.1 presents the three assays feeding profiles.

**Table 6.1** Assay Feeding Profiles

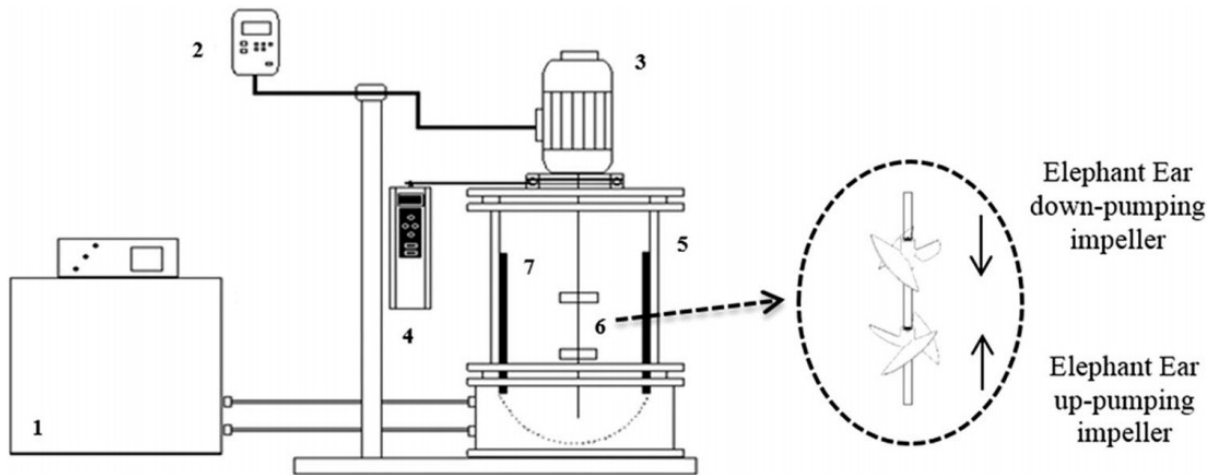
Fitting Assays						Validation Assays		
Assay 1 – High Solids Fed-Batch			Assay 2 – Low Solids Fed-Batch			Assay 3 – Mixed Profile Fed-Batch		
Feeding Time (h)	Solids Feeding ( $\text{g} \cdot \text{L}^{-1}$ )	Enzyme Feeding ( $\text{mg} \cdot \text{g}^{-1}$ )	Feeding Time (h)	Solids Feeding ( $\text{g} \cdot \text{L}^{-1}$ )	Enzyme Feeding ( $\text{mg} \cdot \text{g}^{-1}$ )	Feeding Time (h)	Solids Feeding ( $\text{g} \cdot \text{L}^{-1}$ )	Enzyme Feeding ( $\text{mg} \cdot \text{g}^{-1}$ )
0	100	3.70	0	50	3.70	0	50	3.70
1	50	-	2	50	-	0,5	50	-
2	50	-	12	50	-	1	50	-
-	-	-	24	50	-	2	5	-

**Source:** Author's library

### 6.2.2. Experimental Apparatus

To perform the assays, a 3L working volume reactor was used, this reactor was developed by Corrêa et al. (2016a). The stirring motor was placed on top of a plate with a bearing so the motor was free to rotate when opposing forces acted upon it. A dynamometer was coupled to the lid. This enabled the stirring torque measurement. The experimental apparatus is presented in Figure 6.1.

**Figure 6.1** Experimental Apparatus



Elements key; 1 Thermostatic Bath; 2 Frequency Inverter; 3 Motor; 4 Dynamometer; 5 Reactor; 6 Elephant Ear impeller; 7 Baffles

**Source:** Corrêa et al. (2016a)

### 6.2.3. Solids Monitoring

Solids concentration is not directly obtainable from the torque measurement, since no straight forward correlation is clearly discernible. Thus, an Artificial Neural Network (ANN) was used to transcribe torque data, and other available data, into solids concentration. The ANN models were implemented in SciLab 6.0.0. with the Artificial Neural Network Module 2.0.

### 6.2.4. Instrumentation Data

ANN training requires a relatively large amount of data to fully recognize useful patterns in the data. Solids concentration was calculated stoichiometrically from the free carbohydrates concentration. However, this wouldn't generate enough data to predict concentration. Thus, the solids concentrations were interpolated with a cubic spline algorithm, to generate new data points where previously there were none. It is clear that interpolated data may not be completely accurate to actual state variables profiles, however, this sort of procedure is necessary when the available data set is not sufficient to fit complex empirical models, such as ANNs.

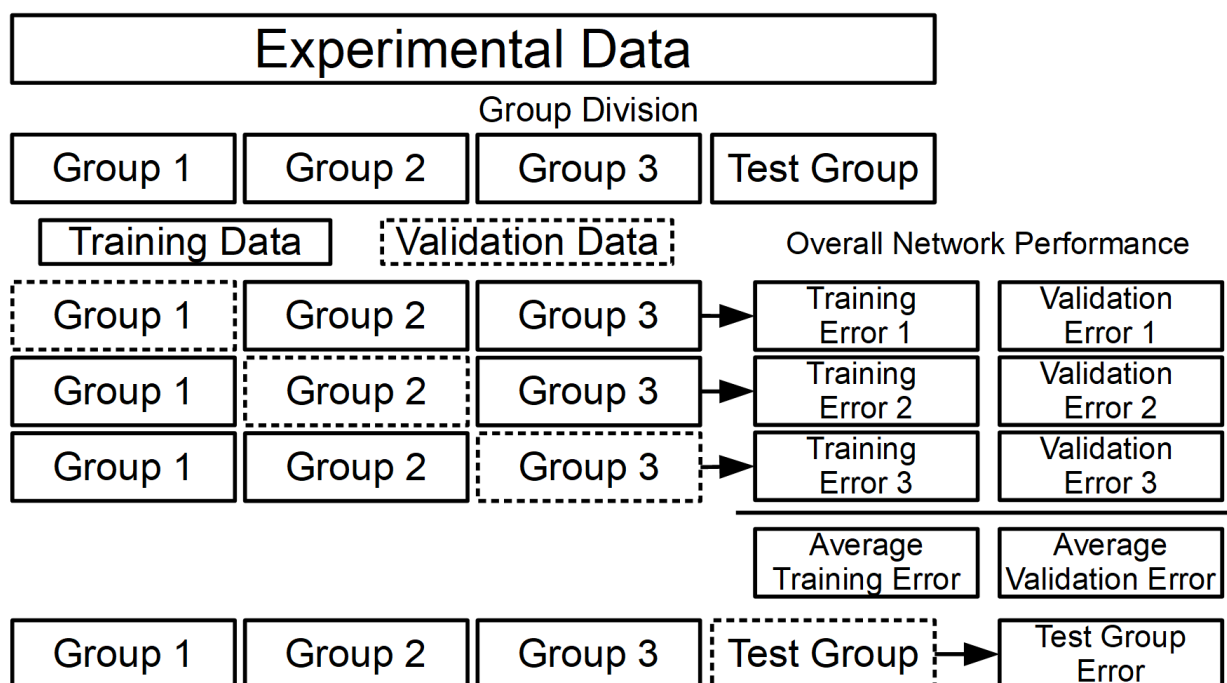
Torque measurement was realized during the assays every 10 seconds. The resulting data was fed through a LoWeSS (Locally Weighted Scatterplot Smoothing) filter to diminish operational noise. The other two input data sets to the neural network were

lignin and enzyme concentrations. Since the feeding was done discretely, and no hydrolysis of lignin or enzyme inactivation was considered, these compounds concentration were calculated with the amount present in each feeding point, plus the previous concentration before the feeding.

### 6.2.5. Neural Network Architecture Optimization

Cross validation approach was used to avoid overfitting issues (Nelles, 2001). The sample universe was first randomized. The samples were then divided in 4 sets. 3 sets were used in a cross-validation approach. 2 sets were used for the training of the network (the current training group) and the unused set was used to validate (the validation group) the current training. This approach was repeated until all the sets were used as validation set. The average of the standard error of training and the average of the standard error of validation were used to evaluate the architecture performance. The last group is the test group. This group does not take place in the cross-validation and training procedure. A graphical representation of this procedure is presented in Figure 6.2.

**Figure 6.2** Cross Validation Procedure

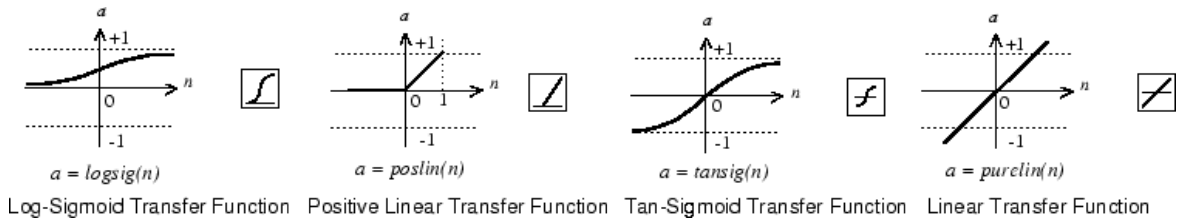


**Source:** Adapted from Nelles (2001)

The architectures taken into account were multilayer perceptrons with one hidden layer, the numbers of neurons in the hidden layer ranged from 1 to 10. The evaluated transfer functions for the hidden layer and the sum layer are displayed in Figure 6.3. Each

transfer function was evaluated both for the hidden layer and the sum layer.

**Figure 6.3** Evaluated Transfer Functions

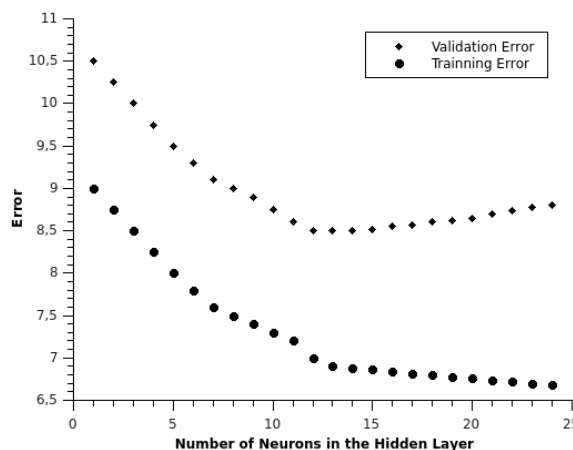


**Source:** Adapted from Nelles (2001)

The NN optimum architecture is achieved when the average standard error from the validation departs from the linear tendency of accompanying the average standard error from the training. When this happens, a possible interpretation is that the complexity of the networks has become larger than the necessary for the system. The networks starts to contemplate, in the pattern recognition, the noise from the samples disrupting the network inference (overfitting).

Therefore, the optimum architecture is when the errors are closely related (Nelles, 2001). An example of the behavior is presented in Figure 6.4. In the presented example, the point in which the validation error departs from the training error is at around 12 neurons in the hidden layer, thus demonstrating to be the optimum architecture for this hypothetical network.

**Figure 6.4** Training and Validation Errors Departure



**Source:** Adapted from Nelles (2001)

### 6.2.6. Mathematical Modeling

The mathematical model used in the state estimator was the fuzzy model described and optimized in Chapter 5. The same parameters and reactions described in that item

were used in the MHE as a mean to obtain the *a-priori* model state estimation.

### 6.2.7. Moving Horizon State Estimator

The moving horizon estimator cost function was presented in equation 3.13.

$$\min_{X(T-N:T)} = V_{T-N}(X(T-N)) + \sum_{j=T-N}^{T-1} L_w(\hat{X} - X^c) + \sum_{j=T-N}^T L_v(\hat{Y} - Y) \quad \text{Equation 3.13}$$

The instrumentation data ( $Y$ ) is obtained by using the torque measurement with the ANN, and the model prediction ( $X^c$ ) is obtained with the fuzzy model. At each observation step, the filter estimation ( $\hat{X}$  and  $\hat{Y}$ ) is optimized via a Levenberg-Marquardt algorithm, with 10 iterations. In this case, the instrumentation data has the same unit as the state variable, and thus  $\hat{X}$  and  $\hat{Y}$  are equal.

The filter estimation is highly sensitive to the optimization weights. To estimate the correct weights, a range of these values were tested with the filter algorithm and the experimental data. A pseudo-code of the tuning algorithm is presented in Table 6.2.

This methodology was used to assess the performance of the filter. In this methodology, only the errors from glucose and xylose were used as performance index.

## 6.3. RESULTS AND DISCUSSION

### 6.3.1. Neural Network Optimization

From all the evaluated ANN structures, the one that obtained the lowest total error, regardless of the group used to train or predict solids concentration, was the network with a Tangent-Sigmoid transfer function in the first layer hidden layer and a pure linear transfer function in the sum layer. The dispersion between the training, validation and test groups for this network, as a function of the number of neurons in the hidden layer is presented in Figure 6.5.

The network training does not present a scatter plot similar from the one expected, represented in Figure 3.4. After the 7<sup>th</sup> neuron the scatter plot becomes erratic, not displaying any clear behavior. One possible explanation is that the algorithm used to train the network is preventing over-fitting by stopping the learning phase before the optimum minimum is reached.

---

**Table 6.2** Moving Horizon Estimator Tuning Pseudo-code

---

```
# Initialization
Set Initial Parameters:  $V_{T,N}=0.5$   $N=4$   $K_m$  and  $k$  Initial Values
Set Weight Values to be Tested:  $L_w = [0.01 \ 1 \ 100]$  and  $L_v = [0.01 \ 1 \ 100]$ 
# Main Loop
For: Every Combination of Weights
  For: Every Feeding Profile
    For:
      If: Window Size < Maximum Size do:
        Adds States to Window
        Measurement from the Neural Network
      Else:
        Updates Window
        Measurement from the Neural Network
      End If
    # Optimization Step
    While: Stopping Criteria = False do:
      Integrate Model for Window
      Evaluate Cost Function
      Update Kinetic Parameters and State Variables Prediction
    End While
    If: Feeding Time = True
      Update State With Substrate
      Reinitialize Moving Horizon Window
    End If
  End For
End For
End For
# Finishing Procedures
Calculate the tracking Error = (Analytical Data - Predicted State)
```

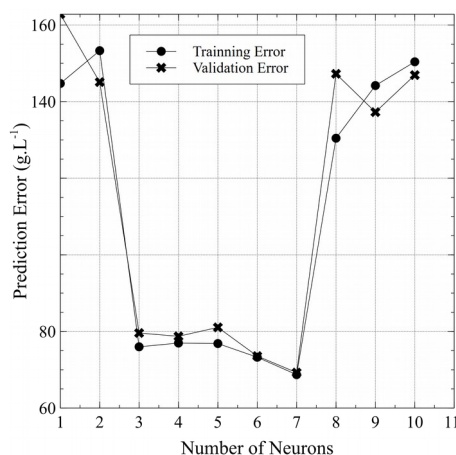
---

Nevertheless, the trend expected by Figure 6.4 can be seen until the 7<sup>th</sup> neuron. Within this interval, the training error decreases greatly with the addition of the 3<sup>rd</sup> neuron and remains somewhat stable. Validation error also remains stable, thus, the considered optimum architecture is the one in where the errors first stabilized, with 3 neurons in the hidden layers. In this structure, the test group error was not much larger than the validation and training groups.

The error scatter plot for all the validation and training groups for the optimum architecture are presented in Figure 6.6.

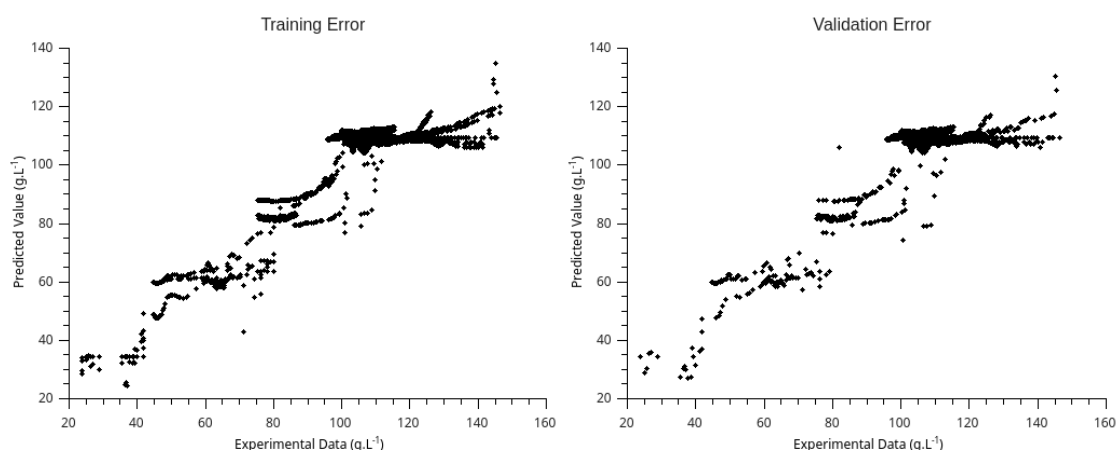
The network presented a fairly adequate relation between the predicted and actual values, demonstrating that it can be used to monitor the concentration of solids inside the reactor. And this trained network was used in the MHE tuning.

**Figure 6.5** Training and Validation Errors for Optimal Network



Source: Author's library

**Figure 6.6** Training and Validation Errors Dispersion



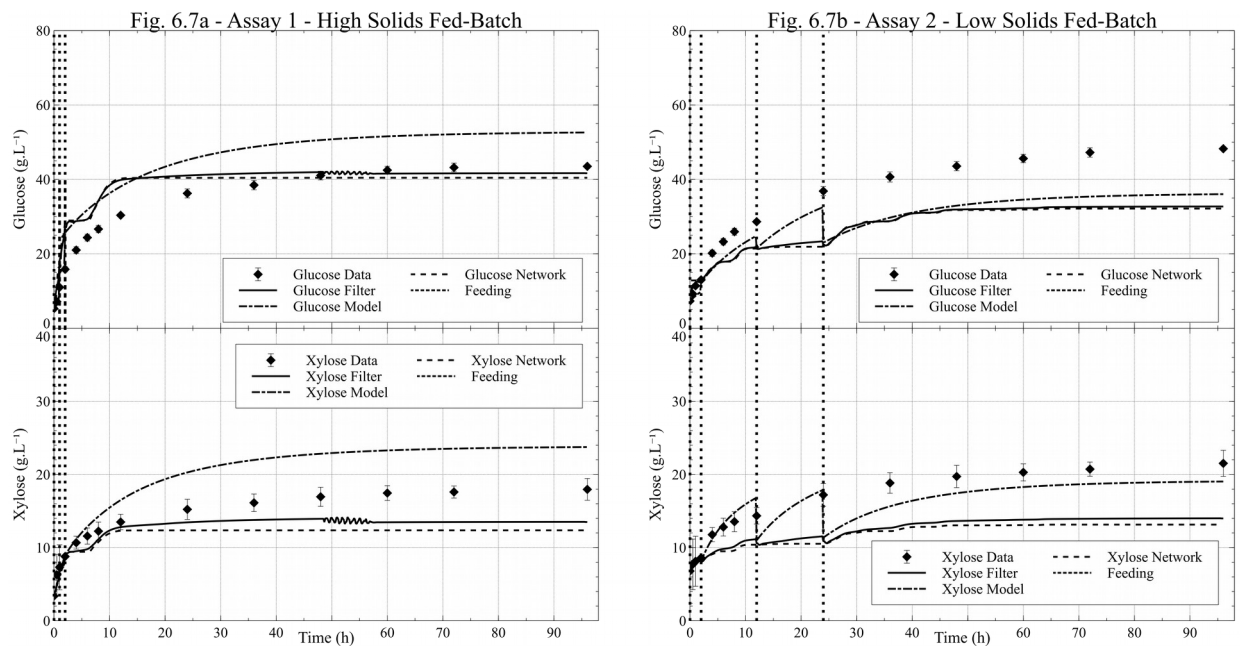
Source: Author's library

### 6.3.2. Moving Horizon Tuning

After the analysis of the several levels for the weights of the filters, the condition that obtained the smallest total tracking error was the one that used 100 for the  $L_v$  and 1 for the  $L_w$ . The best tuning are presented for the training assays are presented in Figures 6.7 and validation assay in Figure 6.8.

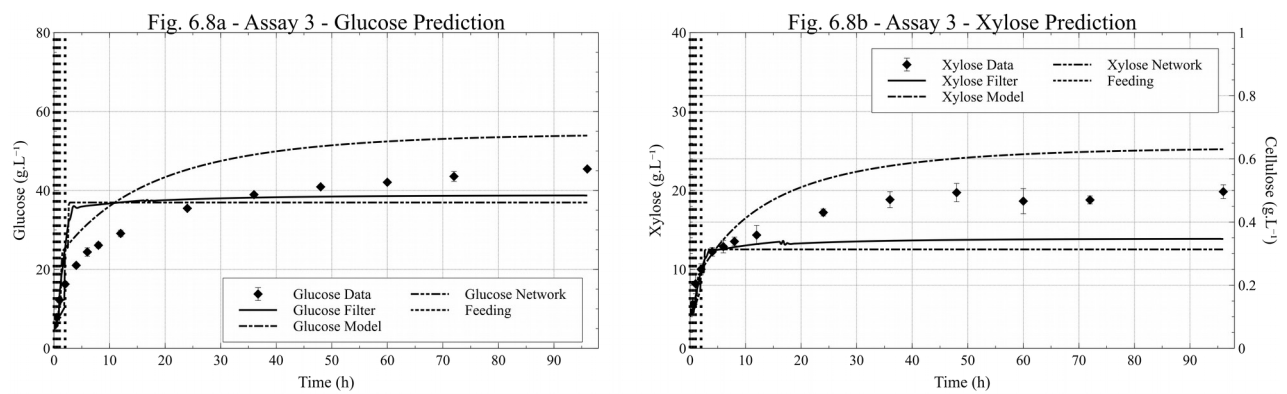
The grid optimization methodology, although simple, generated interesting results. The obtained weights demonstrate that, for these assays, the instrumentation was more significant for the state prediction, as it has a higher penalty in the cost function. Figure 6.7 demonstrates this fact as for both assays, the state prediction is more closely related to the state variable prediction generated by the neural network.

**Figure 6.7 Assay 1 and 2 State Estimation Prediction**



Source: Author's library

**Figure 6.8 Assay 3 State Estimation Prediction – Low Solids Fed-batch**



Source: Author's library

In the initial stage of the process, this is a welcome trend, as the prediction generated by the instrumentation data follows the production of free carbohydrates more closely. However, in the late saccharification stages, when most of the biomass has been liquefied, the instrumentation reaches a plateau of prediction, since changes in the solids concentrations are not significant enough to alter the stirring power.

This generates a deviation between the filtered estimate and the compound concentration, presented in both assays. Using a more thorough tuning methodology can improve the estimator prediction, specially with more tuning weights possibilities.

However, a better alternative is the utilization of a dynamic weight, similar to the



fuzzy rule used in the fuzzy reaction rate model, to increase and decrease value according to the instrumentation necessity. The same trends discussed for the training assays were also observed in the validation assay. Demonstrating the necessity of further optimization in the state estimator.

#### 6.4. CONCLUSION

The ANN optimized in this study was capable of predicting the solids concentration in a robust manner. A state estimator was also constructed and tuned. It proved to be an interesting tool, however, its structure necessitates further optimization.

## 7. SEMISOLID HORIZONTAL SACCHARIFICATION BIOREACTOR DEVELOPMENT

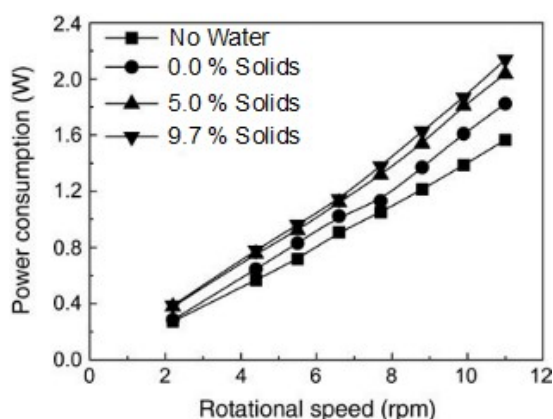
### 7.1. MOTIVATION AND OBJECTIVE

Horizontal Reactors (HR) can greatly increase the economics of the lignocellulosic biomass hydrolysis process, while retaining high conversion rates. However, in horizontal or standard reactors, a build up of insoluble material is unavoidable. The accumulation by the end of a fed-batch process may reach a level of solids close to those in the beginning of a unoptimized batch process.

A secondary characteristic of this type of reactor is the lack of separation between the liquid and solid phases of the slurry. This characteristic seems unnecessary at first, since most reactors do not separate phases. Yet, much can be gained from performing phase separation, both in the sense of energy consumption and reaction kinetics.

In a normal horizontal reactors, where the liquid and solid phases are agitated together, it is feasible to assume that the liquid agitation is responsible by most of the power consumption. This is supported by the work of Jin et al. (2010), where increasing the solids content inside the reactor had a smaller effect than adding more solids in the volumetric power consumption. This trend is presented in Figure 7.1.

**Figure 7.1** Volumetric Power Consumption in Horizontal Reactor



**Source:** Adapted from Jin et al. (2010)

At the rotational speed of 11 RPM, the empty reactor used, approximately, 1.58 W, adding water inside the reactor increased this value to 1.8 W. When 5% solids were added the power consumption increased to 2.1 W. Thus, the solids addition had a small effect in the power consumption when compared to the addition of water into the system. This is expected, since the liquid phase density is greater than the solids density and the mass of water inside the reactor is also higher than the solids mass.

Nevertheless, increasing the solids content from 5% to 9.7 % increased the power consumption to 2.18 W, demonstrating that after a threshold, increasing solids concentration causes a smaller power increment. This further demonstrates, as described previously, that operation at higher solids concentrations is more energy efficient.

Another plausible assumption is that the liquid phase does not requires intense agitation. The work of Liu et al., (2015) reinforces this hypothesis since it showed that an intense mixing liquefaction stage followed by subsequent no mixing saccharification stage did not reduce greatly the process conversion while reducing the total power consumption by 60 %, demonstrating that agitation may only be indispensable in initial hydrolysis stages. However, the initial mixing was realized in STR reactor, and under batch operation, when using a fed-batch policy agitation is required in other times other than the initial mixing, and mixing power can increase.

Thus, one can stipulate that separating liquid and solids phases and diminishing water content in the HR can decrease energy consumption. Furthermore, recirculating the separated liquid back into the HR can diminish enzyme inhibition issues that occurs under low water content.

Separating the phases also enables easy hydrolysis product withdraw. With the separated liquid, already free carbohydrates can be removed from the system, diminishing enzyme activity inhibition by product accumulation. This has been one of the objectives of developing membrane bioreactors. These use ultrafiltration to remove inhibitors from the medium, and increase cellulose conversion (Abels et al., 2013). However, these reactors come with high aggregated costs, since the membrane and its maintenance can be expensive (Pino et al., 2018).

The separated solids also enables more cost-effective manufacture of other high added value products. An interesting alternative is the production of nanocellulose compounds. These are a product of cellulose hydrolysis, under certain conditions, and can be used to generate polymers with application in different fields, from food packing to mechanical reinforcement of structures (Farinas et al., 2018).

Moreover, liquid and solids products independent removals means that their hydraulic retention times are decoupled. This is an important characteristic, as it generates more flexibility in the production plant. The liquid can be extracted earlier than the solids and be used in another process where it is required more rapidly, and solids hydrolysis can

continued unfazed to a desirable degree. This phase separation structure is used in other heterogeneous processes with high solids contents and high hydraulic retention times, as is the case biogas production from anaerobic fermentation.

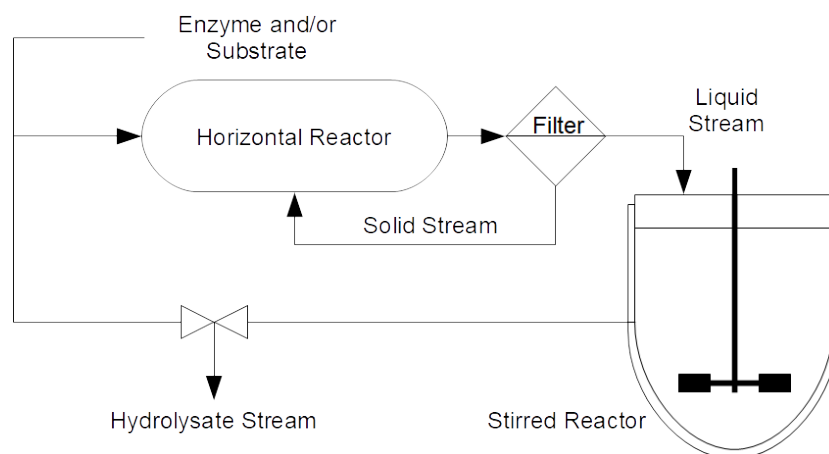
In anaerobic digestion of waste, a process involving several microorganisms immobilized in solids or free in the solution, several architectures of reactors have been developed to decouple liquid and solid phase reactions. These reactors are called Phase-Separated Reactors, and their main focus is diminishing reactor volume and retention time (Xu et al., 2016).

However, in this application, the utilization of phase separation means an increase in reactor cost, since anaerobic fermentation reactors are highly optimized and robust. Thus, increasing reactor complexity becomes unfeasible in waste management (Karthikeyan et al., 2016).

This happens because anaerobic fermentation is, usually, a waste management technology, and increase in investment cost is not easily translated into profitability. For biomass saccharification inside a biorefinery this is not true, since the reactor complexity increase can generate new production pathways inside the plant, from which several new products can be generated.

Due to all the described characteristics, the system presented in Figure 7.2 is proposed.

**Figure 7.2** Initial Proposal for Parallel Phase-Separated Hydrolysis Reactors



**Source:** Author's library

In the proposed architecture, the solids remain in the horizontal reactor, designed to operate at high solids concentrations, while the liquid phase is directed to a stirred tank

reactor. The separation between the phases is done by a passive filter, negating the necessity of additional energy. The liquid phase can be recirculated back into the horizontal reactor on demand.

The proposed system can operate under batch or fed-batch policies, with automated biomass feeding. The feeding system is necessary to diminish the instabilities originated from discrete feeding, specially in modeling, as well as to enable feeding control continuously.

To enhance data gathering, facilitating modeling and other studies, the system also possesses an automated sampler. The sampler enables liquid phase sampling without the necessity of an operator.

Therefore, this chapter objective is to describe the development and construction of horizontal and stirred tank parallel reactor system with phase-separation capabilities through a passive filter. Moreover, the development description of automated solids feeding and liquid phase sampler.

## 7.2. MATERIALS AND METHODS

### 7.2.1. Reactors Construction

The reactors were developed, designed, constructed and operated in the Laboratory for Development and Automation of Bioprocesses, in the Chemical Engineering Department, in the Federal University of São Carlos. The main characteristics that the reactor should attain to were:

- Automatic operation, with little to no operator supervision, besides during manual sampling.
- Phase-separation without the need for extra energy.
- Biomass saccharification energy consumption minimization when compared to STR.
- Automated solids feeding and liquid sampling.
- Scale-up capacity to any necessary volume.

To achieve these goals, different iterations of several parts of the system were tested, and altered if needed. The following items contains a description of the main parts development and their latest iteration.

### 7.2.1.1. Three Dimensional Modeling Software and Fast Prototype Hardware

Most reactors parts were designed in Fusion 360® da Autodesk® software, and were constructed in 3d printer Sethi 3D® S2®. The parts material were poly lactic acid.

### 7.2.2. System Control

The system control, i. e., the activation of motors, valves and pumps of the parallel reactors system was constructed in Arduíno® platform. A Arduíno Mega® was used a microcontroller. The algorithms were programmed and in the language and compiled in the native Arduíno® compiler.

### 7.2.3. Horizontal Reactor Power Consumption

The finished reactor power consumption was estimated by the model proposed by Wang et al. (2013), in this work, experimental data was used to fit a model that can predict the power number of a horizontal reactor, first loaded with only liquid phase and modified to predict power consumption with slurries.

However, Wang et al. (2013) generated a model for a reactor with baffles, and the horizontal reactor designed in this work does not have baffles. Nevertheless, as an initial rough estimate, the equation generated by the authors was extrapolated to an architecture without baffles, but using the original baffle relations.

This is feasible since the authors describes that the utilization of baffles, although improving mixing, increases power consumption. Thus, the value generated would only be overestimated, and can be used in early project stages. The modification of Wang's and collaborators to the baffleless reactor is presented in Equation 7.1

$$N_{PL} = 0.025 \cdot R_e^{0.106} \cdot F_r^{-0.807} \cdot N_R^{0.261} \cdot \left( \frac{V_L}{V_R} \right)^{-0.212} \cdot \left( \frac{L}{D} \right)^{3.85} \quad \text{Equation 7.1}$$

Where  $N_{PL}$  is the power number for the reactor when it is loaded with water,  $N_R$  is the reactor rotational speed ( $s^{-1}$ ),  $V_L$  is the volume of liquid inside the reactor ( $m^3$ ),  $V_R$  is the reactor total volume ( $m^3$ ),  $L$  is the reactor length (m),  $D$  is the reactor diameter (m).  $R_e$  is the Reynolds number described for flow in horizontal reactors, calculated with Equation 7.2, and  $F_r$  is the Froude Number, calculated with Equation 7.3.

$$R_e = \frac{\rho_L \cdot N_R \cdot D^2}{\mu_L} \quad \text{Equation 7.2}$$

$$F_r = \frac{N_R^2 \cdot D}{g} \quad \text{Equation 7.3}$$

Where,  $\rho_L$  is the liquid phase density ( $\text{kg}\cdot\text{m}^3$ ),  $\mu_L$  is the Liquid phase viscosity ( $\text{Pa}\cdot\text{s}$ ) and  $g$  is gravity's acceleration ( $\text{m}\cdot\text{s}^{-2}$ ). With the reactor's power number when loaded with liquid, the reactor's power number when loaded with a slurry ( $N_{ps}$ ) is calculated with Equation 7.4.

$$N_{PS} = \frac{\rho_L}{\rho_{SL}} \cdot N_{PL} \cdot (1 + \varphi^{0.13} + 0.0224 \cdot \varphi^{0.13} \cdot N_{PL}) \quad \text{Equation 7.4}$$

Where,  $\rho_{SL}$  is the slurry density ( $\text{kg}\cdot\text{m}^3$ ),  $\varphi$  is the solid phase volume fraction in the slurry.

With the modified power number, the specific power consumption of the reactor when loaded with a slurry ( $P_{LS}$   $\text{W}\cdot\text{m}^3$ ) is calculated with Equation 7.5.

$$P_{LS} = 2.9 \cdot N_R^{0.59} + \frac{N_{PL} \cdot \rho_L \cdot N_R \cdot D^5}{V_L} \quad \text{Equation 7.5}$$

This value is the estimate of power consumption if the reactor were loaded with a given amount of solids and no reaction occurs. If the value was calculated considering the saccharification of the biomass, it is feasible to assume that it would decrease over time in a batch policy.

### 7.3. RESULTS AND DISCUSSION

The reactors went through several versions to contemplate all the objectives while operating robustly. A global view of the parallel reactors and the Semisolid Horizontal Saccharification Bioreactor (SHSB) is presented in Figure 7.3.

**Figure 7.3** Parallel Phase-Separated Hydrolysis Reactors Design And Prototype

Fig. 7.3a

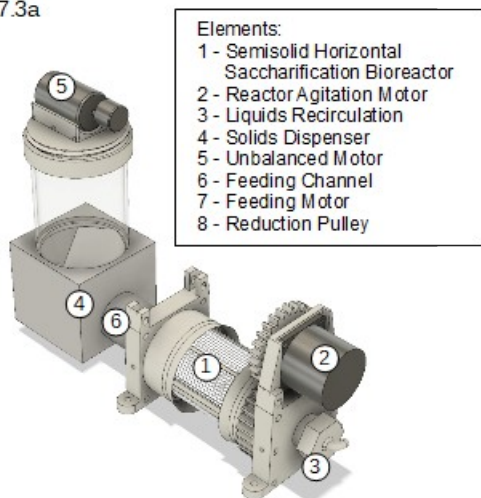
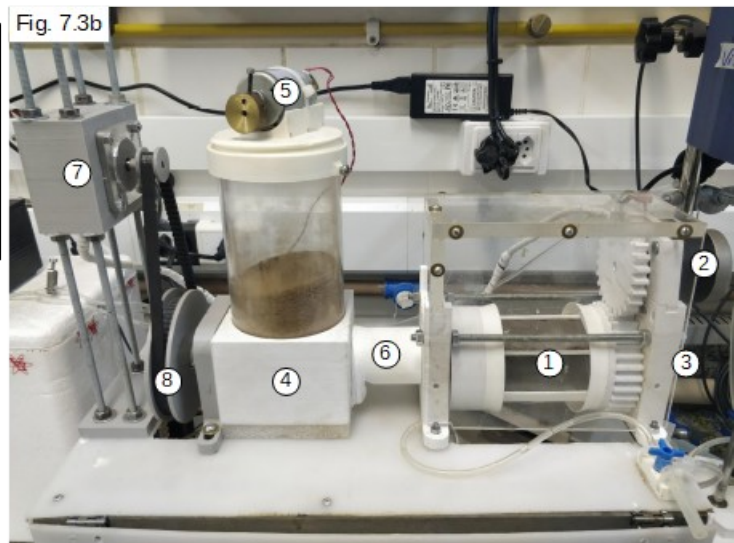


Fig. 7.3b



**Figure 7.3a** SHSB project; **Figure 7.3b** SHSB prototype.

**Source:** Author's library

Figure 7.3a presents the design in the three dimensional modeling software, and

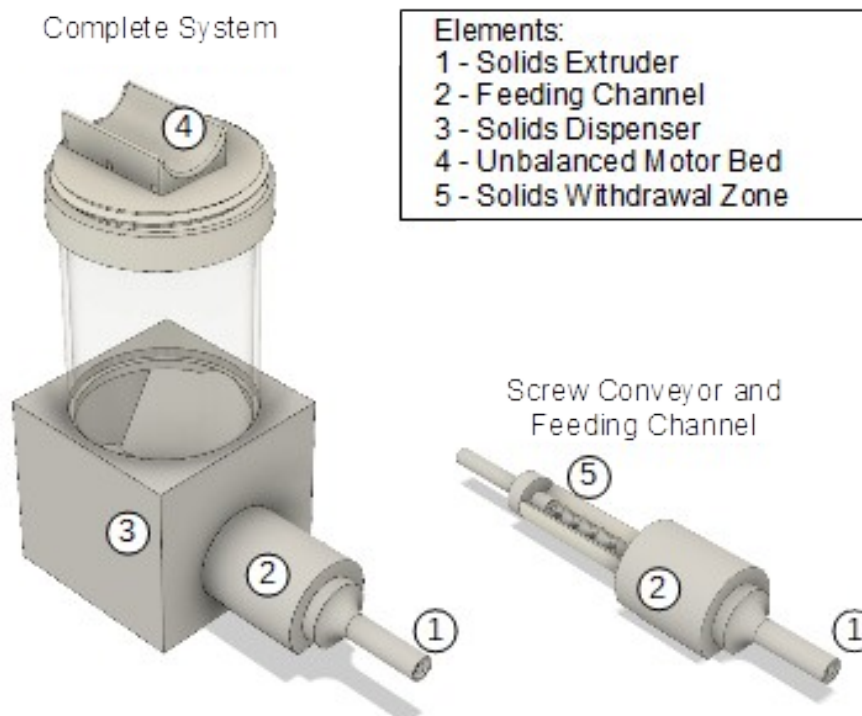
Figure 7.3b the assembled prototype.

### 7.3.1. Solids Feeding Hardware

The developed solids feeding basis is a screw conveyor coupled to a solids reservoir. The project of the system is presented in Figure 7.4. The feeder is powered by a stepper motor Moons® Nema 17 with 200 steps in each turn. The power of the motor is transmitted by a pulley and belt system, where a reduction of 8 times was applied. This was necessary as initial tests demonstrated that the power from the motor was insufficient to maintain a smooth operation. Several ratios were tested, and the 8:1 ratio generated the best results.

The motor is commanded by the system's main microcontroller. A stepper motor driver based on a L293D microchip. In the software, the libraries AccelStepper and AFMotor were used to provide the motor and driver commands functions.

**Figure 7.4** Solids Feeding System



**Source:** Author's library

The feeder operates by rotating the screw conveyor in the bottom of the solids dispenser. The solids used must have humidity close to 5 % to facilitate transport.

Initial tests of the systems demonstrated that after an initial period of constant solids feeding, the transport of biomass was interrupted, despite the screw continuing to rotate.



Troubleshooting demonstrated that the rotation of the screw inside the dispenser generated a packing of the bagasse bed around the screw. To prevent this issue, an unbalanced motor was placed on the top of the dispenser (Figure 7.4, Item 4). The motor was activated periodically, this generates a vibration inside the dispenser that breaks the bed packing and guarantees that the feeding continues.

The solids feeding, more precisely the screw conveyor, channel and extruder had two main versions. A larger initial version, with a bigger diameter, that occupied excessive amount of volume inside the SHSB. Therefore a new, smaller, version of all these components were designed and constructed.

To calibrate the feeder, it was mounted on the SHSB structure, and a scale connected to a computer was placed beneath it. The computer controlled the feeder to rotate 10 times and then read the scale value. This procedure was repeated for 1000 rotations, in three essays to determinate the mass of biomass dispensed by turn. The obtained value was  $7.492 \text{ mg.Turn}^{-1}$  with the associated standard error of  $0.012 \text{ mg.Turn}^{-1}$ .

Using the feeder within the reactor demonstrated that its operation is sensible to humidity. If the solids in the end of the screw becomes humid, either by the liquid vapor inside the reactor or by contact with humid solids, the water permeates quickly towards the solids reservoir. This increases the power to rotate the screw severely, to a point where either the motor begins to slip, or the screw breaks.

Several extruder ends were tested to shield the solids in the screw from becoming humid, these obtained mixed results. The main strategy to ensure that this does not occurs is operating the reactor with smaller solids in the reactor, diminishing the chance of dry and humid solids coming into contact.

### **7.3.2 Autosampler**

The autosampler, although not vital to the operation, is of great value, since it generates much more data from an assay. With more carbohydrate's concentration data obtained, modeling, monitoring and controlling subsequent stages are facilitated. The autosampler is presented in Figure 7.5.

## Figure 7.5 Autosampler System

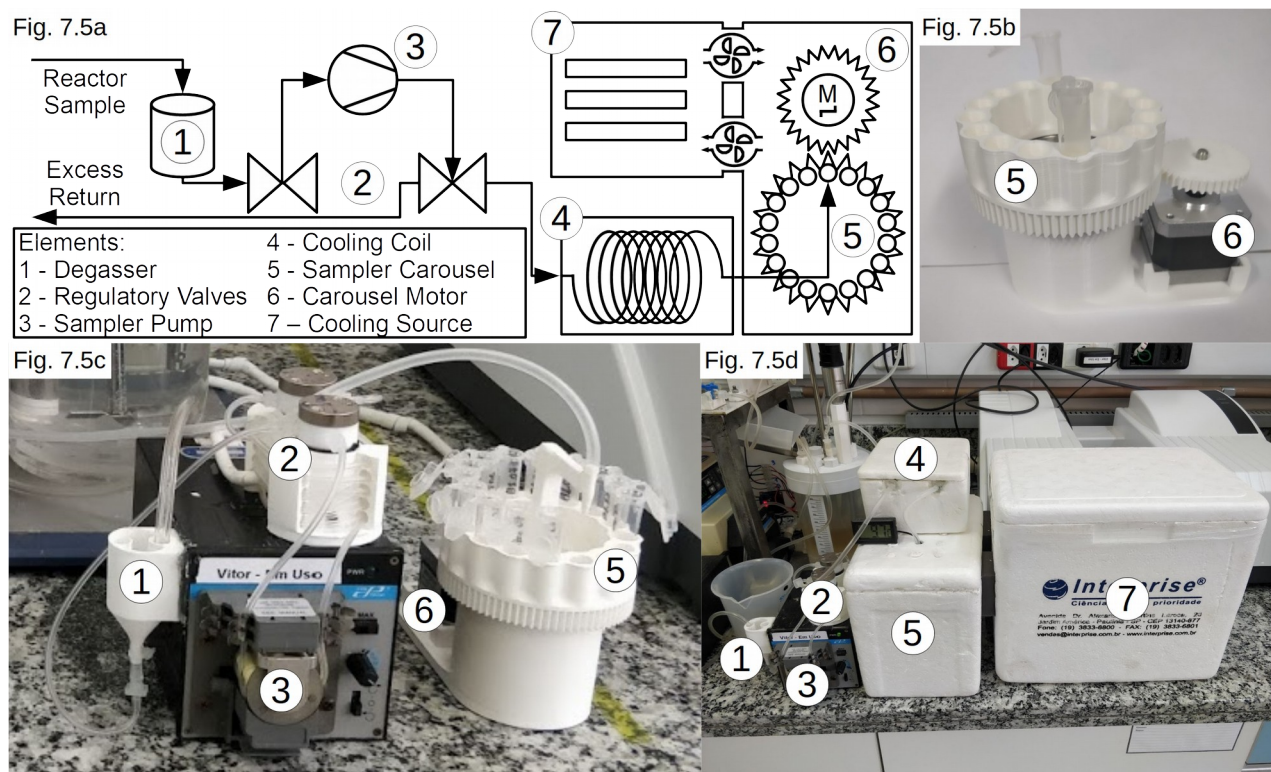


**Figure 7.5a** Autosampler schematics; **Figure 7.5b** Carousel sampler and motor coupling; **Figure 7.5c** Pumping and carousel coupling; **Figure 7.5d** Autosampler prototype.

**Source:** Author's library

Fig. 7.5a presents the sampler schematic and the other internal figures of Figure 7.5 depicts the experimental apparatus. The autosampler is controlled by the system's main microcontroller.

The autosampler operates by first receiving a liquid sample into the Degasser (Figure 7.5 – Item 1), this is an open vessel to remove any bubbles that might have been present in the liquid sample drawn from the reactor.

After the filling of the degasser, the Sampler Pump (Figure 7.5 – Item 3) was activated, this directs the sample through the Regulatory Valves (Figure 7.5 – Item 2). These valves are used to fix the amount of volume liquid that will be sampled. The tubing from the first valve to the second one has a length that amounts to 1.8 mL of sample. When the tubing is filled, the valves are activated, and the trapped liquid between them is directed to the sample vessel.

The sample is pumped through a Cooling Coil (Figure 7.5 – Item 4). This coil is a long section of coiled tubing residing inside a thermal box filled with ice water. It is used to quickly decrease the sample's temperature and diminish hydrolysis rate and preserve the

sample's carbohydrates concentration close to the one inside the reactor in the sampling time.

The sample passes through the cooling stage and is then directed to a sampling vessel. The vessel resides inside another thermal box, connected to another thermal box, the Cooling Source (Figure 7.5 – Item 7). This box contains ice packs used to decrease ambient temperature inside the boxes. Two coolers in the connections between the boxes promote air circulation from the source to the box containing the samples. This is used to keep the samples activity to a minimum, and further preserve the sample nature. Two 500g gel ice packs, at -86 °C, are placed in the cooling source and can keep the temperature at approximately 9 °C for 12 h.

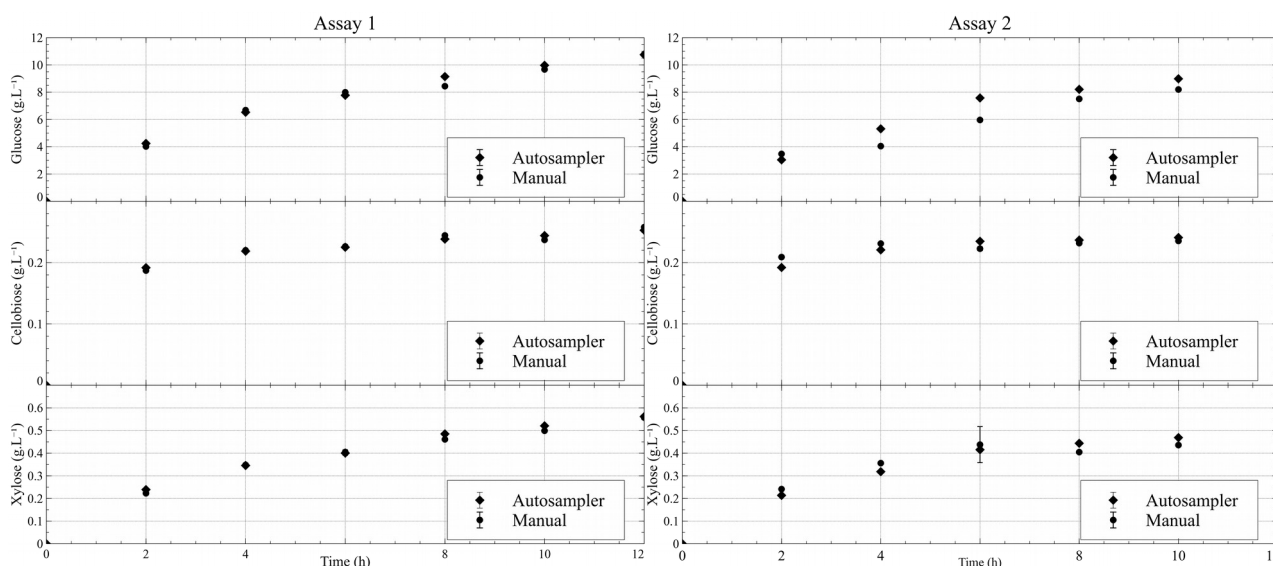
The sample vessels are placed in a rotating Sampler Carousel (Figure 7.5 – Item 5) this is linked to a stepper motor, the Carousel Motor (Figure 7.5 – Item 6). The motor is the same model and uses the same driver and libraries as the motor in the feeder. When the sample pouring into the vessel is completed, the motor is activated and the carousel rotates to the next empty sampling vessel. The carousel can store 18 vessels.

After the sampling procedure is completed, the valves are deactivated, and the remaining liquid inside the degasser is returned to the reactor. The entire sampling automatic operation lasts for approximately 12 min, and thus, this is the minimum sampling period for the instrument.

The sampler cooling system is a second iteration of the apparatus. The first version used no cooling method and instead relied in placing 0,2 mL of sodium hydroxide inside the sampling vessels to interrupt the hydrolysis reaction. This method proveded to be ineffective, as subsequent HPLC carbohydrates analysis showed that these decayed in the sampling vessels.

Thus, the cooling stages were implemented. To guarantee that the system was able to prevent products' concentration alterations, for two 12 h batch assays manual liquid sampling was performed alongside the autosampler every two hours. The manual sample was boiled immediately for 5 min to denature enzymes, halting the reaction and preserving the sample until HPLC was performed. The samples in the autosampler carousel were collected only in the ending of the assay, and boiled then. This enabled the comparison between the methodologies. Figure 7.6 presents methodologies comparison.

**Figure 7.6** Manual and Autosampler Concentrations



Error bar in data points are standard error for the compound concentration.

**Source:** Author's library

The data distribution demonstrated that the automated sampling and delayed denaturation obtained similar results from the manual methodology, and thus, it can be used with the reactor.

### 7.3.3 Semisolid Horizontal Saccharification Bioreactor

The SHSB project was previously presented in Figure 7.3. Its name is derived from the phase separation technology used in the reactor. The reactor wall is lined with filtering material, as presented in Figure 7.7, the mesh retained the solids while liquids were free to permeate. This left very little free water in the horizontal drum, thus generating a semisolid reactive media.

**Figure 7.7** Horizontal Filtering Media Drum

Fig. 7.7a



Fig. 7.7b

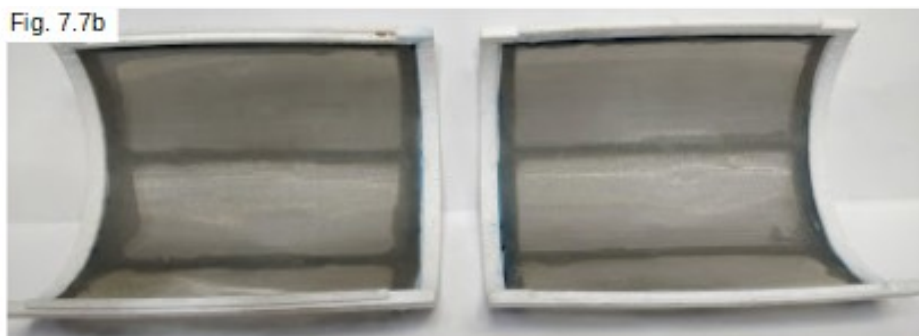


**Figure 7.7a** Filtering media project; **Figure 7.7b** Filtering media prototype.

**Source:** Author's library

The external structures were printed, and the filter was fixated to its interior. As

filtering medium, a stainless steel mesh, with aperture 0.074 mm (Tyler 200). A first version of the horizontal drum had a mesh with aperture 0.500 mm (Tyler 32), this mesh proved to be ineffective, as dry solids would permeate through the sieve.

Another version of the horizontal was constructed with screw like baffles. These were constructed as a coil with a triangular profile fixed to the reactor wall. Two coils were used, if the reactor were to be divided into three sections, one coil was placed in the first third of the reactor, where the solid feeding occurs, it would carry solids to the middle third of the reactor, that was kept empty, and another in the last third, facing the opposite direction, to carry towards the middle section as well. This version prototype is presented in Figure 7.8.

**Figure 7.8** Horizontal Reactor with Screw Baffle – Mid Section Cut



**Source:** Author's library

These were added to improve slurry mixing inside the reactor. However, when applied, the solids were not dry enough to move freely, and the slurry did not have enough liquid to behave as a liquid, and the solids remained in the extremities with the coils walls acting as barriers to movement. Thus, the interior baffles were excluded from subsequent test.

In the extremities of the horizontal drum, septa were used to prevent free water flow through the ends of the reactor instead of the filtering medium. The septa placement is presented in Figure 7.9.

## Figure 7.9 Septa Positioning

Fig. 7.9a



Fig. 7.9b

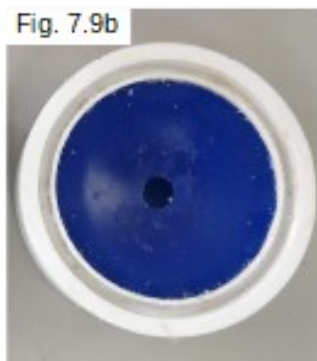


Fig. 7.9c

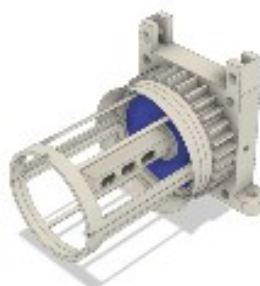


Fig. 7.9d



**Figure 7.9a** Septum project in the feeder side; **Figure 7.9b** Feeder Septum; **Figure 7.9c** Septum project in the dripper side; **Figure 7.9d** Dripper septum.

**Source:** Author's library

The septa have orifices with the size of the hardware that passes through it. This improved the liquid retention inside the SHSB. This was necessary since in initial trials liquid was lost through the reactor's extremities.

The horizontal drum is coupled to a bearing mounted on a flange. On top of the right flange is the stepper motor responsible by the reactor rotation (Figure 7.3, Item 2). The motor and shield is equal to the ones in the feeding and sampler apparatus. The motor is coupled to one the reactors bearing mounts via a gear system in both. There is no reduction applied in this motor.

### 7.3.4 Stirred Tank Reactor and Liquid Recirculation

The SHSB is coupled to a STR. The STR is made of acrylic tubing, and its lid was modeled and printed to be used in the parallel reactor system. The lid has several entrances for different instrumentation probes and hardware from the system. Figure 7.10 demonstrates both reactors coupled.

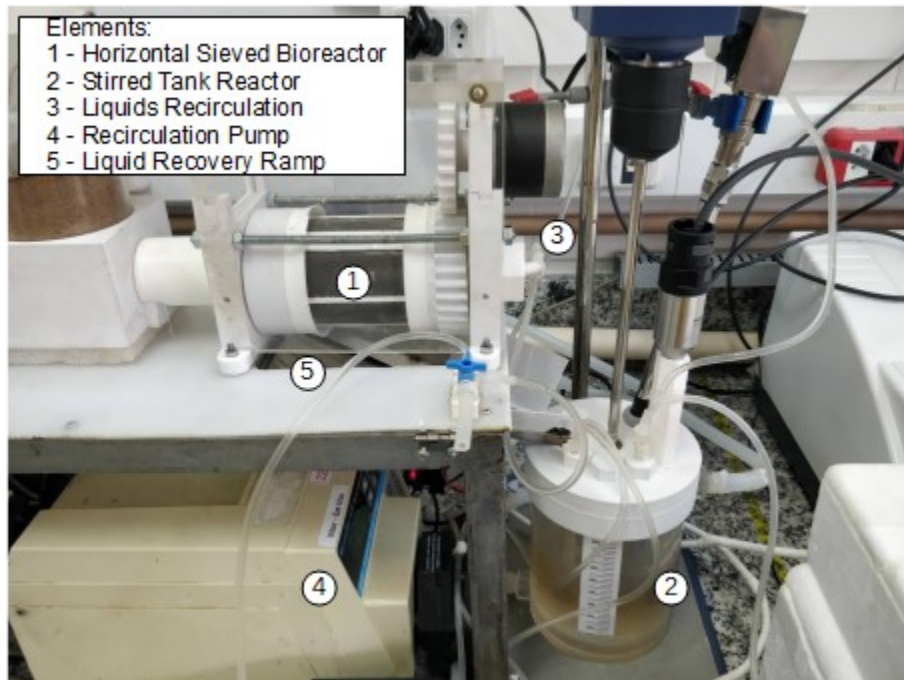
The SHSB is mounted in a stainless steel frame to be raised from the base of the STR. This facilitates integration between the reactors and liquid flow. The frame also has mounts for the solids feeder and the liquid recovery ramp.

Liquid from the STR is transported to the SHSB by a peristaltic pump (Figure 7.10 Item 4), this is directed to a dripper that spreads the liquid inside the horizontal reactor. The dripper (Figure 7.10 Item 3) project and prototype is presented in Figure 7.11.

The dripper was the most altered and redesigned part of the entire system. Several architectures were tested, from using perforated hoses outside of the reactor, to several

tubed in different locations inside the reactor and from all these iterations the dripper was the one that displayed the best trade-off between robust operation and liquid dispersion.

**Figure 7.10** Parallel Reactors Coupling



**Source:** Author's library

**Figure 7.11** Horizontal Reactor Dripper

Fig. 7.11a

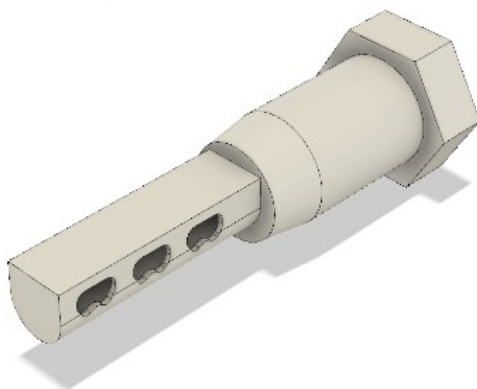


Fig. 7.11b



**Figure 7.11a** Dripper project; **Figure 7.11b** Dripper prototype.

**Source:** Author's library

The orifices are placed in a square profile section, above a semicircular section. The liquid flows from the bottom of the circular section and rises until the holes are reached. This improves flow through all orifices simultaneously. Silicon tubes are tied through the holes from one side of the dripper to the other. This helps to break surface

tension in the liquid and homogenize flow along all the exits in the dripper.

After recirculation to the interior of the SHSB, the liquid mixes with the solids and then permeates through the filter. The liquid is recuperated by slanted ramp, the ramp directs the liquid back to the STR interior.

During operation, to emulate an industrial scale solids feeding, an equivalent amount of liquid is fed to the STR. This is done because it is feasible to assume that with larger scale hardware the solids will not need to be dried to facilitate transport. A secondary peristaltic pump is used to perform this addition. Another pump is responsible for enzymatic cocktail feeding.

### **7.3.5 Power Consumption Estimate**

Using the dimensions of the constructed SHSB, diameter of 75 mm and length 92 mm, power consumption was calculated with Equations 7.1 through 7.5.

To do so a hypothetical process was assumed. The reactor was considered to be loaded slurry composed of 180 ml of liquid with a density of  $1 \text{ kg.L}^{-1}$  and 20 g of solids with a density of  $0,147 \text{ kg.L}^{-1}$ , determined by measuring the volume of a 100 g of biomass. The reactor walls were assumed to be not permeable, i. e., the mass inside the reactor remains constant, and the rotational speed was 5 RPM.

This is an approximation of a batch process initial condition, before the hydrolysis occurred, loaded with the maximum possible amount of a slurry with 15 % solids. This is the worst case scenario for power consumption, when the reactor is at capacity working, and no reduction in the mass inside it occurred. Therefore, it is feasible to assume that the power consumption at this condition is the maximum that the reactor can create.

It is also important emphasize that the reactor architecture deviates from the one used by Wang et al. (2013) to fit the models, and thus, its extrapolation can differ from actual values.

Nevertheless, with these conditions, the reactor obtained a power consumption of  $50.58 \text{ W.m}^{-3}$ . This value is less than half the lower bound ( $100 \text{ W.m}^{-3}$ ) of the specific power range for an industrial reactor (Bouquet and Morin, 2006). This value is also far lower than values obtained during hydrolysis in STRs ( $15.000 \text{ W.m}^{-3}$  in Battista et al. (2018)), and lower than in hydrolysis reactors in similar horizontal architecture ( $560 \text{ W.m}^{-3}$  in Dasari et al. (2009)).



The consumption level, as is expected via analysis of Equation 7.5 and empirical knowledge, increases rapidly with the rotational speed of the reactor. Reducing this velocity to 1 RPM, maintaining the other variables, decreases power consumption to 5.03 W.m<sup>3</sup>, a full order of magnitude smaller than the value with 5 RPM. However, this can hinder reactor mixing. Thus, this is an important variable that need to be optimized.

Further studies are also necessary to fully describe the consumption behavior of the parallel reactors, since other secondary apparatus are necessary, increasing power necessity. Data from actual power consumption during the hydrolysis process are also necessary.

Nevertheless, these values are a major improvement in power consumption for the biomass saccharification stage.

#### 7.4. CONCLUSION

Operating new reactors is a complex task. Unforeseen behaviors can be expected, and a significant amount of empirical knowledge needs to be acquired before the reactor can operate robustly. Frequently, initial assays are discontinued due to severe issues in the reactor operation. The data from the interrupted process is also often lost.

This was the case for the parallel reactors, as from the first 8 assays, only 4 were successful to a degree where the generated data were reliable enough to enable examination.

Nevertheless, these initial experiments with the hardware are necessary to improve the platform overall robustness. With the subsequent operations, and the empirical changes in the parts, the reactor issues were decreased, to a degree where all described independent systems, solids feeder, autosampler and parallel reactor operated concurrently with no issues. Validating this system as a biomass saccharification technology.

The SHSB phase-separation capacity was also validated. Where little to no solids were washed to the interior of the STR.

The solids feeding hardware also operated successfully. After configuration optimization, biomass was fed to the system in a robust manner. The utilization of the unbalanced motor on top of the dispenser was the fundamental system change that enabled the system utilization, without it, it is likely that a screw conveyor based system

would be unsuccessful.

This enables several research opportunities since the fed-batch biomass hydrolysis solids feeding profile is no more bounded to discrete feedings. This is an important result, since, as presented in Table 3.2, only the work of Tai et al. (2015) used an automated feeding system, and in this case, the used instrument was only capable of working with very fine powders. Although an important tool in fed-batch studies, using the biomass as a fine powder can generate deviations from the large scale process, since the biomass state can influence hydrolysis.

Using the architecture proposed here, however, is a more appropriate approximation of the apparatus used in production plants, and thus, a better starting point for scale up calculations. Furthermore, with minor alterations, this system can be applied to other reactors that may benefit from solids feeding.

The autosampler also operated in a satisfactory fashion. With this instrument, more data can be generated from an assay, improving subsequent studies with the generated data. This instrument can also be easily modified to be used in other reactors.

Another important conclusion regards the power consumption of the SHSB. A significant decrease in energy necessity is estimated in this reactor. To a degree that may enable its application in a biorefinery.

Therefore, the SHSB here developed is a novel reactor architecture, that can be easily scaled to larger volumes, and can generate several new production routes within the biorefinery, with or without its utilization parallel to another reactor.

## 8. SEMISOLID HORIZONTAL MESH BIOREACTOR APPLICATION

### 8.1. MOTIVATION AND OBJECTIVE

After the development of the parallel reactors, initial trials with the architecture were performed. These were used to both test the hardware and the reactors' operational characteristics. To establish initial dynamics behavior elucidation, trials under batch and fed-batch operational policies were applied. During the reactors operation, instrumentation in the liquid phase was also applied in order to initiate data gathering for future monitoring softwares.

Monitoring reactions and estimating its state variable is a difficult task. Several methodologies are available, and each application usually demands special tools. The selection of which tool is to be used can occur in different ways, however, in some form or another, different methodologies have to be used to enable performance comparison. As initial monitoring trial, a Partial Least Square algorithm was applied to instrumentation and compounds concentration to determine if this tool is useful in this application. Thus, this chapter objective is to perform assays in the parallel reactors under batch and fed-batch policies with instrumentation and to test initial monitoring software.

### 8.2. MATERIAL AND METHODS

#### 8.2.1. Batch and Fed-batch Assays

With the system described in chapter 7, two assays were performed in duplicate. A 12 h batch and a 48 h fed-batch assay. Both used a total of 20 g of hydrothermally pretreated biomass, as described in item 4.1. In the batch assay all the substrate was added into the SHSB before the beginning of the process, in the fed-batch 5 g was added in the beginning in the horizontal reactor and the 15 g remaining were added by the feeder from the first to the 36<sup>th</sup> h of the process, resulting in a mass flow of approximately 7 mg.min<sup>-1</sup>.

The assays were initiated by adding to the dry pretreated biomass enough buffer to generate a slurry with 15% solids. Enzymatic cocktail was added to the slurry in this stage. Enzyme loading was 12.5 mg<sub>protein</sub>.g<sub>solids</sub><sup>-1</sup> (approximately 10 FPU.g<sub>substrate</sub><sup>-1</sup>), calculated with the 20g of final substrate mass. In the fed-batch assay, a concurrent feeding of buffer was used to simulate a feeding with 15 % solids, by adding, roughly, the 40 μL.min<sup>-1</sup>.

The STR was initiated with 400 mL of citrate buffer. This volume was used to ensure

that the instrumentation inside the liquid reactor could work properly. Every 8 h, 50 mL of distilled water was added to counteract the system evaporation.

### **8.2.2. Analytical Procedures**

Analytical procedures occurred in two ways. With the automated sampler and via manual sampling.

#### **8.2.2.1. Automated Sampling**

Liquid phase from the STR reactor was collected by the autosampler every 2 h, in the method described in item 7.3.2, and the vessels with the samples remained in the autosampler until the next manual sampling period. At this moment, the samples were retrieved, boiled for 5 min and kept under refrigeration until subsequent analysis. In these samples, free and potential carbohydrates were determined. During the manual sampling, fresh ice was added in the autosampler cooling coil and the ice packs in the cooling source were changed.

#### **8.2.2.2. Manual Sampling**

Manual sampling occurred every 6 h in the batch process and every 8 h in the fed-batch. Liquid phase was sampled and FCA was performed in it as described in item 4.5.2.

Sample from the solids were also sampled at this time. Approximately 5 g of slurry were removed from the SHSB. This mass was placed in a glass petri dish and Near Infrared Reflectance Analysis (NIRA) with a Frontier NIR Standard from Perkin Elmer® with NIRA attachment. This instrument scanned the solid through reflectance from 10000  $\text{cm}^{-1}$  to 4000  $\text{cm}^{-1}$  with 4  $\text{cm}^{-1}$  resolution

The slurry sample was divided, 1 g was used to determinate moisture, evaluated in moisture analyzer ID50 from Mater Balanças®, and the rest was suspended in 50 mL of water, boiled for 10 min to stop adsorbed enzymes activities. After boiling, the sample was placed in a vacuum aided filtering apparatus with a general purpose filter paper and washed with 200 mL of water. The washed solids in the filter were then dried for 24h at 40 °C in kiln. The dry solids were scraped of the filter and kept under refrigeration until further analysis could be performed.

### **8.2.3. Process Monitoring**

During the assays, several instrumentation probes were added to the STR. These

instruments were used to generate data, that together with the data from the analytical procedures, could be used in subsequent modeling and monitoring stages.

#### 8.2.3.1. Near Infrared Spectrum Scanning

A reflectance probe Falcata 6 was used coupled to a Frontier NIR Standard from Perkin Elmer®. This instrument performed NIR scans every 6 min of process that ranged from 10000  $\text{cm}^{-1}$  to 1200  $\text{cm}^{-1}$  with 4  $\text{cm}^{-1}$  resolution.

#### 8.2.3.2. Ultraviolet and Visible Spectrum Scanning

A reflectance probe was also applied in the STR, coupled to a Lambda 456 from Perkin Elmer®. This instrument performed scans in the Ultraviolet and Visible (UV/VIS) region of the light spectrum every 6 min of process that ranged from 180 nm to 1100 nm with 1 nm resolution.

#### 8.2.3.3. Capacitance and Conductance Scanning

An Incyte Cell Density Sensor from Hamilton® was placed in the STR. This instrument performed permittivity ( $\text{pF}\cdot\text{cm}^{-1}$ ) and conductance ( $\text{mS}\cdot\text{cm}^{-1}$ ) measurements in the reactive media every 6 min.

#### 8.2.3.4. Software Sensor Modeling

The data obtained with the automated carbohydrate sampling were used with the on-line data from the NIR and UV/VIS spectrum scans from the time where carbohydrate sampling occurred to calibrate PLS model to be used as a soft sensor. Separate models for each spectrum range were developed.

Data from both batch assays and one fed-batch assay were used as fitting data to generate the PLS model, and one fed-batch was used as test data, to evaluate extrapolation.

To determine the number of regressors in each PLS, a cross validation procedure was used, in a manner similar to item 6.2.7. In this instance, 88% of the training data was used in each fitting evaluation, and 12% was used as validation data. The optimum architecture was chosen based on the deviation between training and test data error, as described in Figure 6.4.

### 8.3. RESULTS AND DISCUSSION

#### 8.3.1. Analytical Results

A first important result that should be observed is the slurry moisture analysis, for it did not change during assays, maintaining a level of approximately 85% independent of the reactor policy and hydrolysis degree. This behavior means that effectively the SHSB operates at a fixed value of 15 % solids, irregardless of feeding policy.

At first, this seems to be an issue, since higher solids concentrations are unattainable. However, when considering that the liquid phase hydraulic retention time is decoupled from the solids retention time, and that it can be recirculated back into the horizontal reactor at will, it becomes clear that this is an advantage of this structure.

Since solids are naturally kept at 15%, the product concentration varies only with the volume of recirculated liquid phase. If a more concentrated product is necessary, less liquid phase in the STR can be used.

This can help diminish product concentration after hydrolysis, possibly enabling the usage of the saccharification liquid phase with the sugarcane juicy without dilution of the latter.

Furthermore, the reactor performance is no longer bounded to its maximum solids concentration, and can be operated until its maximum working volume is reached without losing mixing efficiency. Thus, if more biomass needs to be processed, an architecture change is not necessary, only additional reactors or a larger reactor.

Data from the remaining analytical procedures applied in the assays are presented in Figure 8.1 for the batch assay, and in Figure 8.2 for the fed-batch assay.

The figures demonstrate that the parallel reactors were successful in hydrolyzing the biomass, to a degree similar to other studies described in Table 3.2. However, this value may be underestimated.

Since the liquid phase is separated from the solids and recirculates back into the reactor, it is responsible for carrying the sugars formed from the solids into the STR. One can stipulate that if the flow of liquid is not enough, an accumulation of carbohydrates occurs in the liquid surrounding the solids, thus, considering that the sugar concentration is homogeneous throughout the reactor liquid phase can become unrealistic, and the evaluated mass of sugars is smaller than the actual value. Therefore, strategies to retrieve more sugars from the horizontal reactor are necessary.

**Figure 8.1** Parallel Reactors Batch Assay Analytical Data

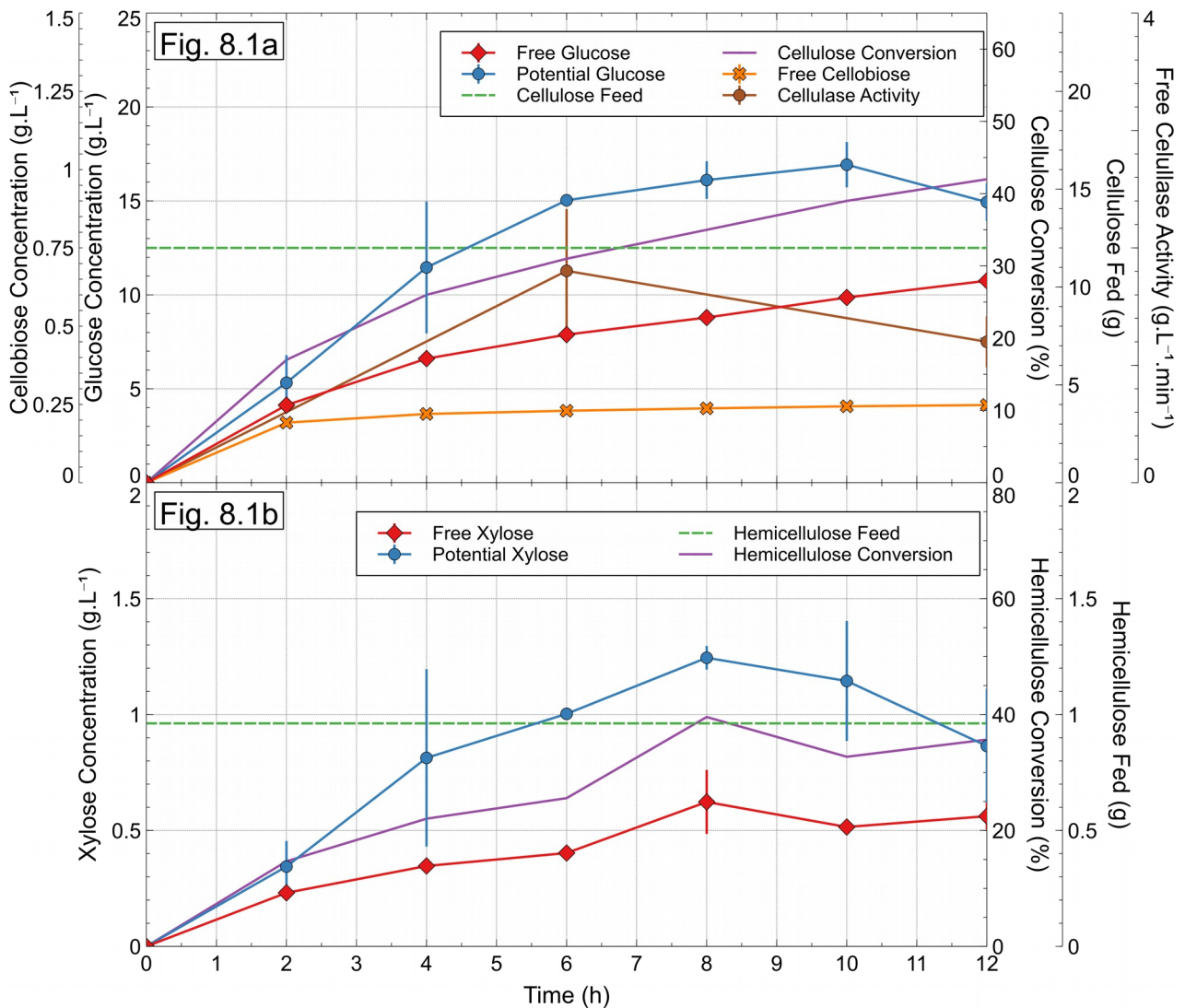


**Figure 8.1a** Data from cellulose related variables; **Figure 8.1b** Data from hemicellulose related variables.

**Source:** Author's library

In both policies, a clear accumulation of polymerized carbohydrates from cellulose and hemicellulose occurs. Conversion can be improved if these were further hydrolyzed. If conversion of cellulose was calculated at the end of the fed-batch assay with the potential glucose concentration instead of the free glucose concentration, conversion would increase from 37.7 % to 68.9 %. Therefore, a significant amount of sugars are not being fully hydrolyzed due to cocktail inhibition.

This is further supported by trend in free cellulase activity from both assays. An initial increase of activity is observed, followed by a sharp decrease. This happens because the enzyme was mixed with the solids prior to adding it to the reactor. It is

feasible to assume that the medium recirculation promotes washing of some enzymes from the solids, increasing the activity in the liquid phase. The subsequent decrease occurs due to several effects, as described in item 3.4.2.4.

**Figure 8.2** Parallel Reactors Fed-batch Assay Analytical Data

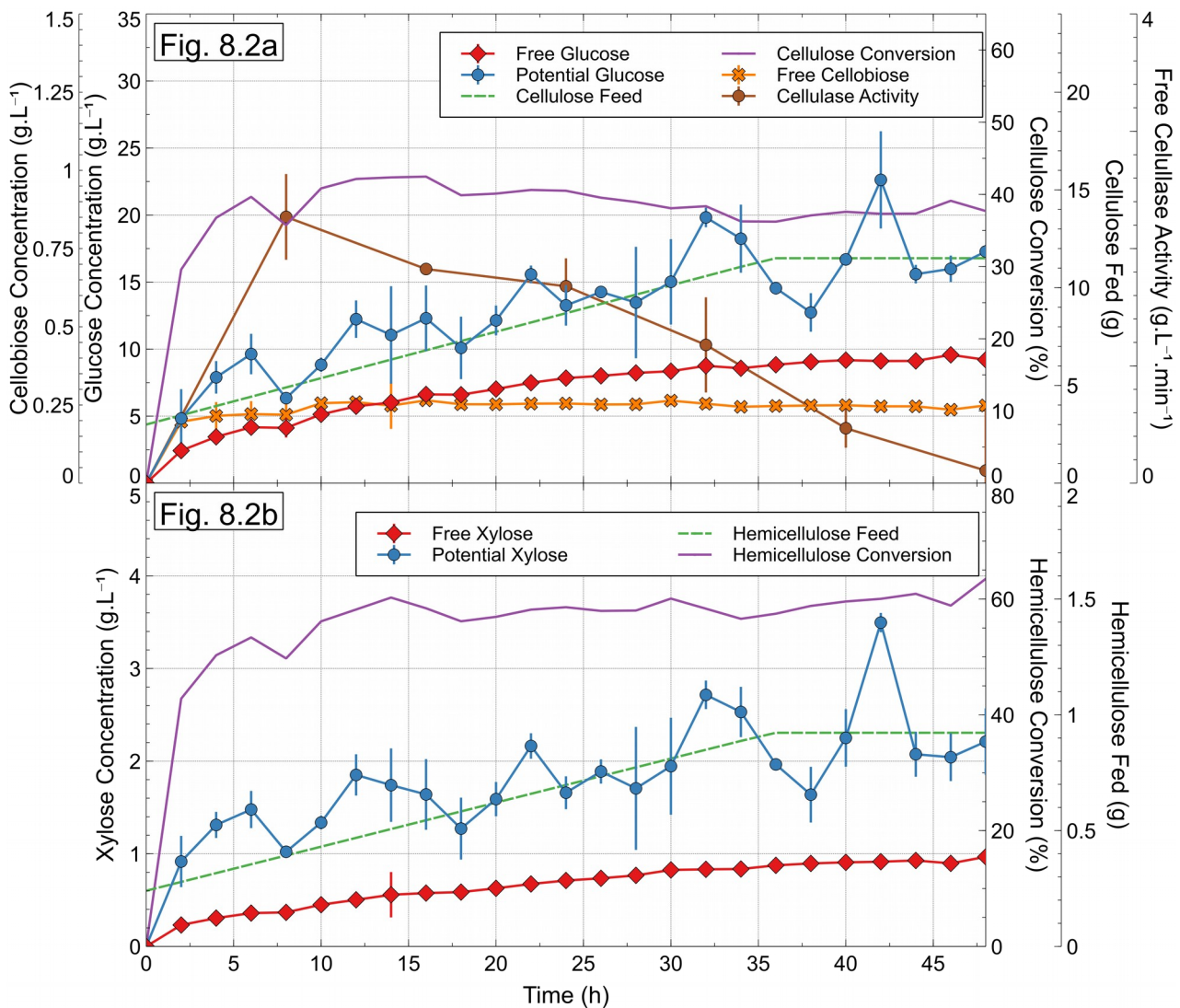


**Figure 8.2a** Data from cellulose related variables; **Figure 8.2b** Data from hemicellulose related variables.

**Source:** Author's library

To overcome this behavior, several strategies can be employed. One alternative is adding more cocktail during the process, in particular,  $\beta$ -glucosidases, as cellobiose quickly rises and enter a pseudo-stationary state. Since cellobiose is an intermediate of glucose production, and described to be an inhibitor of cellulose hydrolysis (Angarita et al., 2015), supplementing this enzyme can improve conversion, but causing an increase process cost. To reduce the cost increase, since this enzyme catalyzes a homogeneous



reaction, an immobilized version of this enzyme can be used in the STR.

However, another critical aspect of the free cellulase activity analysis from both assays must be observed. Even though the assays were initiated with the same amount of cocktail but with different initial solids loadings, free activity was similar between both in the process beginning.

The batch assay, initialized with 20 g of solids and  $12.5 \text{ mg}_{\text{protein}} \cdot \text{g}_{\text{substrate}}^{-1}$ , had in its first data point a free activity and standard error of  $1.80 \pm 0.53 \text{ g} \cdot \text{L}^{-1} \cdot \text{min}^{-1}$ , the fed-batch assay, with the same amount of enzyme but with only 5 g of solids, had  $2.27 \pm 0.37 \text{ g} \cdot \text{L}^{-1} \cdot \text{min}^{-1}$  in its first activity analysis. A T-test with 95 % confidence level demonstrates that there is no significant statistical difference between the means.

This is unexpected. It would be simpler to assume that when mixing a amount of enzyme to two different masses of solids, a smaller free cellulase activated was to be encountered when more solids were used. However, the amount of solids does seem to have little effect in the amount of adsorbed cellulases. This appears to show that the concentration of enzyme is in excess, or, the amount of available substrate is limiting.

The concentrations of potential glucose and free cellobiose further aids this observation, since after two hours no significant statistical difference is observed in this variable between the assays. This may indicate that the solids were liquefied in the same initial rate.

Even though the errors in the activity measurements are relatively high, this is an important conclusion. This demonstrates that high initial loads of enzymes may not increase liquefaction speed. Considering also that enzymes are more susceptible to inhibition the longer they are inside the reactor, adding enzyme throughout the process can greatly improve its performance.

### **8.3.2. Online Instrumentation Data**

Instrumentation data from the assays are presented in Figure 8.3 for the batch assay, and in Figure 8.4 for the fed-batch assay.

Instrumentation from optical scanning of the liquid sample seems to present a trend of increasing absorbance through the processes. In the UV/VIS it appears to be strong in the range of 200 to 380 nm, this is specially interesting since it is the range at which soluble lignin compounds peak absorbance occurs (Sluiter et al., 2012).

**Figure 8.3** Parallel Reactors Batch Assay Instrumentation Data

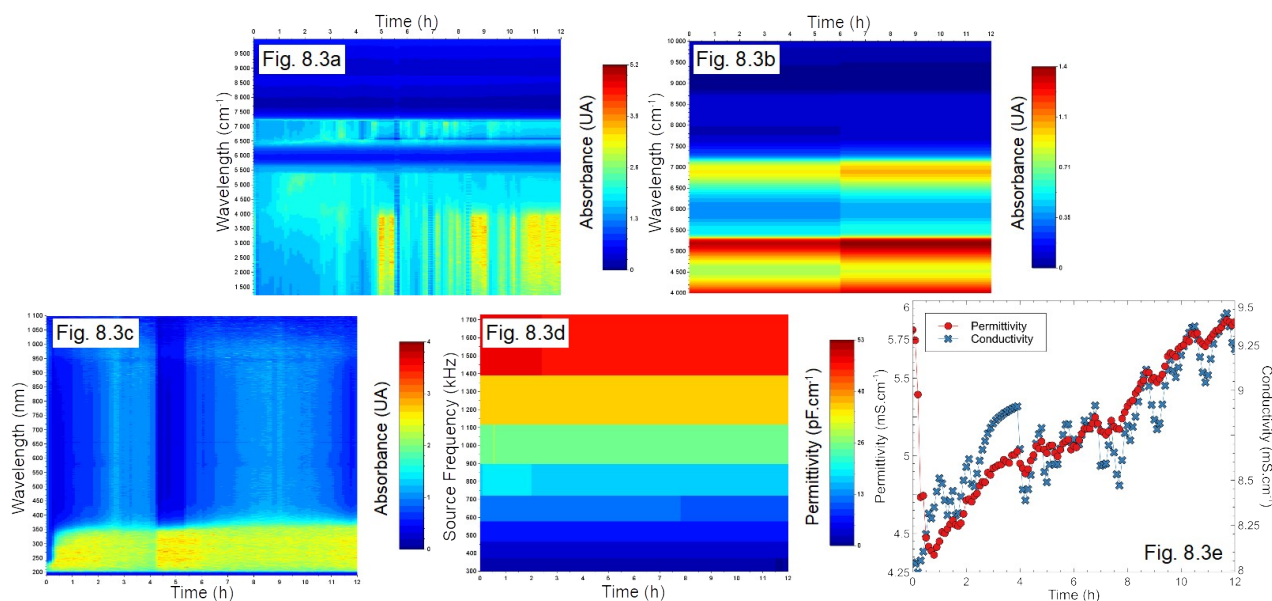


**Figure 8.3a** NIR liquid scanning; **Figure 8.3b** NIR solids scanning; **Figure 8.3c** UV/VIS liquid scanning; **Figure 8.3d** Permittivity scanning; **Figure 8.3e** Permittivity and Conductivity measurement.

Source: Author's library

**Figure 8.4** Parallel Reactors Fed-batch Assay Instrumentation Data

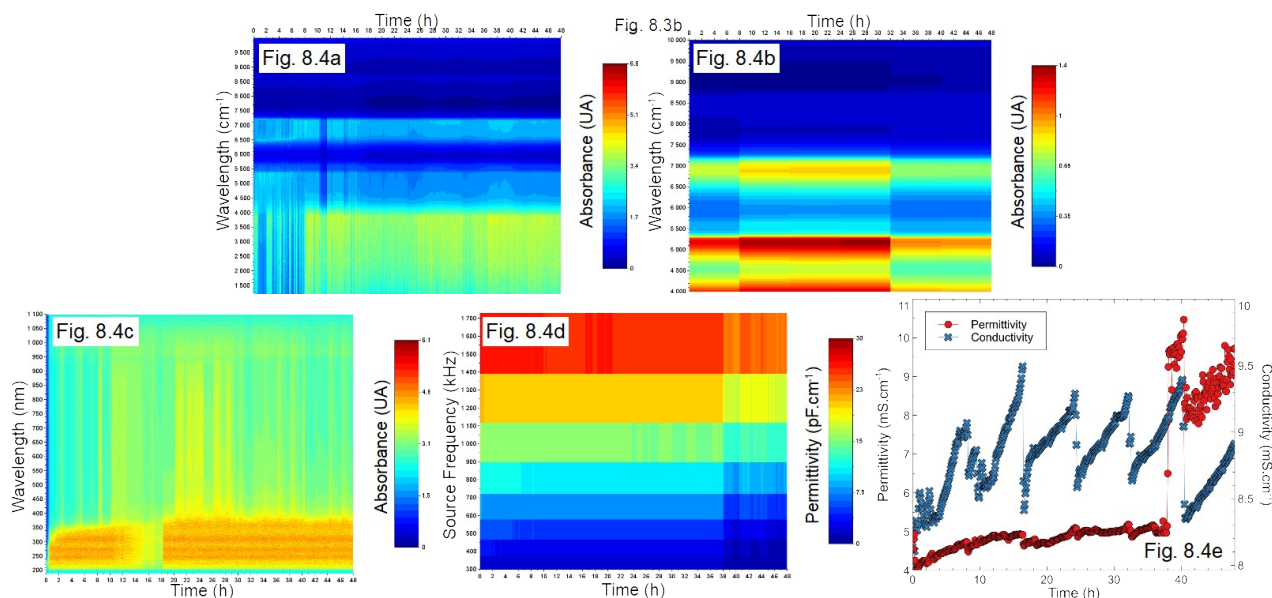


**Figure 8.4a** NIR liquid scanning; **Figure 8.4b** NIR solids scanning; **Figure 8.4c** UV/VIS liquid scanning; **Figure 8.4d** Permittivity scanning; **Figure 8.4e** Permittivity and Conductivity measurement.

Source: Author's library

A similar phenomenon occurs in the NIR liquid scanning, from 7200 to 1100  $\text{cm}^{-1}$ . Even though no clear substance or group of substance can be solely credited as being

responsible for absorbing in this range, it has been proven to be able to monitor the reactions with similar substrates (Pinto et al., 2016).

### 8.3.3. Software Sensor Monitoring

The data from NIR and UV/VIS monitoring presented in the previous item were used to compose the PLS models. Analytical free carbohydrates and instrumentation data from the batch assays and one fed-batch assay were used to fit the model with the cross validation method, and the remaining fed-batch assay data was used to test the model extrapolation capacity.

The algorithm, as it stands, was unable to generate models from the NIR data. This was due to the amount of data generated by each assay, during the fed-batch the NIR scans generate  $4.22 \cdot 10^6$  data-points, thus, any processing of these data is computationally expensive. Even though only the scans from when analytical data is available were used, a data pretreatment stage is still necessary in order to enable modeling, and thus, no model is presented.

For the UV/VIS data, the fitting was possible, and the cross validation result for number of eigenvectors in the regression is presented in Figure 8.5.

**Figure 8.5** Cross Validation for PLS Fitting With UV/VIS Data

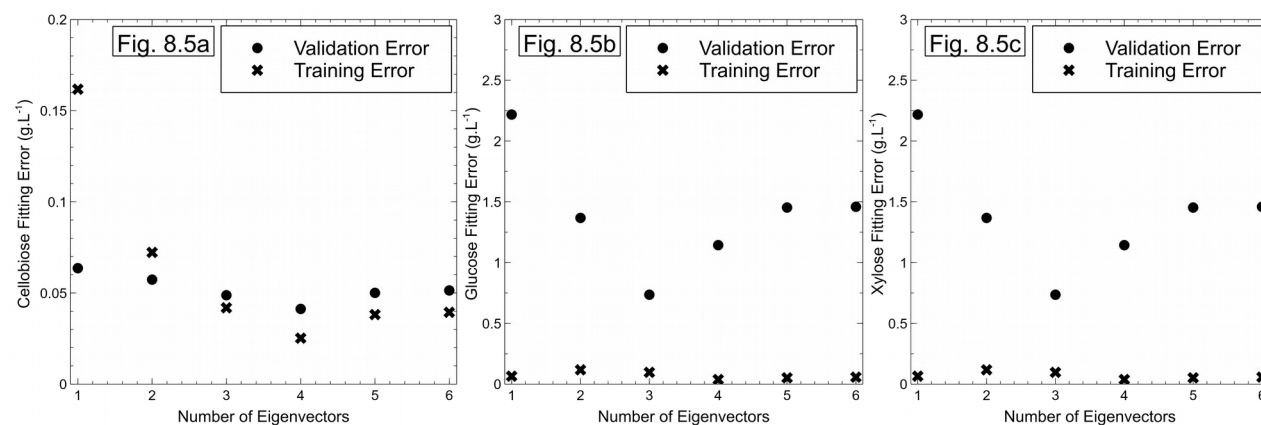


**Figure 8.5a** Cross Validation for Glucose Concentrations; **Figure 8.5b** Cross Validation for Cellobiose Concentrations; **Figure 8.5c** Cross Validation for Xylose Concentrations.

**Source:** Author's library

For all the predicted carbohydrates, the deviation between training and validation error occurred when 3 eigenvectors were used as dimensions for the partial regression. Thus, this value was used for the regression. The model prediction for the test fed-batch data is presented in Figure 8.6.

**Figure 8.6** Prediction for PLS Regression With UV/VIS Data

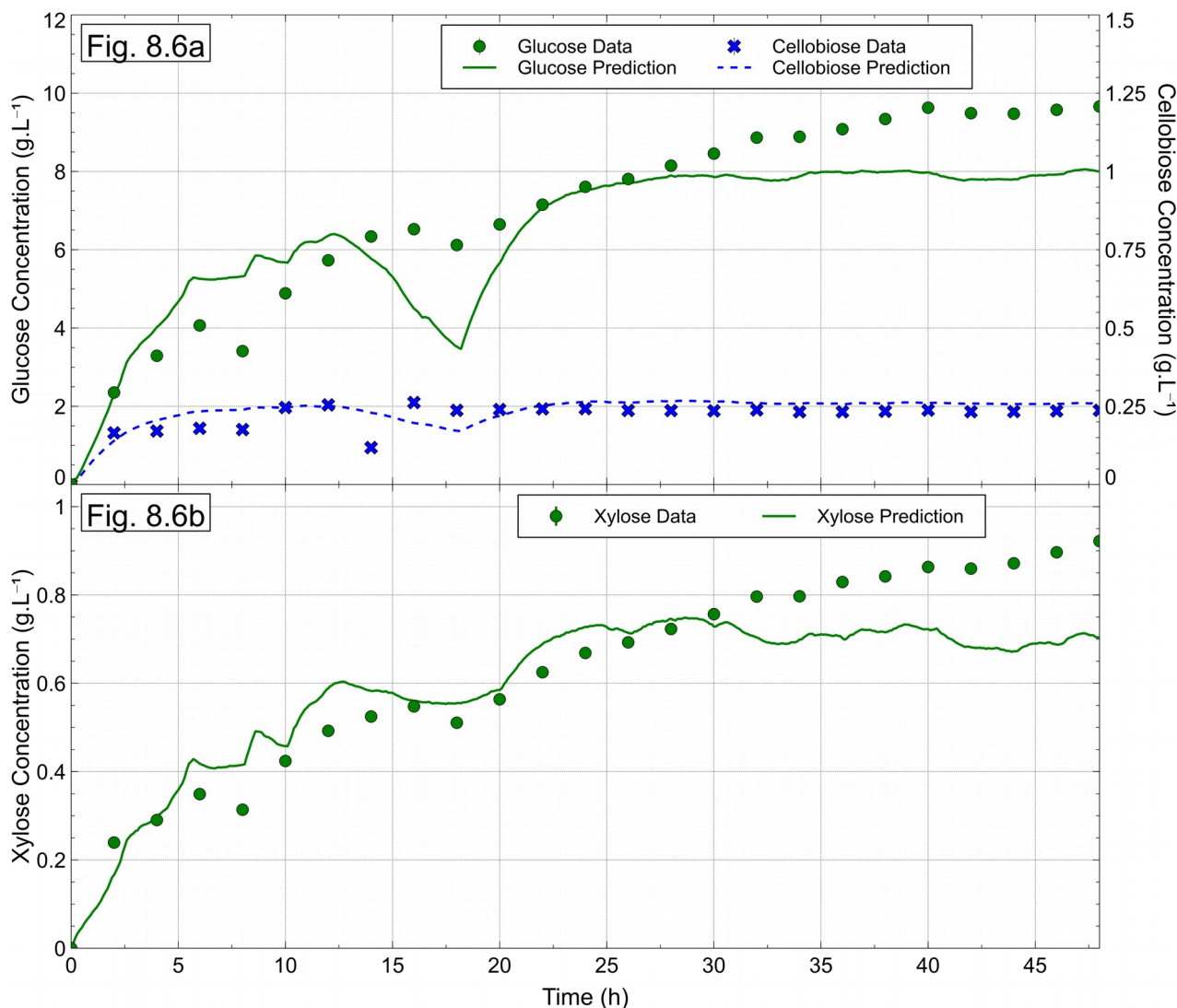


**Figure 8.6a** Cellulose Related State Variables UV/VIS PLS Prediction; **Figure 8.6b** Xylose UV/VIS PLS Prediction.

**Source:** Author's library

A good adherence was achieved with the model as is. However, it is highly susceptible to instrumentation data noise. Specially the formation of unexpected bubbles in the probes, as this is an optical measurement. To overcome this effect, the data from the other instruments must be added into the software sensor layer. Furthermore, the studies of modeling and state estimation described in previous chapter should also be applied in the parallel reactors.

#### 8.4. CONCLUSIONS

Lignocellulosic biomass hydrolysis performance with the parallel reactors was similar to other reactors conversionwise, with the added capacity of separating reaction

phases. The SHSB reactor operates under conditions that are not common in other reactors, opening new possibilities of control policies, that could improve overall process efficiency.

PLS proved to be a promising tool to monitor the saccharification process. However, further studies are necessary to apply the full data generated from instruments, as well as to improve monitoring capacity.

## 9. CONCLUSIONS

Several conclusions can be drawn from the studies presented in this thesis. First by enhancing modeling and monitoring of the saccharification process under different operational policies, and also by altering the reactor in which the process is conducted.

Fuzzy enhanced modeling improved the prediction of simple kinetic models in high solids saccharification in stirred tank reactors. Monitoring was also possible using simplified instrumentation and models in this architecture.

The main result here presented is the new reactor structure for lignocellulosic material hydrolysis. Using a horizontal reactor capable of separating the liquid and solid phases of the reaction and using a parallel stirred tank coupled to it can not only diminish the energy necessary to conduct the process, but can also generate new processing technologies within the biorefinery. This is achieved with small reactor complexity increase, and while retaining process performance when compared to similar architectures.

Further studies are necessary to fully described the saccharification process in the reactors in order to fully optimize its performance and explore new process technologies.

## **10. FURTHER STUDIES**

- Apply more feeding profiles to the parallel reactors systems. Specially policies with continuous addition of enzyme.
- Apply the soft-sensor methodology to the remaining instrumentation data. Including the solids analysis data in the soft-sensor.
- Modify the modeling and monitoring softwares developed for the stirred-tank reactor to operate with the data from the parallel reactors.

## REFERENCES

- Abels, C., Thimm, K., Wulfhorst, H., Christine, A., Wessling, M., 2013. Membrane-based recovery of glucose from enzymatic hydrolysis of ionic liquid pretreated cellulose. *Bioresour. Technol.* 149, 58–64. <https://doi.org/10.1016/j.biortech.2013.09.012>
- Aditiya, H.B., Mahlia, T.M.I., Chong, W.T., Nur, H., Sebayang, A.H., 2016. Second generation bioethanol production : A critical review. *Renew. Sustain. Energy Rev.* 66, 631–653. <https://doi.org/10.1016/j.rser.2016.07.015>
- Adney, B., Baker, J., 2008. Measurement of Cellulase Activities - Laboratory Analytical Procedure.
- Aguiar, R.S., Silveira, M.H.L., Pitarelo, A.P., Corazza, M.L., Ramos, L.P., 2013. Kinetics of enzyme-catalyzed hydrolysis of steam-exploded sugarcane bagasse. *Bioresour. Technol.* 147, 416–423. <https://doi.org/10.1016/j.biortech.2013.08.067>
- Al-hadithi, B.M., Jiménez, A., Matía, F., 2012. A new approach to fuzzy estimation of Takagi – Sugeno model and its applications to optimal control for nonlinear systems. *Appl. Soft Comput. J.* 12, 280–290. <https://doi.org/10.1016/j.asoc.2011.08.044>
- Amornchai, A., Shomchoam, N., 2009. Neurocomputing Control of fed-batch bioreactors by a hybrid on-line optimal control strategy and neural network estimator. *Neurocomputing* 72, 2297–2302. <https://doi.org/10.1016/j.neucom.2009.01.002>
- Angarita, J.D., Souza, R.B.A., Cruz, A.J.G., Biscaia Jr, E.C., Secchi, A.R., 2015. Kinetic modeling for enzymatic hydrolysis of pretreated sugarcane straw. *Biochem. Eng. J.* 104, 10–19. <https://doi.org/10.1016/j.bej.2015.05.021>
- Bailey, C.J., 1989. Enzyme kinetics of cellulose hydrolysis. *Biochem. J.* 262, 1001–1002.
- Balat, M., 2011. Production of bioethanol from lignocellulosic materials via the biochemical pathway : A review. *Energy Convers. Manag.* 52, 858–875. <https://doi.org/10.1016/j.enconman.2010.08.013>
- Bansal, P., Hall, M., Realf, M.J., Lee, J.H., Bommaris, A.S., 2009. Modeling cellulase kinetics on lignocellulosic substrates. *Biotechnol. Adv.* 27, 833–848. <https://doi.org/10.1016/j.biotechadv.2009.06.005>
- Bastin, G., Dochain, D., 1990. *On-line Estimation and Adaptive Control of Bioreactors*, 1st



ed. ed. Elsevier, Amsterdam, Neatherlands.

- Battista, F., Almendros, M.G., Rousset, R., Boivineau, S., 2018. Enzymatic hydrolysis at high dry matter content : The influence of the substrates' physical properties and of loading strategies on mixing and energetic consumption. *Bioresour. Technol.* 250, 191–196. <https://doi.org/10.1016/j.biortech.2017.11.049>
- Battista, F., Bolzonella, D., 2018. Some critical aspects of the enzymatic hydrolysis at high dry-matter content: a review. *Biofuels, Bioprod. Biorefining* 12, 711–723. <https://doi.org/10.1002/bbb.1883>
- Beeson, W.T., Phillips, C.M., Cate, J.H.D., Marletta, M.A., 2011. Oxidative Cleavage of Cellulose by Fungal Copper-Dependent Polysaccharide Monooxygenases. *IEEE J. Quantum Electron.* 134, 890–892. <https://doi.org/10.1109/JQE.1997.641329>
- Berry, H., 2002. Monte Carlo Simulations of Enzyme Reactions in Two Dimensions : Fractal Kinetics and Spatial Segregation. *Biophys. J.* 83, 1891–1901.
- Bezerra, R.M., Dias, A.A., 2004. Discrimination Among Eight Modified Michaelis-Menten Kinetics Models of Cellulose Hydrolysis With a Large Range of Substrate/Enzyme Ratios. *Appl. Biochem. Biotechnol.* 112, 173–184.
- Bhowmick, G. De, Sarmah, A.K., Sen, R., 2018. Lignocellulosic biorefinery as a model for sustainable development of biofuels and value added products. *Bioresour. Technol.* 247, 1144–1154. <https://doi.org/10.1016/j.biortech.2017.09.163>
- Bondancia, T.J., Corrêa, L.J., Cruz, A.J.G., Badino, A.C., Mattoso, L.H.C., Manoel, J., 2018. Enzymatic production of cellulose nanofibers and sugars in a stirred-tank reactor: determination of impeller speed, power consumption, and rheological behavior. *Cellulose* 25, 4499–4511. <https://doi.org/10.1007/s10570-018-1876-2>
- Bouquet, F., Morin, D., 2006. BROGIM®: A new three-phase mixing system testwork and scale-up. *Hydrometallurgy* 83, 97–105. <https://doi.org/10.1016/j.hydromet.2006.03.040>
- Bryant, D.N., Firth, E., Kaderbhai, N., Taylor, S., Morris, S.M., Logan, D., Garcia, N., Ellis, A., Martin, S.M., Gallagher, J.A., 2013. Monitoring real-time enzymatic hydrolysis of Distillers Dried Grains with Solubles ( DDGS ) by dielectric spectroscopy following hydrothermal pre-treatment by steam explosion. *Bioresour. Technol.* 128, 765–768. <https://doi.org/10.1016/j.biortech.2012.09.021>

- Campbell, M.K., Farrel, S.O., 2007. *Bioquímica - Combo*, 1st ed. ed. São Paulo, Brazil.
- Canilha, L., Chandel, A.K., Suzane, T., Antunes, F., Luiz, W., Grac, M., Felipe, A., Silv, S., 2012. Bioconversion of Sugarcane Biomass into Ethanol: An Overview about Composition , Pretreatment Methods , Detoxification of Hydrolysates , Enzymatic Saccharification , and Ethanol Fermentation 2012. <https://doi.org/10.1155/2012/989572>
- Cara, C., Moya, M., Ballesteros, I., Negro, M.J., González, A., Ruiz, E., 2007. Influence of solid loading on enzymatic hydrolysis of steam exploded or liquid hot water pretreated olive tree biomass. *Process Biochem.* 42, 1003–1009. <https://doi.org/10.1016/j.procbio.2007.03.012>
- Cardona, C.A., Quintero, J.A., Paz, I.C., 2010. Production of bioethanol from sugarcane bagasse: Status and perspectives. *Bioresour. Technol.* 101, 4754–4766. <https://doi.org/10.1016/j.biortech.2009.10.097>
- Carrillo, F., Lis, M.J., Colom, X., López-Mesas, M., Valldeperas, J., 2005. Effect of alkali pretreatment on cellulase hydrolysis of wheat straw: Kinetic study. *Process Biochem.* 40, 3360–3364. <https://doi.org/10.1016/j.procbio.2005.03.003>
- Carvalho, M.L., Jr, R.S., Suarez, C.A.G., 2013. Kinetic study of the enzymatic hydrolysis of sugarcane bagasse. *Brazilian J. Chem. Eng.* 30, 437–447.
- Cavalcanti-montaña, I.D., Alberto, C., Suarez, G., Giordano, R.D.C., Júnior, R.D.S., 2013. Optimal Bioreactor Operational Policies for the Enzymatic Hydrolysis of Sugarcane Bagasse. *BioEnergy Res.* 6, 776–785. <https://doi.org/10.1007/s12155-013-9294-7>
- Chandra, R.P., Au-yeung, K., Chanis, C., Roos, A.A., Mabee, W., Pablo, A., Ghatora, S., Saddler, J.N., 2011. The Influence of Pretreatment and Enzyme Loading on the Effectiveness of Batch and Fed-Batch Hydrolysis of Corn Stover. *Biotechnol. Prog.* 27, 77–85. <https://doi.org/10.1002/btpr.508>
- Chen, H., Qiu, W., 2010. Key technologies for bioethanol production from lignocellulose. *Biotechnol. Adv.* 28, 556–562. <https://doi.org/10.1016/j.biotechadv.2010.05.005>
- Chiamonti, D., Prussi, M., Ferrero, S., Oriani, L., Ottonello, P., Torre, P., Cherchi, F., 2012. Review of pretreatment processes for lignocellulosic ethanol production , and development of an innovative method. *Biomass and Bioenergy* 46, 25–35. <https://doi.org/10.1016/j.biombioe.2012.04.020>

- Cornish-Bowden, A., 2013. The origins of enzyme kinetics. *FEBS Lett.* 587, 2725–2730. <https://doi.org/10.1016/j.febslet.2013.06.009>
- Corrêa, A.C., Teixeira, E. de M., Pessa, L.A., Mattoso, L.H.C., 2010. Cellulose nanofibers from curaua fibers Cellulose nanofibers from curaua fibers. <https://doi.org/10.1007/s10570-010-9453-3>
- Corrêa, L.J., Badino, A.C., Cruz, A.J.G., 2016a. Power consumption evaluation of different fed-batch strategies for enzymatic hydrolysis of sugarcane bagasse. *Bioprocess Biosyst. Eng.* 39, 825–833. <https://doi.org/10.1007/s00449-016-1562-4>
- Corrêa, L.J., Badino, A.C., Cruz, A.J.G., 2016b. Mixing design for enzymatic hydrolysis of sugarcane bagasse : methodology for selection of impeller configuration. *Bioprocess Biosyst. Eng.* 39, 285–294. <https://doi.org/10.1007/s00449-015-1512-6>
- Daniel, R.M., Danson, M.J., 2013. Temperature and the catalytic activity of enzymes : A fresh understanding. *FEBS Lett.* 587, 2738–2743. <https://doi.org/10.1016/j.febslet.2013.06.027>
- Dantas, G.A., Legey, L.F.L., Mazzone, A., 2013. Energy from sugarcane bagasse in Brazil : An assessment of the productivity and cost of different technological routes. *Renew. Sustain. Energy Rev.* 21, 356–364. <https://doi.org/10.1016/j.rser.2012.11.080>
- Dasari, R.K., Dunaway, K., Berson, R.E., 2009. A Scraped Surface Bioreactor for Enzymatic Saccharification of Pretreated Corn Stover Slurries. *Energy & Fuels* 492–497.
- Dias, M.O.S., Cunha, M.P., Jesus, C.D.F., Rocha, G.J.M., Geraldo, J., Pradella, C., Rossell, C.E. V, Maciel, R., Bonomi, A., 2011. Second generation ethanol in Brazil : Can it compete with electricity production ? *Bioresour. Technol.* 102, 8964–8971. <https://doi.org/10.1016/j.biortech.2011.06.098>
- Dias, M.O.S., Junqueira, T.L., Cavalett, O., Cunha, M.P., Jesus, C.D.F., Rossell, C.E. V, Maciel, R., Bonomi, A., 2012. Integrated versus stand-alone second generation ethanol production from sugarcane bagasse and trash. *Bioresour. Technol.* 103, 152–161. <https://doi.org/10.1016/j.biortech.2011.09.120>
- Dias, M.O.S., Junqueira, T.L., Cavalett, O., Pavanello, L.G., Cunha, M.P., Jesus, C.D.F., Maciel, R., Bonomi, A., 2013. Biorefineries for the production of first and second generation ethanol and electricity from sugarcane. *Appl. Energy* 109, 72–78.

<https://doi.org/10.1016/j.apenergy.2013.03.081>

- Dochain, D., 2003. State and parameter estimation in chemical and biochemical processes : a tutorial 13, 801–818. [https://doi.org/10.1016/S0959-1524\(03\)00026-X](https://doi.org/10.1016/S0959-1524(03)00026-X)
- Dodds, S.A., Heath, W.P., 2005. Construction of an online reduced-spectrum NIR calibration model from full-spectrum data B 76, 37–43. <https://doi.org/10.1016/j.chemolab.2004.09.002>
- Du, J., Zhang, F., Li, Y., Zhang, H., Liang, J., Zheng, H., Huang, H., 2014. Enzymatic liquefaction and saccharification of pretreated corn stover at high-solids concentrations in a horizontal rotating bioreactor. *Bioprocess Biosyst. Eng.* 37, 173–181. <https://doi.org/10.1007/s00449-013-0983-6>
- Dyk, J.S. Van, Pletschke, B.I., 2012. A review of lignocellulose bioconversion using enzymatic hydrolysis and synergistic cooperation between enzymes — Factors affecting enzymes , conversion and synergy. *Biotechnol. Adv.* 30, 1458–1480. <https://doi.org/10.1016/j.biotechadv.2012.03.002>
- Eko, Y., Sugiharto, C., Harimawan, A., Tri, M., Penia, A., Purwadi, R., Mariyana, R., Nur, H., Fathmadinda, H., 2016. Enzyme feeding strategies for better fed-batch enzymatic hydrolysis of empty fruit bunch. *Bioresour. Technol.* 207, 175–179. <https://doi.org/10.1016/j.biortech.2016.01.113>
- Farinas, C.S., Marconcini, J.M., Mattoso, L.H.C., 2018. Enzymatic Conversion of Sugarcane Lignocellulosic Biomass as a Platform for the Production of Ethanol, Enzymes and Nanocellulose 6, 203–216. <https://doi.org/10.7569/JRM.2017.6341578>
- Fenila, F., Shastri, Y., 2016. Optimal control of enzymatic hydrolysis of lignocellulosic biomass. *Resour. Technol.* 2, S96–S104. <https://doi.org/10.1016/j.reffit.2016.11.006>
- Furlan, F.F., Filho, R.T., Pinto, F.H.P.B., Costa, C.B.B., Cruz, A.J.G., Giordano, R.L.C., Giordano, R.C., 2013. Bioelectricity versus bioethanol from sugarcane bagasse : is it worth being flexible ? 1–12.
- Furlong, V.B., 2015. Automation of a reactor for enzymatic hydrolysis of sugar cane bagasse : Computational intelligence-based adaptive control.
- Gandla, M.L., Martín, C., Jönsson, L.J., 2018. Analytical Enzymatic Saccharification of Lignocellulosic Biomass for Conversion to Biofuels and Bio-Based Chemicals.

Energies 11, 1–20. <https://doi.org/10.3390/en11112936>

Ghose, T.K., 1987. Measurement of Cellulase Activities. *Pure Appl. Chemistry* 59, 257–268. <https://doi.org/10.1111/j.1468-2389.1995.tb00038.x>

Gouveia, E.R., Nascimento, R.T., Souto-Maior, A.M., 2009. Validacao de metodologia para a caracterização química de bagaco de cana-de-açucar. *Quim. Nova* 32, 1500–1503.

Guo, F., Shi, W., Sun, W., Li, X., Wang, F., Zhao, J., Qu, Y., 2014. Differences in the adsorption of enzymes onto lignins from diverse types of lignocellulosic biomass and the underlying mechanism 1–10.

Gupta, R., Kumar, S., Gomes, J., Kuhad, R.C., 2012. Kinetic study of batch and fed-batch enzymatic saccharification of pretreated substrate and subsequent fermentation to ethanol. *Biotechnol. Biofuels* 5, 16. <https://doi.org/10.1186/1754-6834-5-16>

Haaland, D.M., Thomas, E. V., 1988. Partial Least-Squares Methods for Spectral Analyses. 1. Relation to Other Quantitative Calibration Methods and the Extraction of Qualitative Information. *Anal. Chem.* 60, 1193–1202. <https://doi.org/10.1021/ac00162a020>

Haerifar, M., Azizian, S., 2014. Fractal-Like Kinetics for Adsorption on Heterogeneous Solid Surfaces. *J. Phys. Chem.* 118, 1129–1134.

Haseltine, E.L., Rawlings, J.B., 2005. Critical Evaluation of Extended Kalman Filtering and Moving-Horizon Estimation. *Ind. Eng. Chem. Res.* 44, 2451–2460. <https://doi.org/10.1021/ie034308l>

Hernández-beltrán, J.U., Hernández-escoto, H., 2018. Enzymatic hydrolysis of biomass at high-solids loadings through fed-batch operation. *Biomass and Bioenergy* 119, 191–197. <https://doi.org/10.1016/j.biombioe.2018.09.020>

Hildén, L., Johansson, G., 2004. Recent developments on cellulases and carbohydrate-binding modules with cellulose affinity. *Biotechnol. Lett.* 26, 1683–1693. <https://doi.org/10.1007/s10529-004-4579-8>

Hodge, D.B., Karim, M.N., Schell, D.J., Mcmillan, J.D., 2009. Model-Based Fed-Batch for High-Solids Enzymatic Cellulose Hydrolysis. *Appl. Biochem. Biotechnol.* 152, 88–107. <https://doi.org/10.1007/s12010-008-8217-0>

Hodge, D.B., Karim, M.N., Schell, D.J., Mcmillan, J.D., 2008. Soluble and insoluble solids

- contributions to high-solids enzymatic hydrolysis of lignocellulose. *Bioresour. Technol.* 99, 8940–8948. <https://doi.org/10.1016/j.biortech.2008.05.015>
- Huang, A.A., 1975. Kinetic studies on insoluble cellulose–cellulase system. *Biotechnol. Bioeng.* 17, 1421–1433. <https://doi.org/10.1002/bit.260171003>
- IEA Bioenergy, 2014. Task 42 - Biorefining.
- Jawad, H., Madhab, D., Murthy, G.S., 2019. A novel method for real-time estimation of insoluble solids and glucose concentrations during enzymatic hydrolysis of biomass. *Bioresour. Technol.* 275, 328–337. <https://doi.org/10.1016/j.biortech.2018.12.071>
- Jin, J., Liu, G.L., Shi, S.Y., Cong, W., 2010. Studies on the performance of a rotating drum bioreactor for bioleaching processes - Oxygen transfer, solids distribution and power consumption. *Hydrometallurgy* 103, 30–34. <https://doi.org/10.1016/j.hydromet.2010.02.013>
- Jørgensen, H., Pinelo, M., 2017. Enzyme recycling in lignocellulosic biorefineries. *Biofuels, Bioprod. Biorefining* 11, 150–167. <https://doi.org/10.1002/bbb>
- Jørgensen, H., Vibe-pedersen, J., Larsen, J., Felby, C., 2007. Liquefaction of Lignocellulose at High-Solids Concentrations. *Biotechnol. Bioeng.* 96, 862–870. <https://doi.org/10.1002/bit>
- Kadam, K.L., Rydholm, E.C., Mcmillan, J.D., 2004. Development and Validation of a Kinetic Model for Enzymatic Saccharification of Lignocellulosic Biomass. *Biotechnol. Prog.* 20, 698–705.
- Kadlec, P., Gabrys, B., Strandt, S., 2009. Data-driven Soft Sensors in the process industry 33, 795–814. <https://doi.org/10.1016/j.compchemeng.2008.12.012>
- Karimi, K., Taherzadeh, M.J., 2016. A critical review of analytical methods in pretreatment of lignocelluloses: Composition, imaging, and crystallinity. *Bioresour. Technol.* 203, 348–356. <https://doi.org/10.1016/j.biortech.2015.11.022>
- Karthikeyan, O.P., Selvam, A., Wong, J.W.C., 2016. Hydrolysis-acidogenesis of food waste in solid-liquid-separating continuous stirred tank reactor (SLS-CSTR) for volatile organic acid production. *Bioresour. Technol.* 200, 366–373. <https://doi.org/10.1016/j.biortech.2015.10.017>
- Klein-Marcuschamer, D., Oleskowicz-Popiel, P., Simmons, B.A., Blanch, H.W., 2011. The

Challenge of Enzyme Cost in the Production of Lignocellulosic Biofuels. *Biotechnol. Bioeng.* 109, 1083–1087. <https://doi.org/10.1002/bit.24370>

Kline, L.M., Hayes, D.G., Womac, A.R., Labbé, N., 2010. Simplified determination of lignin content in hard and soft woods via UV-spectrophotometric analysis. *BioResources* 5, 1366–1383.

Kopelman, R., 1988. Fractal Reaction Kinetics. *Science.* 241, 1620–1625.

Kristensen, J.B., Felby, C., Jørgensen, H., 2009. Yield-determining factors in high-solids enzymatic hydrolysis of lignocellulose. *Biotechnol. Biofuels* 2, 1–10. <https://doi.org/10.1186/1754-6834-2-11>

Kumar, S., Dheeran, P., Singh, S.P., Mishra, I.M., Adhikari, D.K., 2015. Kinetic studies of two-stage sulphuric acid hydrolysis of sugarcane bagasse. *Renew. Energy* 83, 850–858. <https://doi.org/10.1016/j.renene.2015.05.033>

Larsen, J., Østergaard, M., Thirup, L., 2012. Inbicon makes lignocellulosic ethanol a commercial reality. *Biomass and Bioenergy* 46, 36–45. <https://doi.org/10.1016/j.biombioe.2012.03.033>

Li, X., Zheng, Y., 2017. Lignin-enzyme interaction: Mechanism, mitigation approach, modeling, and research prospects. *Biotechnol. Adv.* 35, 466–489. <https://doi.org/10.1016/j.biotechadv.2017.03.010>

Li, Y., Irwin, D.C., Wilson, D.B., 2007. Processivity, substrate binding, and mechanism of cellulose hydrolysis by *Thermobifida fusca* Cel9A. *Appl. Environ. Microbiol.* 73, 3165–3172. <https://doi.org/10.1128/AEM.02960-06>

Liguori, R., Soccol, C.R., de Souza Vandenberghe, L.P., Woiciechowski, A.L., Faraco, V., 2015. Second generation ethanol production from brewers' spent grain. *Energies* 8, 2575–2586. <https://doi.org/10.3390/en8042575>

Liguori, R., Ventrino, V., Pepe, O., Faraco, V., 2016. Bioreactors for lignocellulose conversion into fermentable sugars for production of high added value products. *Appl. Microbiol. Biotechnol.* 110, 597–611. <https://doi.org/10.1007/s00253-015-7125-9>

Lima, F. V, Rawlings, J.B., 2011. Nonlinear Stochastic Modeling to Improve State Estimation in Process Monitoring and Control. *AIChE J.* 57, 996–1007. <https://doi.org/10.1002/aic>

- Limayem, A., Ricke, S.C., 2012. Lignocellulosic biomass for bioethanol production: Current perspectives, potential issues and future prospects. *Prog. Energy Combust. Sci.* 38, 449–467. <https://doi.org/10.1016/j.pecs.2012.03.002>
- Lin, Y., Lee, W., Duan, K., Lin, Y., 2013. Ethanol production by simultaneous saccharification and fermentation in rotary drum reactor using thermotolerant *Kluyveromyces marxianus*. *Appl. Energy* 105, 389–394. <https://doi.org/10.1016/j.apenergy.2012.12.020>
- Liu, K., Zhang, J., Bao, J., 2015. Two stage hydrolysis of corn stover at high solids content for mixing power saving and scale-up applications. *Bioresour. Technol.* 196, 716–720. <https://doi.org/10.1016/j.biortech.2015.07.054>
- Longati, A.A., Lino, A.R.A., Giordano, R.C., Furlan, F.F., 2018. Defining research & development process targets through retro-techno-economic analysis: The sugarcane biorefinery case. *Bioresour. Technol.* 263, 1–9. <https://doi.org/10.1016/j.biortech.2018.04.102>
- Łukajtis, R., Rybarczyk, P., Kucharska, K., Konopacka-Łyskawa, D., Słupek, E., Wychodnik, K., Kamiński, M., 2018. Optimization of saccharification conditions of lignocellulosic biomass under alkaline pre-treatment and enzymatic hydrolysis. *Energies* 11, 1–27. <https://doi.org/10.3390/en11040886>
- Luttmann, R., Bracewell, D.G., Cornelissen, G., Gernaey, K. V., Glassey, J., Hass, V.C., Kaiser, C., Preusse, C., Striedner, G., Mandenius, C.F., 2012. Soft sensors in bioprocessing: A status report and recommendations. *Biotechnol. J.* 7, 1040–1048. <https://doi.org/10.1002/biot.201100506>
- Lynd, L.R., Weimer, P.J., Zyl, W.H. Van, Pretorius, I.S., 2002. Microbial cellulose utilization: Fundamentals and Biotechnology. *Bioresour. Technol.* 66, 506–577. <https://doi.org/10.1128/MMBR.66.3.506>
- McCabe, W.L., Smith, J.C., Harriott, P., 2005. *Unit Operations in Chemical Engineering*, 7<sup>th</sup> Edition, New York, USA.
- Menon, V., Rao, M., 2012. Trends in bioconversion of lignocellulose: Biofuels, platform chemicals & biorefinery concept. *Prog. Energy Combust. Sci.* 38, 522–550. <https://doi.org/10.1016/j.pecs.2012.02.002>
- Miller, G.L., 1959. Use of Dinitrosalicylic Acid Reagent for Determination of Reducing



Sugar. Anal. Chem. 31, 426–428. [https://doi.org/10.1016/S0140-6736\(08\)60884-3](https://doi.org/10.1016/S0140-6736(08)60884-3)

Modenbach, A.A., Nokes, S.E., 2013. Enzymatic hydrolysis of biomass at high-solids loadings - A review. *Biomass and Bioenergy* 56, 526–544. <https://doi.org/10.1016/j.biombioe.2013.05.031>

Mohagheghi, A., Tucker, M., Grohmann, K., Wyman, C., 1992. High solids simultaneous saccharification and fermentation of pretreated wheat straw to ethanol. *Appl. Biochem. Biotechnol. Part A Enzym. Eng. Biotechnol.* 33, 67–81. <https://doi.org/10.1007/BF02950778>

Mohd, J., Hoang, N.H., Hussain, M.A., Dochain, D., 2015. Review and classification of recent observers applied in chemical process systems. *Comput. Chem. Eng.* 76, 27–41. <https://doi.org/10.1016/j.compchemeng.2015.01.019>

Moncada, J.B., Aristizábal, V.M., Cardona, C.A.A., 2016. Design strategies for sustainable biorefineries. *Biochem. Eng. J.* 116, 122–134. <https://doi.org/10.1016/j.bej.2016.06.009>

Morales-Rodríguez, R., Capron, M., Huusom, J.K., 2010. Controlled fed-batch operation for improving cellulose hydrolysis in 2G bioethanol production, in: 20th European Symposium on Computer Aided Process Engineering – ESCAPE20. pp. 1–6.

Mosier, N., Wyman, C., Dale, B., Elander, R., Lee, Y.Y., Holtzapple, M., Ladisch, M., 2005. Features of promising technologies for pretreatment of lignocellulosic biomass 96, 673–686. <https://doi.org/10.1016/j.biortech.2004.06.025>

Naik, S.N., Goud, V. V, Rout, P.K., Dalai, A.K., 2010. Production of first and second generation biofuels : A comprehensive review. *Renew. Sustain. Energy Rev.* 14, 578–597. <https://doi.org/10.1016/j.rser.2009.10.003>

Nelles, O., 2001. *Nonlinear System Identification*, first. ed. Springer-Verlag, Berlin, Germany. <https://doi.org/10.1007/978-3-662-04323-3>

Nikzad, M., Movagharnejad, K., Talebnia, F., 2012. Comparative Study between Neural Network Model and Mathematical Models for Prediction of Glucose Concentration during Enzymatic Hydrolysis. *Int. J. Comput. Appl.* 56, 43–48. <https://doi.org/10.5120/8859-2818>

O'Dwyer, J.P., Zhu, L., Granda, C.B., Chang, V.S., Holtzapple, M.T., 2008. Neural network

prediction of biomass digestibility based on structural features. *Biotechnol. Prog.* 24, 283–292. <https://doi.org/10.1021/bp070193v>

Özdenkçi, K., Blasio, C. De, Muddassar, H.R., Melin, K., Oinas, P., Koskinen, J., Sarwar, G., Järvinen, M., 2017. A novel biorefinery integration concept for lignocellulosic biomass. *Energy Convers. Manag.* 149, 974–987. <https://doi.org/10.1016/j.enconman.2017.04.034>

Palmqvist, B., Lidén, G., 2012. Torque measurements reveal large process differences between materials during high solid enzymatic hydrolysis of pretreated lignocellulose 1–9.

Parada, M.P., Osseweijer, P., Duque, J.A.P., 2017. Sustainable biorefineries, an analysis of practices for incorporating sustainability in biorefinery design. *Ind. Crop. Prod.* 106, 105–123. <https://doi.org/10.1016/j.indcrop.2016.08.052>

Pereira, L., Comelli, A., Paula, A., Marcele, L., Henrique, M., Silveira, L., 2015. Enzymatic hydrolysis of steam-exploded sugarcane bagasse using high total solids and low enzyme loadings. *Bioresour. Technol.* 175, 195–202. <https://doi.org/10.1016/j.biortech.2014.10.087>

Phanthong, P., Reubroycharoen, P., Hao, X., Xu, G., 2018. Nanocellulose : Extraction and application. *Carbon Resour. Convers.* 1, 32–43. <https://doi.org/10.1016/j.crcon.2018.05.004>

Pino, M.S., Rodríguez-jasso, R.M., Michelin, M., Flores-gallegos, A.C., 2018. Bioreactor design for enzymatic hydrolysis of biomass under the biorefinery concept. *Chem. Eng. J.* 347, 119–136. <https://doi.org/10.1016/j.cej.2018.04.057>

Pino, M.S., Rodríguez-jasso, R.M., Michelin, M., Ruiz, H.A., 2019. Enhancement and modeling of enzymatic hydrolysis on cellulose from agave bagasse hydrothermally pretreated in a horizontal bioreactor. *Carbohydr. Polym.* 211, 349–359. <https://doi.org/10.1016/j.carbpol.2019.01.111>

Pinto, A.S.S., Pereira, S.C., Ribeiro, M.P.A., Farinas, C.S., 2016. Monitoring of the cellulosic ethanol fermentation process by near-infrared spectroscopy. *Bioresour. Technol.* 203, 334–340. <https://doi.org/10.1016/j.biortech.2015.12.069>

Rahikainen, J.L., Evans, J.D., Mikander, S., Kalliola, A., Puranen, T., Tamminen, T., Marjamaa, K., Kruus, K., Liisa, J., David, J., Mikander, S., Kalliola, A., Puranen, T.,

- Tamminen, T., Marjamaa, K., Kruus, K., 2013. Cellulase–lignin interactions — The role of carbohydrate-binding module and pH in non-productive binding. *Enzyme Microb. Technol.* 53, 315–321. <https://doi.org/10.1016/j.enzmictec.2013.07.003>
- Rambla, F.J., Garrigues, S., Guardia, M. De, 1997. PLS-NIR determination of total sugar , glucose , fructose and sucrose in aqueous solutions of fruit juices. *Anal. Chim. Acta* 344, 41–53.
- Rastogi, M., Shrivastava, S., 2017. Recent advances in second generation bioethanol production: An insight to pretreatment, saccharification and fermentation processes. *Renew. Sustain. Energy Rev.* 80, 330–340. <https://doi.org/10.1016/j.rser.2017.05.225>
- Reilly, P.J., 2007. Amylase and Cellulase Structure and Function, in: *Bioprocessing for Value-Added Products from Renewable Resources*. pp. 119–130. <https://doi.org/10.1016/B978-044452114-9/50006-2>
- Ren, H., Zhang, J., 2018. Enhanced High-Solids Fed-Batch Enzymatic Hydrolysis of Sugar Cane Bagasse with Accessory Enzymes and Additives at Low Cellulase Loading. *ACS Sustain. Chem. Eng.* 6, 12787–12796. <https://doi.org/10.1021/acssuschemeng.8b01972>
- Ribeiro, M.P.A., Pádua, T.F., Leite, O.D., Giordano, R.L.C., Giordano, R.C., 2008. Multivariate calibration methods applied to the monitoring of the enzymatic synthesis of ampicilin. *Chemom. Intell. Lab. Syst.* 90, 169–177. <https://doi.org/10.1016/j.chemolab.2007.09.006>
- Rocha-martín, J., Martínez-bernal, C., Pérez-cobas, Y., Reyes-sosa, F.M., García, B.D., 2017. Additives enhancing enzymatic hydrolysis of lignocellulosic biomass. *Bioresour. Technol.* 244, 48–56.
- Roche, C.M., Dibble, C.J., Stickel, J.J., 2009. Lignocellulosic biomass at high-solids loadings. *Biotechnol. Biofuels* 11, 1–11. <https://doi.org/10.1186/1754-6834-2-28>
- Rodríguez-zúñiga, U.F., Farinas, C.S., Carneiro, R.L., Giordano, R.D.C., Perencin, M., Ribeiro, D.A., 2014. Fast Determination of the Composition of Pretreated Sugarcane Bagasse Using Near-Infrared Spectroscopy 1441–1453. <https://doi.org/10.1007/s12155-014-9488-7>
- Rosgaard, L., Andric, P., Dam-Johansen, K., Pedersen, S., Meyer, A.S., 2007. Effects of substrate loading on enzymatic hydrolysis and viscosity of pretreated barley straw.

- Appl. Biochem. Biotechnol. 143, 27–40. <https://doi.org/10.1007/s12010-007-0028-1>
- Sagmeister, P., Wechselberger, P., Jazini, M., Meitz, A., Langemann, T., Herwig, C., 2013. Soft sensor assisted dynamic bioprocess control: Efficient tools for bioprocess development. *Chem. Eng. Sci.* 96, 190–198. <https://doi.org/10.1016/j.ces.2013.02.069>
- Salles, P., 2013. Avaliação de um reator tipo tambor rotativo para hidrólise enzimática do bagaço de cana-de-açúcar.
- Samaniuk, J.R., Scott, C.T., Root, T.W., Klingenberg, D.J., 2011. The effect of high intensity mixing on the enzymatic hydrolysis of concentrated cellulose fiber suspensions. *Bioresour. Technol.* 102, 4489–4494. <https://doi.org/10.1016/j.biortech.2010.11.117>
- Santos, F.A., Queiróz, J.H. De, Colodette, J.L., Fernandes, S.A., Guimarães, V.M., Sebastião T Guimarães, 2012. Potencial da palha de cana-de-açúcar para produção de etanol. *Quim. Nova* 35, 1004–1010.
- Schwald, W., Breuil, C., Brownell, H.H., Chan, M., Saddler, J.M., 1989. Assessment of pretreatment conditions to obtain fast complete hydrolysis on high substrate concentrations. *Appl. Biochem. Biotechnol.* 20–21, 29–44. <https://doi.org/10.1007/BF02936471>
- Scott, C.T., Samaniuk, J.R., Scott, C.T.; Samaniuk, J.R.; Klingenberg, D.J., Scott, C.T., Samaniuk, J.R., Klingenberg, D.J., 2011. Rheology and extrusion of high-solids biomass. *Tappi J.* 10, 47–53.
- Skvaril, J., Kyprianidis, K.G., Dahlquist, E., 2017. Applications of near-infrared spectroscopy (NIRS) in biomass energy conversion processes: A review. *Appl. Spectrosc. Rev.* 52, 675–728. <https://doi.org/10.1080/05704928.2017.1289471>
- Sluiter, A., Hames, B., Ruiz, R., Scarlata, C., Sluiter, J., Templeton, D., Crocker, D., 2012. Determination of Structural Carbohydrates and Lignin in Biomass Laboratory Analytical Procedure (LAP) Determination of Structural Carbohydrates and Lignin in Biomass Laboratory.
- Sluiter, A., Hames, B., Ruiz, R., Scarlata, C., Sluiter, J., Templeton, D., Crocker, D., 2008. Determination of Sugars, Byproducts, and Degradation Products in Liquid Fraction Process Samples - Technical Report NREL/TP-510-42623, National Renewable Energy Laboratory.

- Sotaniemi, V.H., Taskila, S., Ojamo, H., Tanskanen, J., 2016. Controlled feeding of lignocellulosic substrate enhances the performance of fed-batch enzymatic hydrolysis in a stirred tank reactor. *Biomass and Bioenergy* 91, 271–277. <https://doi.org/10.1016/j.biombioe.2016.05.037>
- Sousa Jr, R., Carvalho, M.L., Giordano, R.L.C., Giordano, R.C., 2011. Recent trends in the modeling of cellulose hydrolysis. *Brazilian J. Chem. Eng.* 28, 545–564.
- Souza, A.P. De, Leite, D.C.C., Buckeridge, M.S., 2013. Composition and Structure of Sugarcane Cell Wall Polysaccharides : Implications for Second-Generation Bioethanol Production 564–579. <https://doi.org/10.1007/s12155-012-9268-1>
- Suarez, C.A.G., Cavalcanti-montaña, I.D., Marques, R.G. da C., Furlan, F.F., Aquino, P.L. da M. e, Giordano, R. de C., Souza Jr, R., 2014. Modeling the Kinetics of Complex Systems : Enzymatic Hydrolysis of Lignocellulosic Substrates. *Appl. Biochem. Biotechnol.* 173, 1083–1096. <https://doi.org/10.1007/s12010-014-0912-4>
- Sun, S.S., Sun, S.S., Cao, X., Sun, R., 2016. The role of pretreatment in improving the enzymatic hydrolysis of lignocellulosic materials. *Bioresour. Technol.* 199, 49–58. <https://doi.org/10.1016/j.biortech.2015.08.061>
- Sun, Y., Cheng, J., 2002. Hydrolysis of lignocellulosic materials for ethanol production: A review 83, 1–11.
- Tai, C., Arellano, M.G., Keshwani, D.R., 2014. Epidemic based modeling of enzymatic hydrolysis of lignocellulosic biomass. *Biotechnol. Prog.* 30, 1021–1028. <https://doi.org/10.1002/btpr.1960>
- Tai, C., Keshwani, D.R., Voltan, D.S., Kuhar, P.S., Engel, A.J., 2015. Optimal Control Strategy for Fed-Batch Enzymatic Hydrolysis of Lignocellulosic Biomass Based on Epidemic Modeling. *Biotechnol. Bioeng.* 112, 1376–1382. <https://doi.org/10.1002/bit.25552>
- Takagi, T., Sugeno, M., 1985. Fuzzy identification of systems and its applications to modeling and control. *IEEE Trans. Syst. Man. Cybern.* SMC-15, 116–132. <https://doi.org/10.1109/TSMC.1985.6313399>
- Tervasmäki, P., Sotaniemi, V., Kangas, J., Taskila, S., Ojamo, H., Tanskanen, J., 2017. A discretized model for enzymatic hydrolysis of cellulose in a fed-batch process. *Bioresour. Technol.* 227, 112–124. <https://doi.org/10.1016/j.biortech.2016.12.054>

- Teter, S.A., Sutton, K.B., Emme, B., 2014. Enzymatic processes and enzyme development in biorefining, *Advances in Biorefineries: Biomass and Waste Supply Chain Exploitation*. <https://doi.org/10.1533/9780857097385.1.199>
- Trevor Palmer, 1985. *Understanding Enzymes*. Hertfordshire, England.
- Väljamäe, P., Kipper, K., Pettersson, G., Johansson, G., 2003. Synergistic Cellulose Hydrolysis Can Be Described in Terms of Fractal-Like Kinetics. *Biotechnol. Bioeng.* 84, 2001–2004. <https://doi.org/10.1002/bit.10775>
- Varga, E., Klinke, H.B., Réczey, K., Thomsen, A.B., 2004. High solid simultaneous saccharification and fermentation of wet oxidized corn stover to ethanol. *Biotechnol. Bioeng.* 88, 567–574. <https://doi.org/10.1002/bit.20222>
- Vojinovi, V., Cabral, J.M.S., Fonseca, L.P., 2006. Real-time bioprocess monitoring Part I: In situ sensors. *Sensors Actuators B* 114, 1083–1091. <https://doi.org/10.1016/j.snb.2005.07.059>
- Wang, W., Zhuang, X., Yuan, Z., Yu, Q., Qi, W., Wang, Q., Tan, X., 2012. High consistency enzymatic saccharification of sweet sorghum bagasse pretreated with liquid hot water. *Bioresour. Technol.* 108, 252–257. <https://doi.org/10.1016/j.biortech.2011.12.092>
- Wang, Z., Feng, H., 2010. Fractal kinetic analysis of the enzymatic saccharification of cellulose under different conditions. *Bioresour. Technol.* 101, 7995–8000. <https://doi.org/10.1016/j.biortech.2010.05.056>
- Wang, Z., Wen, S., Zhang, Q., Liu, G., Wu, X., Cong, W., 2013. Power Consumption of Liquid and Liquid / Solid Systems in a Rotating-Drum Bioreactor. *Chem. Eng. Technol.* 36, 1395–1401. <https://doi.org/10.1002/ceat.201200523>
- Wold, S., Sjostrom, M., Eriksson, L., Sweden°, S., 2001. PLS-regression, a basic tool of chemometrics. *Chemom. Intell. Lab. Syst.* 58, 2001–109. [https://doi.org/10.1016/S0169-7439\(01\)00155-1](https://doi.org/10.1016/S0169-7439(01)00155-1)
- Xie, L., Ye, X., Liu, D., Ying, Y., 2009. Quantification of glucose , fructose and sucrose in bayberry juice by NIR and PLS. *Food Chem.* 114, 1135–1140. <https://doi.org/10.1016/j.foodchem.2008.10.076>
- Xiong, Z., Zhang, J., 2005. Neural network model-based on-line re-optimisation control of fed-batch processes using a modified iterative dynamic programming algorithm.

Chem. Eng. Process. 44, 477–484. <https://doi.org/10.1016/j.cep.2004.07.001>

- Xu, F., Ding, H., 2007. A new kinetic model for heterogeneous (or spatially confined) enzymatic catalysis: Contributions from the fractal and jamming (overcrowding) effects 317, 70–81. <https://doi.org/10.1016/j.apcata.2006.10.014>
- Xu, F., Yu, J., Tesso, T., Dowell, F., Wang, D., 2013. Qualitative and quantitative analysis of lignocellulosic biomass using infrared techniques: A mini-review. *Appl. Energy* 104, 801–809. <https://doi.org/10.1016/j.apenergy.2012.12.019>
- Xu, S., Luo, L., Selvam, A., Wong, J.W.C., 2016. Strategies to Increase Energy Recovery From Phase-Separated Anaerobic Digestion of Organic Solid Waste. *Curr. Dev. Biotechnol. Bioeng. Solid Waste Manag.* 113–134. <https://doi.org/10.1016/B978-0-444-63664-5.00006-X>
- Yang, J., Zhang, X., Yong, Q., Yu, S., 2011. Three-stage enzymatic hydrolysis of steam-exploded corn stover at high substrate concentration. *Bioresour. Technol.* 102, 4905–4908. <https://doi.org/10.1016/j.biortech.2010.12.047>
- Yao, M., Wang, Z., Wu, Z., Qi, H., 2011. Evaluating Kinetics of Enzymatic Saccharification of Lignocellulose by Fractal Kinetic Analysis. *Biotechnol. Bioprocess Eng.* 16, 1240–1247. <https://doi.org/10.1007/s12257-011-0283-4>
- Yao, S., Nie, S., Yuan, Y., Wang, S., Qin, C., 2015. Efficient extraction of bagasse hemicelluloses and characterization of solid remainder. *Bioresour. Technol.* 185, 21–27. <https://doi.org/10.1016/j.biortech.2015.02.052>
- Zabed, H., Sahu, J.N., Suely, A., Boyce, A.N., Faruq, G., 2017. Bioethanol production from renewable sources: Current perspectives and technological progress. *Renew. Sustain. Energy Rev.* 71, 475–501. <https://doi.org/10.1016/j.rser.2016.12.076>
- Zhang, J., Chu, D., Huang, J., Yu, Z., Dai, G., Bao, J., 2010. Simultaneous Saccharification and Ethanol Fermentation at High Corn Stover Solids Loading in a Helical Stirring Bioreactor. *Biotechnol. Bioeng.* 105, 718–728. <https://doi.org/10.1002/bit.22593>
- Zhang, L., Carlos, A., Ximenes, E., Ladisch, M., 2017. Proteins at heterogeneous (lignocellulose) interfaces. *Curr. Opin. Chem. Eng.* 18, 45–54. <https://doi.org/10.1016/j.coche.2017.09.003>

- Zhang, Y., Liu, Y.-Y., Xu, J.-L., Yuan, Z.-H., Qi, W., Zhuang, X.-S., He, M.-C., 2012. High Solid and Low Enzyme Loading Based Saccharification of Agricultural Biomass. *BioResources* 7, 345–353.
- Zhang, Y.P., Lynd, L.R., 2004. Toward an Aggregated Understanding of Enzymatic Hydrolysis of Cellulose: Noncomplexed Cellulase Systems. *Biotechnol. Bioeng.* 88, 797–824. <https://doi.org/10.1002/bit.20282>
- Zhu, Y., Malten, M., Torry-smith, M., Mcmillan, J.D., Stickel, J.J., 2011. Calculating sugar yields in high solids hydrolysis of biomass. *Bioresour. Technol.* 102, 2897–2903. <https://doi.org/10.1016/j.biortech.2010.10.134>





